POLITECNICO DI TORINO

Corso di Laurea Magistrale in Ingegneria Elettronica

Tesi di Laurea Magistrale

pNML to Skyrmions interface for logic in memory application

Relatori:
Prof. Maurizio Zamboni
Prof. Marco Vacca
Ing. Fabrizio Riente

Candidato:
Gianluca Palmeri

Aprile 2021

A scientist studies what is,
whereas an engineer creates what never was.
- Theodore von Kármán

To my grandparents Giovanni and Angelina

Acknowledgments

I would like to thank all the people who have supported me since the beginning of my university career: my family and in particular my mother who encouraged me to always do better and helped me in every possible way to achieve my dream.

My girlfriend Elisabetta for helping me and giving me advices in those situations where I was in trouble and for always supporting my decisions. My sister Serena for motivating me and always being there for me when it was necessary.

My friends and colleagues Pierpaolo and Giuseppe for sharing with me many nights of study and fun. My childhood friend Carmelo to always be a sunny support.

My supervisors Prof Maurizio Zamboni, Marco Vacca and Fabrizio Riente for helping me in this research path and providing me a solution for every problem I encountered.

And a special thanks to Ph.Luca Gnoli for always helping me and giving advice by stimulating my imagination.

Abstract

The progressive improvement of the common complementary metal-oxide semiconductor (CMOS) technology implies growing technological challenges and a drastic increase in manufacturing costs for each new technological node. Because of physical, technological and economic constraints of future nodes, several emerging technologies beyond CMOS are explored, which compete for the succession of CMOS or implementation in hybrid integrated circuits (ICs). Two promising candidates are Nanomagnetic Logic (NML) technology, which uses the interaction of coupled non-volatile magnets to perform logic operations, and Skyrmions technology, which uses magnetic nanovortices used to permanently store data in a CoPt strip.

This work investigates the communication between perpendicular nanomagnetic logic (pNML) technology and skyrmions (Sk) to obtain devices able to take advantage of the best characteristics of both technologies. In pNML technology ferromagnetic islands can have a bi-stable perpendicular (up / down) state of magnetization, which is binary coded to represent digital states 1 and 0. This technology presents clear advantages for logic application thanks to its great efficiency and the possibility to the ease to realize multilayer circuits. In skyrmions technology the presence or absence of the skyrmion represents respectively the digital states 1 and 0. This technology is more suitable for memory thanks to the small dimensions of skyrmions compared to the pNML ferromagnetic states and thanks to the higher stability of information. In the proposed hybrid solution the skyrmions, used as memory elements, are used as a seed to construct valid data in pNML. This data can then be elaborated with pNML devices and finally be converted back into a skyrmion to be stored efficiently in a magnetic memory. The devices have been studied through mumax3, a micromagnetic GPU-accelerated simulation software.

This study demonstrated that a connection between skyrmion and pNML technology is definitely possible. This opens many interesting scenarios in which complex devices can take advantage of multiple magnetic technologies to obtain optimal solution both for memory and processing. In this direction also a preliminary evaluation of logic in memory systems has been done. Different valid algorithms was found compatible to this hybrid system. Among them a max/min search algorithm was analyzed. An outline and optimizations have been carried out but no full LiM system simulations have been performed.

Table of contents

List of figures

List of tables

Chapter 1

Summary

In this thesis work we want to describe how it is possible to hybridize the two technologies pNML and Skyrmions, while a particular attention was give to the possible applications LiM.

We will start with Chapter 2 where we will see a brief introduction regarding the technologies currently in use (CMOS) and the emerging ones, of which we will talk about in this work of thesis (Skyrmion, pNML), presenting briefly the magnetic phenomena that dominate these micromagnetic technologies. Finally a hint at the architecture LiM, extremely suitable with these two technologies.

Chapter 3 summarizes the various structures studied during the work and there are countless extracts from the simulations to understand how it is possible to perform conversions.

In Chapter 4 a series of characterizations are collected mainly concerning the skyrmions able to eventually make an hybrid system Skyrmion-pNML.

In Chapter 5 we can appreciate some options of complete conversion structure Sk-DW-pNML-DW-Sk which is the basic element of the hybrid technology described above with a respective simulation of parts of the structure.

Finally in chapter 6 is shown a possible logic in memory architecture excellent to test this hybrid technology that allows the search for the Max/ Min in a Skyrmions memory.

Chapter 2

Introduction

in this section there are some basic notions and some considerations that led to this thesis work.

In particular we will focus on existing technologies (CMOS) and the possible evolution of the latter, as well as technologies that could replace them or expand their capabilities.

We will briefly see some physical phenomena that intervene in the functioning of the main magnetic technologies in detail the hysteresis, the laws of Maxwell and other phenomena that intervene in the technologies studied in the period of the thesis (pNML, Skyrmions).

Finally, a summary of the research already conducted on technologies of central importance in this thesis, namely the pNML technology based on Domain Wall (DW) and the skyrmions based on magnetic nanovortices.

2.1 CMOS technology

The evolution of CMOS circuits has followed the path defined by Moore's law from the 70 till today [26]. In fact, CMOS technology improved by 30% every 2 years by reducing size and increasing the speed of integrated circuits. This allowed a progressive increase in the performance of CMOS systems both as a computing power (by increasing the number of transistors and processing units inside a Die) and from the point of view of the energy.

The progressive downsizing predicted by Moore's law allows to increase by a factor 2 the density of the transistors for each technological node. This increases the speed of the integrated circuits (about 30% per node) and on the other hand it reduces the power passing from one node N to a node N + 1 (See Figure [2.1]) [1].

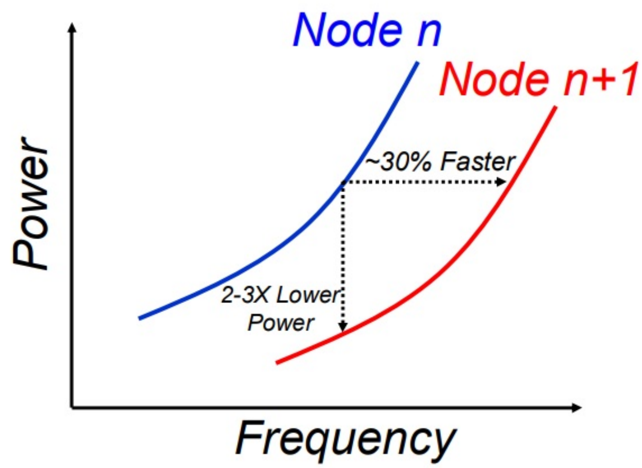

Figure 2.1: Moving from node "n" to node "n+1" and operating at lower voltage, one could obtain faster and/or lower power are obtained, taken from [1]

Thanks to the downsizing of solid-state integrated devices there was an improvement in performance, power and costs that caused an evolution in the industry that has led us from integrated structures at $10\mu m$ in 1970 to $14nm$ in 2013 [2].

This improvement continues with the steps establishes by the International Technology Road map for Semiconductors (ITRS) which predicted the path to follow until 2024 [27]. Every time you move from one technological node to another, there are several technological challenges to overcome (e.g. lithography, transistor resizing, interconnections and circuit design).

In fact, reducing the size of the transistors causes an increase in the parasitic parameters (Resistance, capacitance) which become dominant in the case of planar CMOS technology around the technological node at 20nm (See Figure [2.2]) [2].

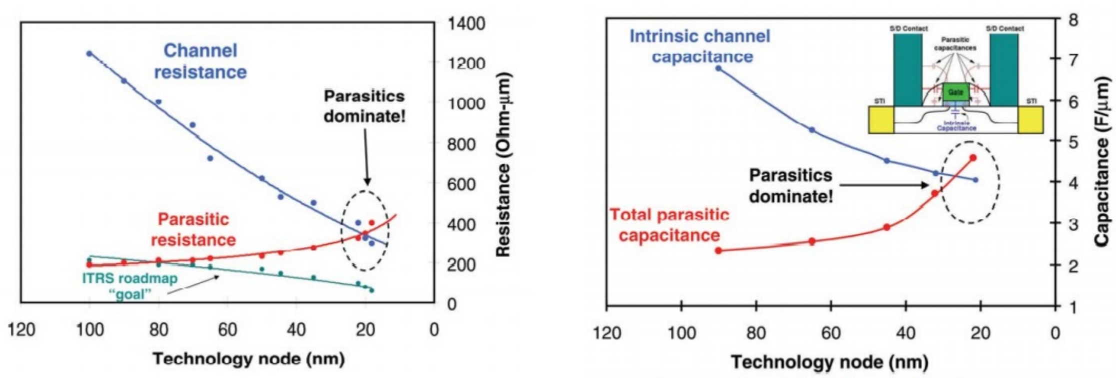

Figure 2.2: Estimated total planar CMOS parasitic and channel resistance and capacitance are compared to technology node,taken from [2].

The total production costs increased significantly (See Figure [2.3]), in particular the costs of photo lithography and masks[3].

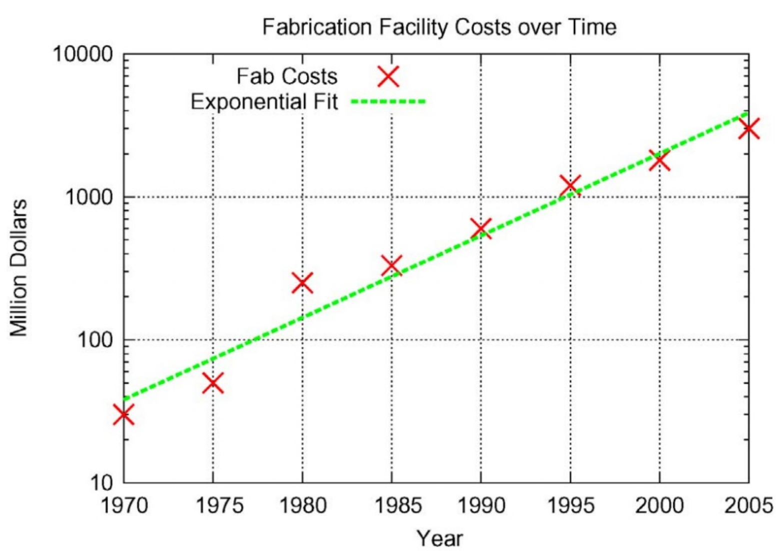

Figure 2.3: Fabrication facility costs over time, taken from[3]

Of course, this trend cannot be maintained forever. In fact Sooner or later, insuperable technological or economic limits will arise and will no longer allow it (See Figure [2.4]). Nowadays we are very close to this limit with the technological node at 7 nm[28], this physical limit is inevitable and forces us to think outside the

CMOS world and about devices that work in symbiosis with this technology or that completely replace it [4].

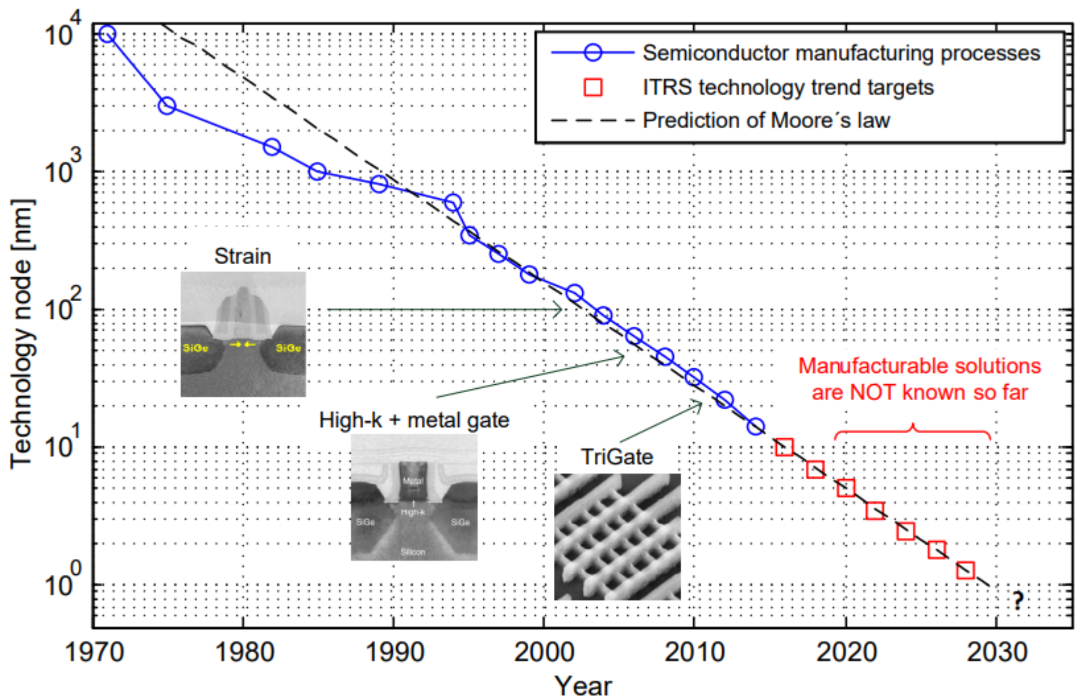

Figure 2.4: Technology node of the semiconductor manufacturing process from 1971 until the next 15 years are scheduled in the International Technology Road map for Semiconductors (ITRS) [4]

2.1.1 New Technology

The favourite way of the industry to continue with the conventional dimensional and functional resizing according to Moore's law (”More Moore”)[5]is the expansion of CMOS technology and in particular of new technologies that work in symbiosis with it.

The search for ”More-Then-Moore” and ”Beyond-CMOS” devices has been applied a lot in recent years [3] because of the increasing technological and economic challenges for the development of future technological nodes. These two approaches differ in their purpose [5]

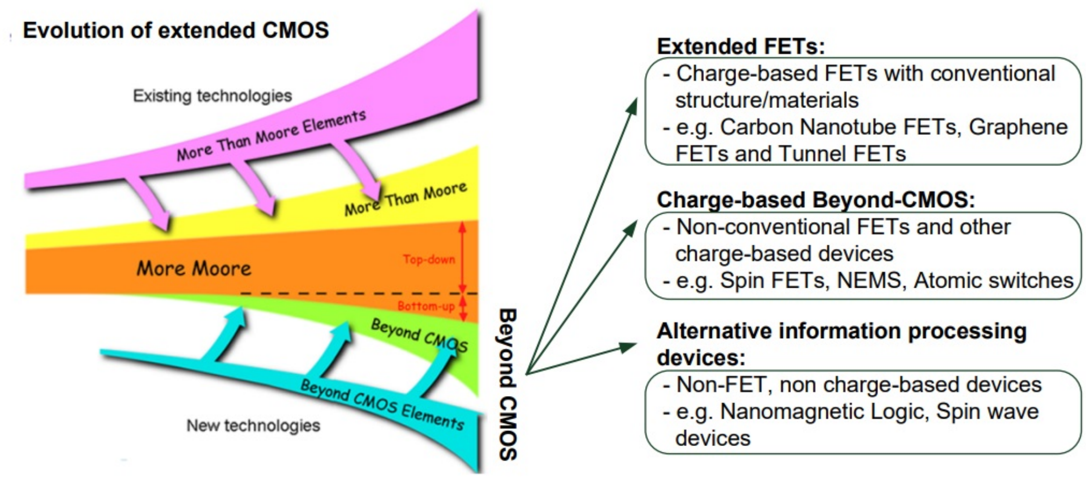

Figure 2.5: Relationship among ”More Moore”, ”More-than-Moore” and ”Beyond-CMOS” taken from [5]. Beyond-CMOS devices are classified basing on their state variable, structure and material

2.1.2 More than Moore

More-than-Moore devices (See Figure [2.5]) are managed as non-digital information processing devices to extend CMOS functionality. The principle of the operation is simple and it consists in reproducing generic functions of a high level in functions at low level. Thanks to these technologies it is possible to replace the elements originally in CMOS making it simpler. Thus in this way the costs for their implementation become acceptable and encourage the development and the maintenance of long-term CMOS technology for the.

2.1.3 Beyond-CMOS

Devices beyond CMOS (See Figure [2.5]) are classified as alternative information processing devices to extend or partially replace functionality of the CMOS platform.[5].

are classified as logical and alternative information processing devices not only to extend but also to partially replace functionality of the CMOS platform[5]. Changing the design and materials of MOSFETs would make an improvement possible for few generations, but to make something enduring, it is necessary to think about a new device that allows continuous long-term scaling.

Nowadays, these devices are studied and evaluated both by industry and by academia research (See Figure [2.6]). However, to replace the current CMOS technology, a new technology must satisfy several fundamental characteristics in order to be able to consider them effectively as post-CMOS devices [6].

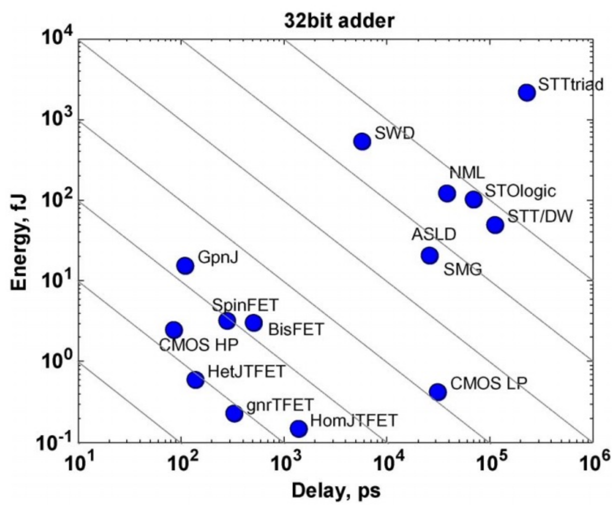

Figure 2.6: Energy versus delay of 32-bit adders in different technology, taken from [6]

This is the approach with which the work was carried out in this Thesis referring to thinking of hardware accelerators that replace the circuit areas that could initially be made in CMOS technology.

2.2 Magnetic phenomena

2.2.1 Magnetic hysteresis

Magnetic hysteresis is at the center of magnetic materials behaviour. All applications of these materials are based on particular aspects of hysteresis.

The variety of working conditions shows the richness of the phenomena that can guide the behavior of different materials.

An identifying element of ferromagnetic materials is the hysteresis loop, obtained by applying a specific cyclic magnetic field H and recording the variations of the magnetization M or the magnetic induction B along the direction of the field. As shown in Figure [2.7] and in Figure [2.8]there are two hysteresis loops for the materials largely used in this work: the $Co_{0.8}Pt_1$ singlelayer (thickness = 1.8nm) and the $[Co_{0.8}Pt_1]_{x7} + Co_{0.8}$ multilayer (thickness = 13.4nm).

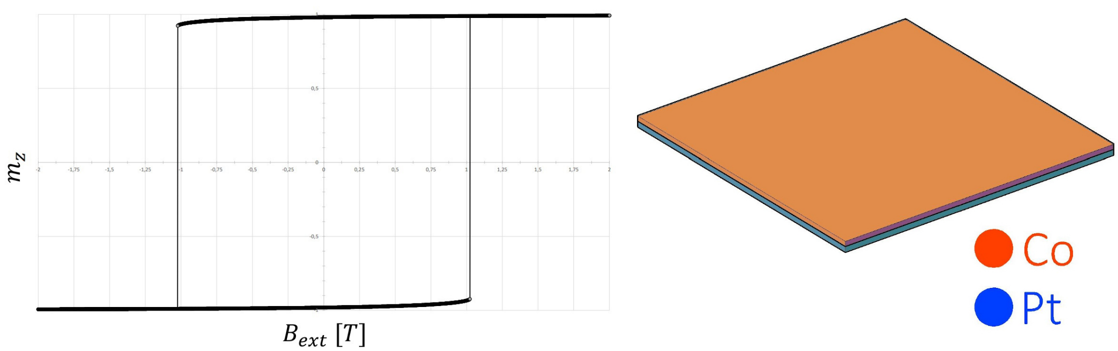

Figure 2.7: Hysteresis loop of $CoPt$ singlelayer made by 50 nm·50 nm·1.8 nm magnet obtained by MUMAX3 at T=0K. Loop width is 2.04 T less than the multilayer case.

M_z measures the average magnetic moment per unit volume of material along the +Z direction that characterizes the magnetic state, B_{ext} the Magnetic field [T].

The hysteresis cycle can take several different shapes according to the material and its thickness. Thanks to this characteristic, different materials can be used for very different applications. As highlighted above there is a difference between the

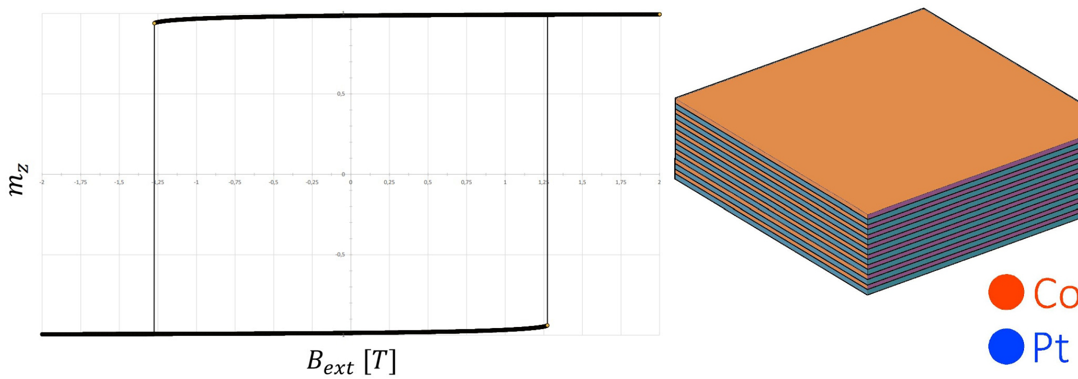

Figure 2.8: Hysteresis loop of $CoPt$ multilayer made by 50 nm · 50 nm · 13.4 nm magnet obtained by MUMAX3 at T=0K. Loop width is 3.6 T greater than the singlelayer case.

hysteresis cycle of the CoPt singlelayer and CoPt Multilayer specifically a different field value for the status switch. A magnetic material can be imagined as a set of permanent magnetic moment m_i, of quantum-mechanical origin.

Ferromagnetic materials can exhibit a large spontaneous magnetization even at low fields as the elementary magnetic moments are not independent. In fact, they are strongly coupled by an internal field proportional to the magnetization itself. This field introduces a positive feedback mechanism.

The variety of the shape of the hysteresis loop observed is the direct consequence of the variety of the magnetic domains' possible structures. The magnetic domain results from the balance of several competing energy terms. Domains with magnetization that point approximately in the direction of the applied field are energetically favored. At high fields, the material is magnetized everywhere along the direction of the applied fields. In this way a large domain is covering the entire spectrum taken from [29]

2.2.2 Thermal relaxation

The velocity-independent hysteresis is an approximation only possible at zero temperature. In this condition the system remains in an initially occupied local minimum. At a temperature superior than 0k, the system naturally tends to occupy a state which is determined by the Boltzmann statistics.

When free energy has many extremes and saddle points, relaxation towards balance results to be a complicated process. thermal agitation offers a change to overcome one of the energy barriers that separate the system from neighboring states. This happens when the system is trapped in local minimum energy for long periods.

The magnetic domain is progressively modified and when balance is reached, the system shifts to a new minimum energy state.

In the velocity-independent approximation, the system is influenced by the action of the external field that will make it jump to a new state only when the total energy is reduced to zero. When thermal agitation is activated, the jump occur more quickly, before the total energy is reduced to zero. It happens thanks to the barrier that is lower.

2.2.3 Bi-stability

A system whose free energy is given by the Equation (2.1)

$$f(x) = x^4 - 2ax^2 \tag{2.1}$$

In the Equation a is a positive constant, the problem has been reduced to a convenient dimensionless form including all variables and parameters. $f(x)$ is shown in the Figure [2.9]. has two equal minima located at $x = \pm a^{(1/2)}$ and a maximum at $x = 0$.

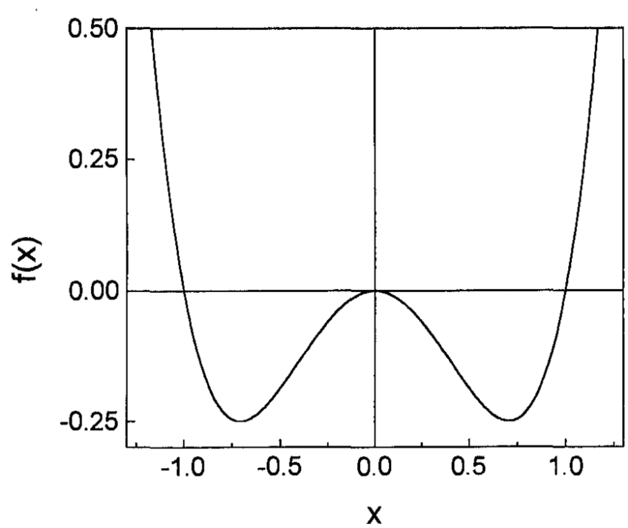

Figure 2.9: Free energy of bi-stable system described by Equation (2.1), with the energy minima are located at $x = \pm a^{(1/2)}$ and a maximum at $x = 0$, taken from [7]

The free energy under a non-zero input h is given by the Equation (2.2)

$$g_L(x,h) = x^4 - 2ax^2 - hx \tag{2.2}$$

The metastable states under the generic field h are determined by the condition $\delta g_L/\delta x^2 = 0$, whit $\delta^2 g_L/\delta x^2 = 0$, which identifies the minimum local g_L.

The qualitative behavior value of $g_L(x,h)$ for the various values of h is shown in Figure [2.10].

When h is large (eg. $-\infty$), the energy of interaction with the external field dominates and shows only a minimum (See Figure [2.10.1]). When h increases from $h = -\infty$, to a certain field $h = -hc$, a new energy minimum is formed. At $h = 0$ the two minima have the same energy (See Figure [2.10.2]). At $h = hc$ the minimum initially occupied by the system becomes an inflection point(See Figure [2.10.3]): the system is no longer stable and makes a spontaneous and irreversible Barkhausen jump to the lower energy state. There is only a minimum for the higher fields and that is where our system is.

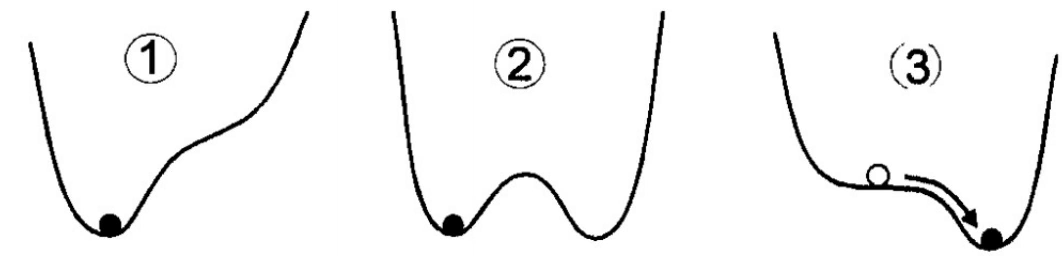

Figure 2.10: Sequence of energy profiles calculated from Equation (2.2) under different external field, showing genesis of barkhausen jump and hysteresis loop. 1:$h = -\infty$, 2:$h = 0$, 3:$h = hc$, taken from [7]

A similar situation occurs when the field is progressively decremented from $+\infty$, except that the barkhausen jump will now occur in $h = -hc$. The bheavior is visible in Figure [2.11])

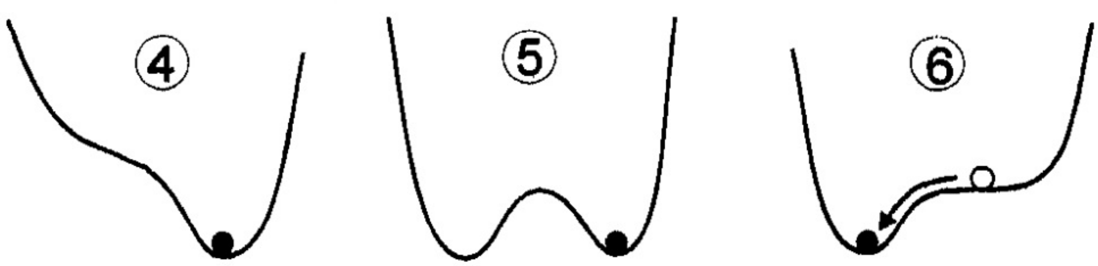

Figure 2.11: Sequence of energy profiles calculated from Equation (2.2) under different external field, showing genesis of barkhausen jump and hysteresis loop. 4:$h = +\infty$, 5:$h = 0$, 6:$h = -hc$, taken from [7]

2.2.4 Maxwell's equations

An interesting characteristic of the magnetic material is that it can produce a static magnetic field in surounding space. According to Maxwell's equations, in fact a static magnetic field is produced by stationary electric currents.

The magneto static studies the magnetic phenomena produced by stationary currents. Its same principles can be extended to all those situations in which the current changes slowly (dynamic case). In fact if we assume short time period, the system can be consider stationary in a good approximation.

Maxwell's equations expressed in the following form[30]:

$$\mathit{\Delta} \cdot B = 0 \tag{2.3}$$

$$\mathit{\Delta} \times E + \frac{\delta B}{\delta t} = 0 \tag{2.4}$$

$$\epsilon_0 \cdot E = \rho \tag{2.5}$$

$$\frac{1}{\mu_0} \times B - \epsilon_0 \frac{\delta E}{\delta t} = j \tag{2.6}$$

the constants are:

$$\epsilon_0 = \frac{1}{c^2 \mu_0} \approx 8.8510^{-12}[F \cdot m] \tag{2.7}$$

$$\mu_0 = 4\pi 10^{-7}[H \cdot m] \tag{2.8}$$

These equations refer to the elementary volume $\mathit{\Delta}V$. the electric field $E(r{,}t)$ and the magnetic field $B(r{,}t)$ are taken on the elementary volume $\mathit{\Delta}V$ centered on the position r, ρ and j represent the $\mathit{\Delta}V$ averages of the electric charge density and the electric current density .

2.2.5 Micromagnetism

Micromagnetism is the evolution of the magnetic moments theory, developed to combine the phenomenological Maxwell's theory and quantum one. Maxwell's theory of electromagnetic fields is valid for macroscopic dimensions and specifies material properties such as global permeabilities and susceptibilities. By contrast, the quantum theory describes magnetic properties on the atomic level.

Micromagnetism represents the magnetic properties by mediating them on a certain volume and mapping the magnetic characteristics from a discrete representation (like the quantum one) to a continuous representation. This is based on Brown's theory
The turning point was achieved by Landau and Lifshitz, who formulated an expression for the exchange energy and describe a first interpretation of domain patterns [31].

The theory of micromagnetism allows to describe domain patterns, magnetization processes on magnetic materials as well as the switching properties.

Micromagnetic energies

The basic principle of micromagnetics is the minimization of the total energy of the magnetization vector [32]. The formation of magnetic domains are a necessary consequence to reach the minimum energy level. Thus the following magnetization-dependent contributions to the total energy are the origin to describe both the magnetization dynamics and the domain theory.

The basic principle of micromagnetics is the minimization of the total energy of the magnetization vector [32]. The reaching of the minimum energy level causes the formation of magnetic domains as a necessary consequence.

The contributions to the total energy are the origin of both the magnetization dynamics and the domain theory.
Exchange energy : The exchange interaction establishes magnetic ordering in magnetic materials. It describes a quantum effect between two contiguous spins, which tend to align in a parallel.
It describes the intensity of the magnetic coupling needed to deviate a spin from the direction of the exchange field. the exchange energy is minimized for all spins

aligned in parallel.

Anisotropy energy : The magnetic anisotropy energy may arise for multiple reasons and it depends on the direction of the magnetization respect to the crystal structure of the magnetic material.

Magnetostatic energy : It originates from two different sources: the external magnetic field and the demagnetization one (or stray field) that derives from the magnetization of the material m.

- *Zeeman energy (external field energy)* : It is the energy generated by the interaction of the magnetization M with the external magnetic field. To minimize it, the magnetization M and the external field have to be aligned in parallel.
- *Demagnetization energy (stray field energy)* : It is generated by the divergence of the magnetization M itself and it is minimized for a minimum stray field.

Total energy : Summing up all contributions mentioned above gives the total energy :

$$E_{total} = E_{exchange} + E_{ani} + E_{Zeeman} + E_{demag} + ... \tag{2.9}$$

2.2.6 Landau-Lifshitz-Gilbert (LLG) equation

Landau and Lifshitz published the Landau-Lifshitz-equation (LL-equation) in 1992 for the motion of magnetic moments in an applied magnetic field [31]. It describes the precession of the magnetization M around an effective magnetic field H_{eff}.

Gilbert and Kelly added the damping term to the LL-equation that describes the damping in thin films [33]. This brought us Landau-Lifshitz-Gilbert (shortllg) equation, used to describe the magnetization dynamics:

$$\frac{\delta M(r,t)}{\delta t} = -\gamma M(r,t) \times H_{eff}(r,t) - \frac{\alpha}{M_a} M(r,t) \times \frac{\delta M(r,t)}{\delta t} \tag{2.10}$$

with the damping constant of the magnetization precession α. The effective field H_{eff} is given by summing up all effective field components.

2.2.7 Spin Hall Effect

The Spin Hall Effect (SHE) is a phenomena in which an out-of-plane spin current j_s is generated by an in-plane charge current j_e. The plane is polarized perpendicularly to j_e and the film. The Spin Hall Effect works as a strong damping-like torque acting on a magnetic layer.

$$\xi_{SH} m \times [m \times [m \times j_e] \tag{2.11}$$

where the constant $\xi_{SH} = \hbar\Theta_{SH}T_{int}j_e/(2|e|M_s\tau)$, T_{INT} stands for the coefficient of spin transparency [34] [8], and $\Theta_{SH} = j_s/j_e$ for the spin Hall angle, which characterizes the strength of the Spin Hall effect. The magnitude of the spin Hall pair is generally proportional to the thickness of the heavy metal, saturating as the thickness approaches the diffusion length of the spin λ.

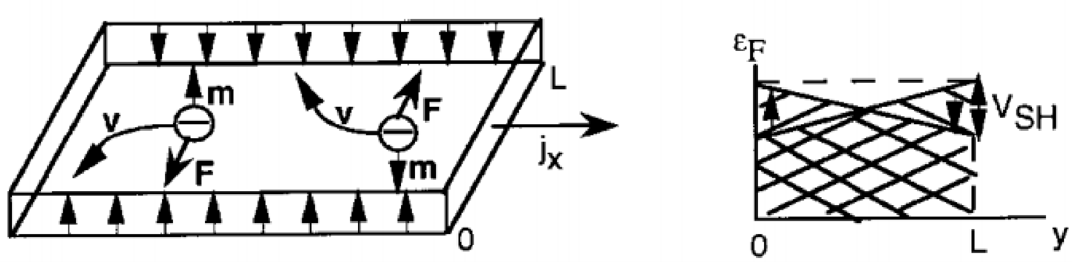

Figure 2.12: In the spin Hall effect skew scattering of the moving magnetic moments causes spin imbalance perpendicular to the current flow, taken from [8]

2.3 Skyrmions Technology

Skyrmions are named after Tony Skyrme, a nuclear physicist who developed a non-linear field theory for interacting pions.

Magnetic skyrmions are chiral spin structures with a whirling configuration (Figure [2.13]).

They are topologically protected and this means that their topological representation does not allow their complete deformation. This physically results into a particular stability compared to other magnetic textures such as vortices or bubbles[9].

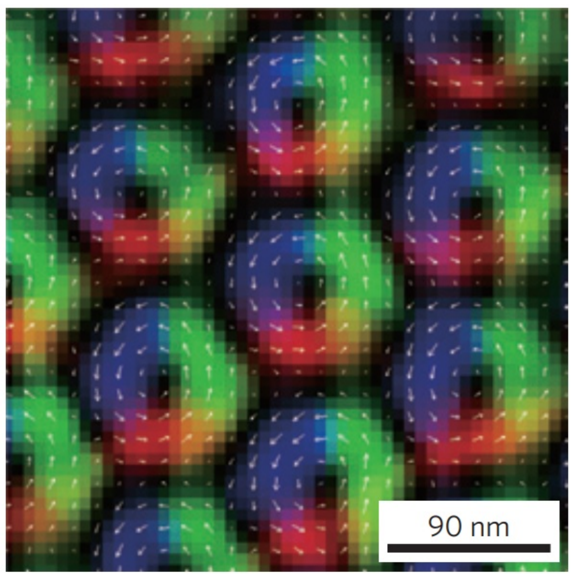

Figure 2.13: Lorentz microscopy image of a skyrmion lattice of Bloch-type skyrmions in $Fe_{1-x}Co_xSi$, taken from [9]

A skyrmion is characterized by three numbers: vorticity Q_v, the Pontryagin number Q_s and the the helicity Q_h [24].

Vorticity of a skyrmion (Q_v) is defined by the winding number of the spin configurations projected into the $s_x - s_y$ plane.

The skyrmion number Q_s can be evaluated by taking into account this Equation (2.12):

$$Q_s = -\frac{1}{4\pi} \cdot \int d_x d_y (m(r) \cdot (\delta_x m(r) \times \delta_y m(r))) \tag{2.12}$$

It is called a skyrmion when the Pontryagin number Q_s is positive otherwise it is called anti-skyrmions.

The helicity of a skyrmion(Q_h) is determined by the type of the Dzyaloshinskii-Moriya (DMI). A skyrmion with a helicity of 0 and π corresponds to the Neel-type skyrmion (See Figure [2.14 left]), while a skyrmion with a helicity of $\pi/2$ and $3\pi/2$ corresponds to the Bloch-type skyrmions(See Figure [2.14 center])[35]

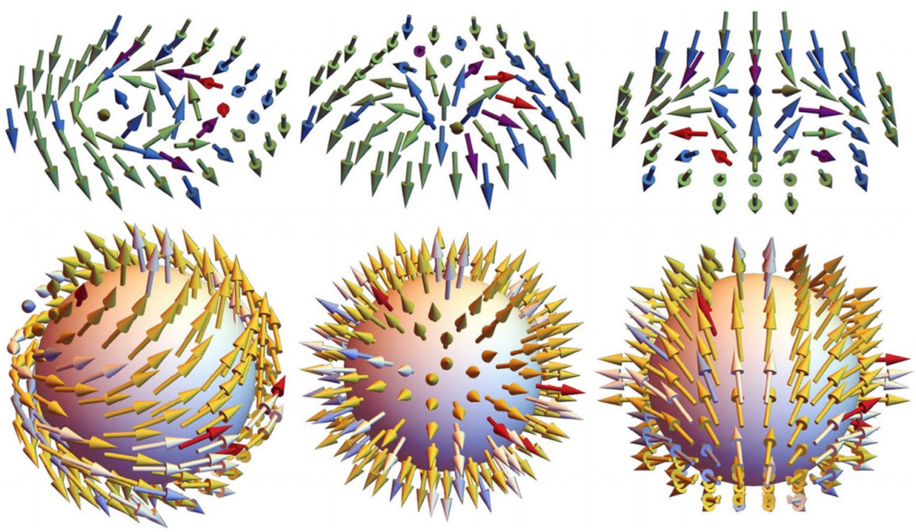

Figure 2.14: Bloch skyrmion (Top-left) and Neel skyrmion (Top-middle) have topological charge $Qs = 1$ and $p = 1$ (polarity). Antiskyrmion (Top-right) has topological charge $Qs = -1$. (Bottom) they move around a unit sphere upon application of stereographic projection. Figures extracted from [10]

Skyrmions originate from the chiral Dzyaloshinskii-Moriya interaction, Breaking simetry at the interface or in the lattice. The Hamiltonian of DMI between two atomic spins can be expressed in the Equation (2.13) [9]

$$H_{DMI} = -\vec{D_{12}} \cdot (\vec{S_1} \times \vec{S_2}) \tag{2.13}$$

the DMI at the interface provides 3-indirect sites and forms a triangle in presence of an ultra thin magnetic film. Between the nearby atom and the two atomic spins there is a strong SOC. This kind of interaction tends to promote a rotation of close magnetic moments. The DMI vector D_{12} is directed perpendicular to the plane of the triangle (Figure [2.15]) its maximum is reached when the two vectors are perpendicular to each other. This is different from the exchange interaction which encourages the alignment of close magnetic moments. [9].

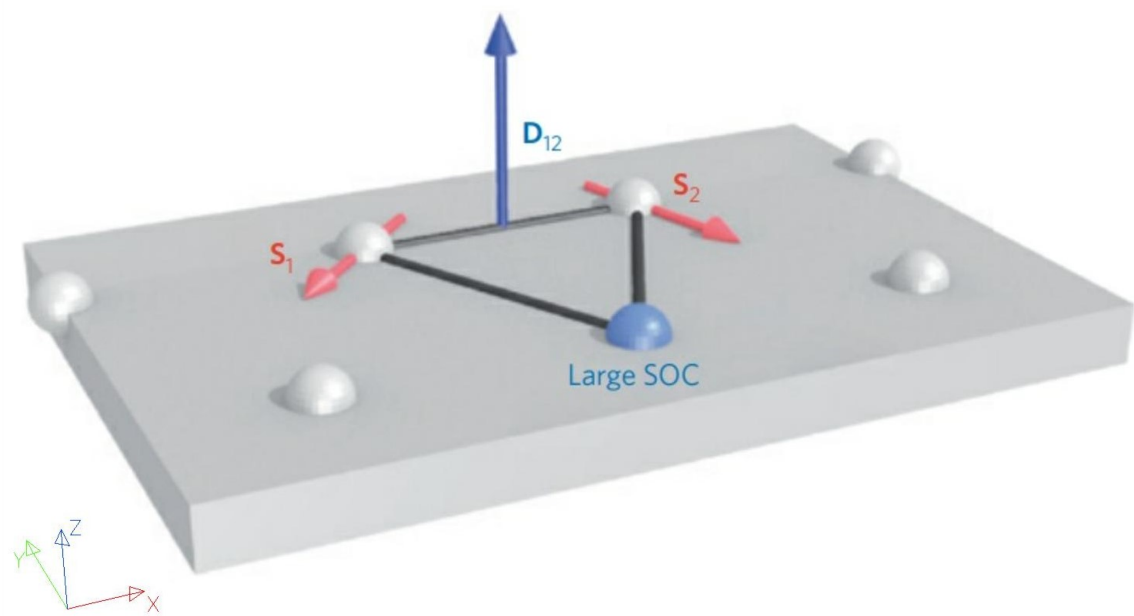

Figure 2.15: DMI generated by indirect exchange between the two atomic spins and an atom with a strong SOC, taken from [9]

The interface between a thin ferromagnetic layer and a metal with a strong SOC generates a DMI for the two atomic spins interfaces with the DMI vector D_{12} as in Figure [2.16] [9]

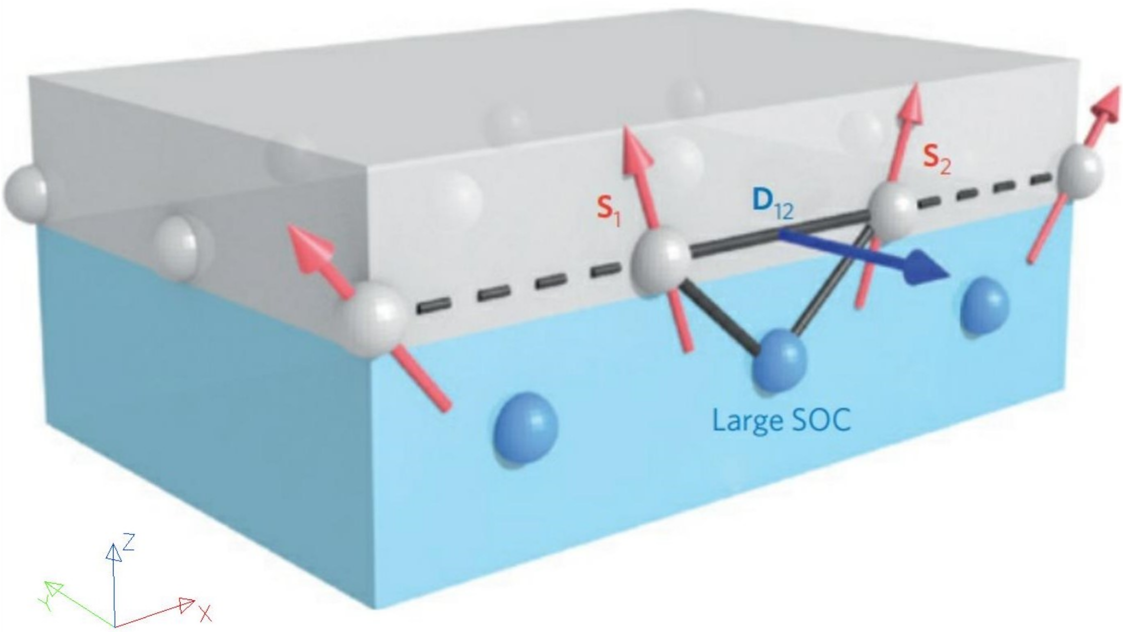

Figure 2.16: DMI at the interface between a FM (grey) and a metal with a strong SOC (blue). The DMI vector D_{12} is perpendicular to the plane of the triangle (composed of two magnetic sites and an atom with a large SOC), taken from [9]

The DMI module at the interface can be 10%-20% of the exchange interaction. Therefore, the energy is minimized by the Skyrmions structure when the material is ferromagnetic (uniaxial anisotropy) with non-negligible DMI.

2.3.1 Skyrmion creation and annihilation

Skyrmion creation can occur in several ways:

A skyrmion can be created by injecting an external electric current into the disk and employing the spin transfer torque (STT) [15] as shown in Figure [2.17] ,

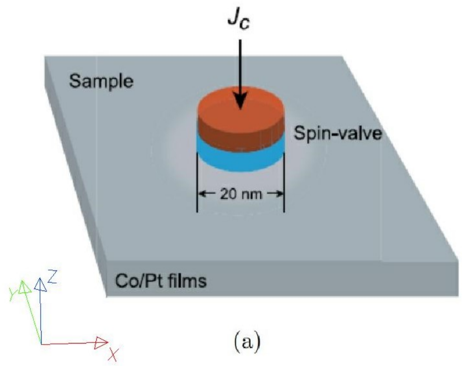

(a)

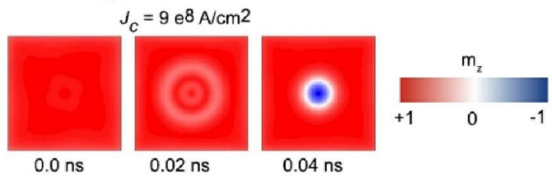

(b)

Figure 2.17: skyrmion creation by injection of an electrical current. (b) temporal progression of skyrmion creation under a current density of $J_c = 9 \times 10^8 A/cm^2$, taken from [11]

Skyrmions can also be obtained through the conversion of a Domain Wall (DW) [12]. The Domain Wall inside the nanowire is forced to leave the bottleneck if subjected to an external electric current (Figure [2.18.A]). There is a moment in this process in which its extremes are still anchored to the interfaces while its body continues to move. Finally a skyrmion is created (Figure [2.18.F]).

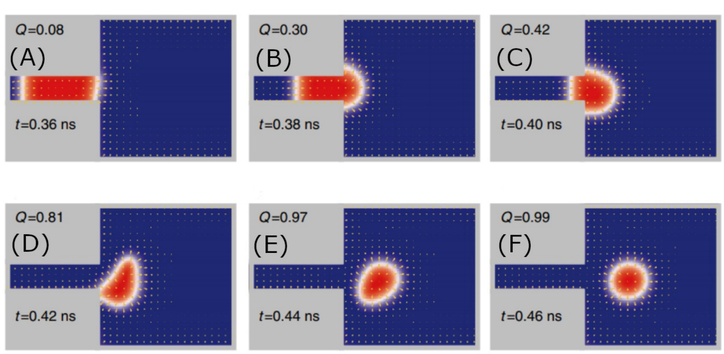

Figure 2.18: Domain Wall to skyrmion conversion, taken from [12]

Another method to create a skyrmion happens in a stripline-shaped system with a square notch structure (Figure [2.19]) [13]. the eclectic current flows, the spin transfer pair (STT) curve and the weft in the notch expands. This happens because of the presence of the DMI that causes the creation of the skyrmion.

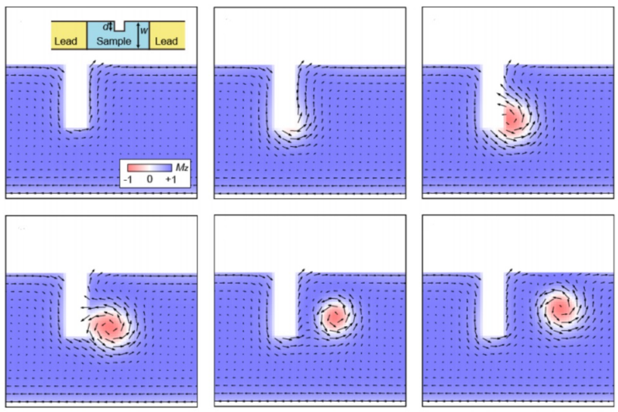

Figure 2.19: Nucleation of a skyrmion around a rectangular notch for $J = 3.6 \times 10^{11} Am^{-2}$, taken from [13]

Skyrmions can be annihilated by pushing it against the boundary under a driving current. This method can be seen in Figure [2.20] [36].

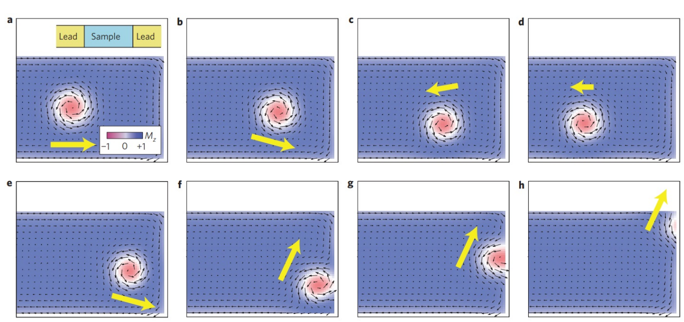

Figure 2.20: Dynamical spin configurations at selected times near the edge of the track for two different current densities j. The colour plot represents the z-components of the magnetic moments.A-D : $J = 1 * 10^{11} A/m^2$ E-H : $J = 3 * 10^{11} A/m^2$, taken from [13]

To annihilate a skyrmion avoiding the raise of current density, it is possible to modify the track geometry [14] by adding a triangular notch with a rounded tip at the end of the track (see Figure [2.21])

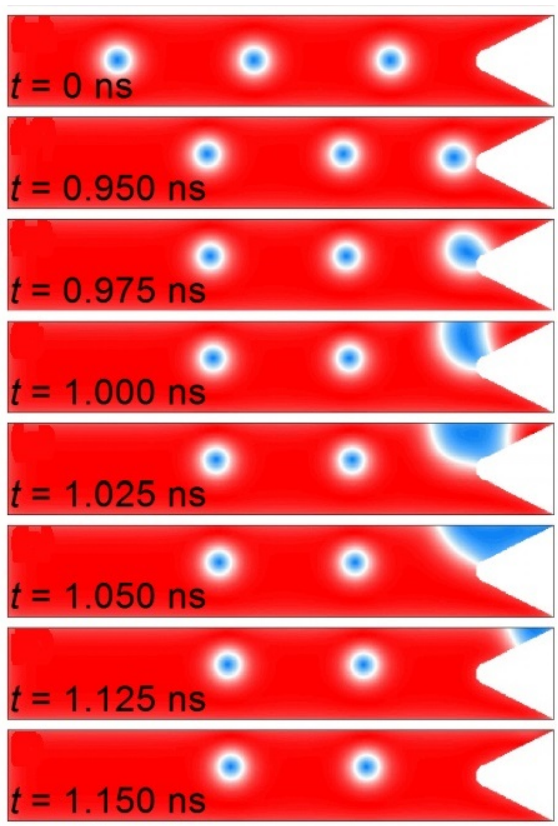

Figure 2.21: Motion of a skyrmions at the end of the racetrack with a notch. The current density is $J = 5 \times 10^{10} A/m^2$, taken from [14]

2.3.2 Skyrmion motion

Skyrmion moves if subjected to an electric current by means of Spin Hall Effect (SHE) or the spin Transfer Torque (STT).

Considering the STT [15], spin-polarized currents are injected into the ferromagnet, where an adiabatic and non-adiabatic induced spin transfer torque pair causes a rotation of the magnetic moment. As result the skyrmion moves with a horizontal speed of about $u\beta/\alpha$ [15] (u: proportional to the current density j, β : spin transfer torque non-adiabatic constant, α : damping constant) along the ferromagnet as shown in Figure [2.22].

Figure 2.22: Trajectory of a single skyrmion pushed by a vertical current $J = 5MA/m^2V = 57m/s$, taken from [15]

In Figure [2.23] can be seen the relationship between the current that induces the skyrmions to move and the ΔP_{xy} (deviation of the resistivity of the Hall effect) [13]. From this relationship the speed can be evaluated.

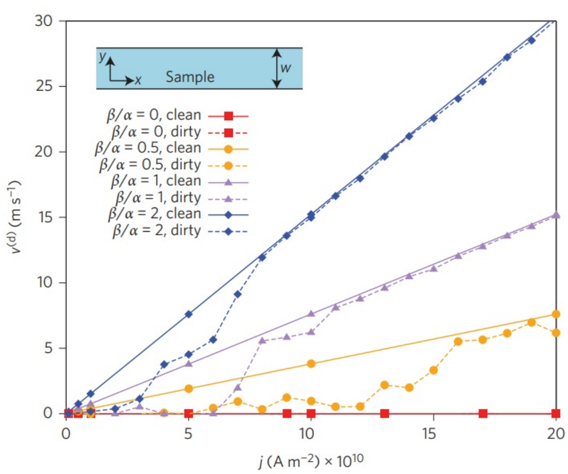

Figure 2.23: The graph represent the velocity of current-induced motion of a skyrmion. Drift velocity $V(d)$ is a function of current density j for several values of β/α, taken from [13]

regarding the values reported in Figure [2.23] above and in literature [13], two important comments can be made :

1. To move a skyrmion is needed less current than that needed to move a plain Domain Wall.

2. Once the minimum threshold of current that allows Domain Wall movement has been exceeded, skyrmions and DW move at the same speed if subjected to the same current.

The difference is in the deepening current j_c which is smaller in skyrmions.

2.3.3 Skyrmion detection

To detect a skyrmion is necessary to take into account the Hall Effect (THE) or the magnetoresistance effect [37]

The detection can be performed thanks to the effect of the tunnel magnetoresistance at room temperature The sensing device is composed by a heavy metal layer (HM), which is used to obtain high levels of DMI and of Spin Hall Effect (SHE). Ferromagnetic layers are used as a base for MTJ deposition [16] (Figure [2.24]).

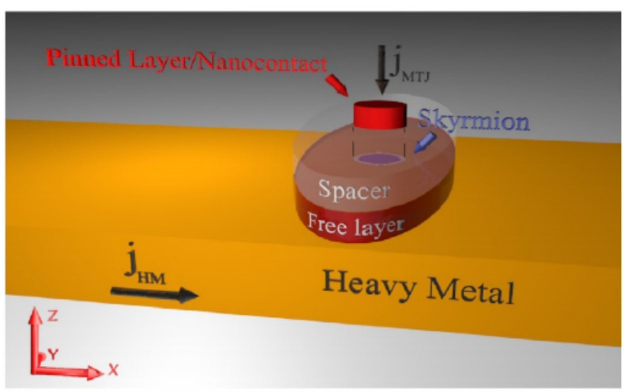

Figure 2.24: Schematic of the device, taken from [16]

An electric current is spin-polarized if it passes through a ferromagnetic layer with fixed magnetization. the density of states (DOS) of a ferromagnetic metal is different from the DOS of a normal metal. The electrons injected into the ferromagnetic perceive different value of resistivity based on their spin [16] (Figure [2.25]):

the spin-down electrons have a greater resistivity ($\rho \uparrow$) compared to spin up electrons ($\rho \downarrow$).

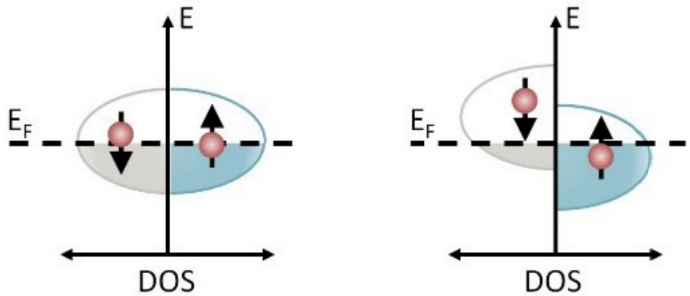

Figure 2.25: Representation the density of states at the Fermi level in a metal (left) and in a FM (right). The density of states at the Fermi level is unbalanced for the two branches, taken from [16]

2.3.4 Skyrmions logic gates

skyrmions have several properties such as low deepening current density, small size, low power dissipation and versatility that enables them to carry out different tasks like for example duplication and logic functions.

Skyrmion Logic [17] is based on particular gates visible in Figure [2.26] and Figure [2.27]. It can be defined as "conservative", because the number of skyrmions in the output is the same of the one in the input every time an operation is performed. This is a huge advantage because it reducing energy consumption.

There are two different basic logic functions: AND/OR (figure [2.26]) and INV/-COPY (figure [2.27]).

The Spin Hall Effect pushes the skyrmions towards the $+y$ direction and generates an x direction force which is opposed by the repulsive effect of the track edges (Figure [2.26]) [17]. This phenomenon occurs when A = 0 and B = 1, for this reason the right exit of the gate stands for AND function and the left exit stand for OR function.

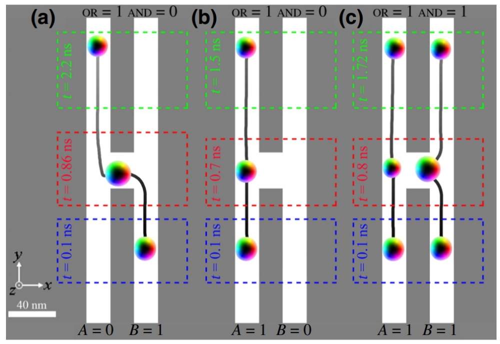

Figure 2.26: Simulation of conservative AND/OR logic gate with input combinations (a) A = 0 B = 1, (b) A = 1 B = 0 and (c) A = B = 1, taken from [17]

The INV/COPY gate provides the result of a basic NOT gate (Figure [2.27]) [17]. So this structure has two inputs: IN, which is the entrance to be denied and CTRL, which enables the gate to work thanks skyrmion-skyrmion repulsion. The INV/COPY gate provides two additional output: the left (COPY1) and the right (COPY2) that duplicate the skyrmion IN.

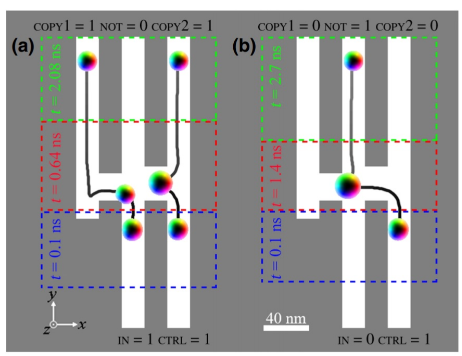

Figure 2.27: Simulation of conservative INV/COPY logic gate with input combinations (a) IN = 1 CTRL = 1, (b) IN = 0 CTRL = 1, taken from [17]

Besides these two logic gates, in the Article [17] a synchronization mechanism is described (Figure [2.28]). This element functioning depends on the current injected : if this value is under than the threshold, the skyrmion stops permanently; if the current is above the threshold the skyrmion reduces its size and overcomes the notch element.

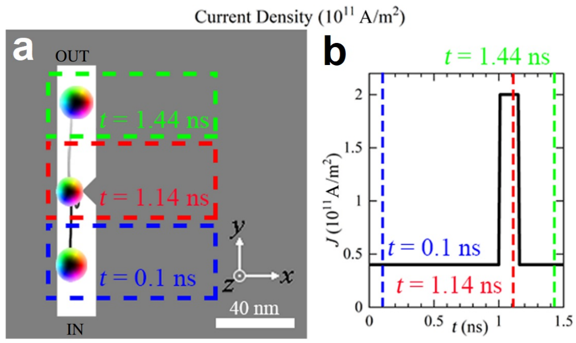

Figure 2.28: (a) Simulation of notch element and (b) electrical current injected, taken from [17]

2.4 PNML Technology

2.4.1 Domain Wall Logic

Domain Wall Logic (DWL) is a magnetic logic that uses domain walls propagation to perform operations [38]. Here, logic operations are carried out by the external rotating magnetic field by means of geometric gates.

However, these devices seem to be unsuitable as technology beyond CMOS because of the sensitivity to geometric imperfections.
The application of magnetic materials with PMA brought interest to both DWL and DW based memory devices [39].

2.4.2 Perpendicular Nanomagnetic Logic (pNML)

The imminent end of scaling of conventional CMOS technology has increased the research on magnetic logic devices (iNML and pNML).

The milestone of pNML evolution is the demonstration of the majority gate (made of Co/ Pt with PMA)[19]. Thanks to the majority gate a 1-bit full adder has been experimentally demonstrated [18].

The pNML has been included in the ITRS (chapter for Emerging Research Devices) as an individual device technology [40].

In Figure [2.29] is shown an integrated pNML system with all its logic parts for digital computing: electrical input / output devices and on-chip clock structures.

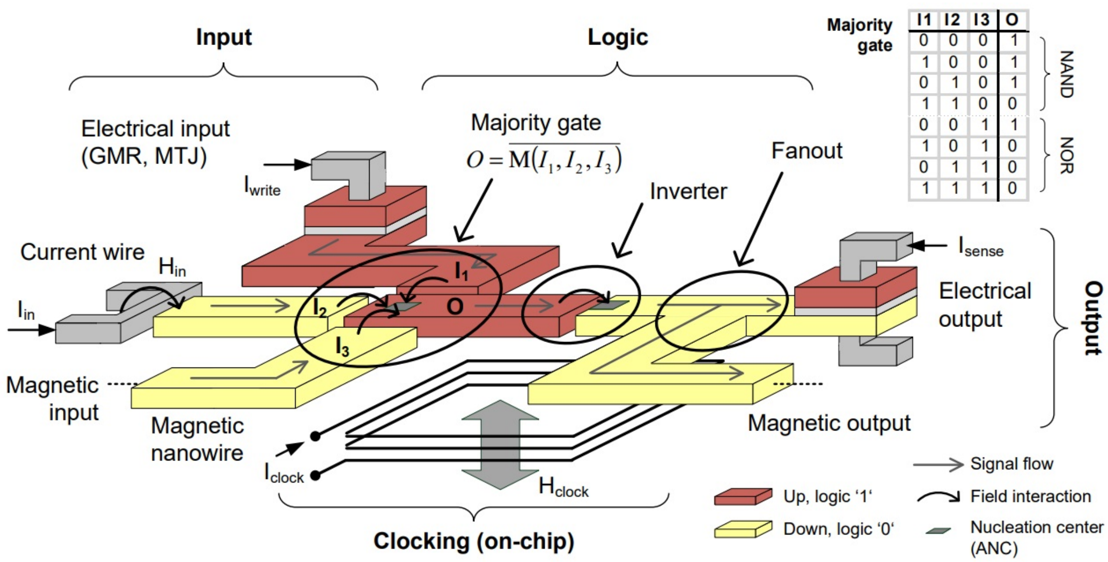

Figure 2.29: Integrated pNML system: Majority gates, inverters and fan out structure that provide logic computation, taken from [18]

2.4.3 Basic working principle

The pNML uses nanomagnets with PMA, which interact by antiferromagnetic coupling [41]. Due to PMA, the magnet has only two possible state that encodes the data: logic ”1” (magnetization up) or logic ”0” (magnetization down).

The commutation of the magnet is composed of two phases: the first starts with the Domain Wall nucleation at the weakest point of the magnet; The second one the Domain Wall propagates through the entire magnet to reverse it. To establish artificial nucleation center (ANC) the PMA is locally reduced by irradiation FIB.

The magnet (output) is sensitive to near magnets (inputs) [42]. The energy necessary to switch the magnets is given by the perpendicular external magnetic field [43].

2.4.4 Digital logic computation

To enable logic operation, the external magnetic field induces Domain Wall nucleation in the ANC. During this process the external magnetic field is strengthened or weakened by the overlapping frontal fields of the input magnets that depends on their magnetization state [19]. The inverter is the most simple logical element. The coupling field between close magnets allows to reverse the output magnetization as function of the input magnetization [18].

The majority gate is the fundamental computing element for logic operation (see Figure [2.30]). The ANC of the output magnet is surrounded by at least three magnet inputs whose overlapping fringe fields strengthen or prevent Domain Wall Nucleation (depending on most input states) [19].

the majority gate provides the basic logic operations NAND and NOR setting the states of the input (e.g. I3): '0' stands for O = NAND (I1, I2) and '1' stand for O = NOR (I1, I2).

The Domain Wall propagation uses magnetic nanowires as interconnections between successive logic gates [18]. When a magnet switches, it assumes the function of input for subsequent gates. Therefore, the information movement is synchronized with the oscillating external field [44]. If it is necessary to drive more than one output (fan out) structures, the magnetic nanowire can be splitted into multiple branches [45].

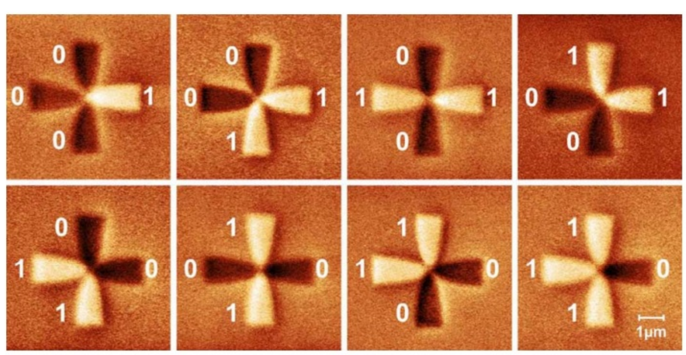

Figure 2.30: MFM images of the majority gate for all configurations. The output is the right magnet while the other are the input, taken from [19]

2.5 Logic in Memory

Nowadays, most of all computer systems are based on the Von Neumann paradigm, which is characterized by the data exchange between a central processing unit (CPU) and a memory. The CPU executes operations and stores the results in memory.

CPU and memory speed influences the data exchange mechanism. However, CPU speed performance has increased much more than memory one, causing a ”bottle-neck” [46].

To overcome these limits, an alternative architecture has been studied. The main advantages of the Logic-in-Memory architecture (LiM) are:

1. solving the problem of bottleneck because it brings the calculation directly into the memory.
2. reducing the amount of memory accesses and the energy consumption because there is no data exchange between CPU and storage.

2.5.1 In Memory Architecture

In-memory architecture is composed of four different categories [20]:

(A) **Computation-near-Memory** - Logic and storage are two structures close to each other and the data exchange between them occur by using 3D stacked integration technologies [47]. The advantages of this approach are the short distance of the interconnects and the length of memory bandwidth (See Figure [2.31.A]).

(B) **Computation-in-Memory** - the structure does not change but its analogical functionality is used to perform calculations. In particular, these operations are obtained by taking the data from the memory file [48] (detected by sense amplifier) where the results are rewritten (See Figure [2.31.B]).

(C) **Computation-with-Memory** - the memory in this approach is seen as a Content Addressable Memory (CAM) file, which takes the data from a lookup table (LUT) [49] (See Figure [2.31.C]).

(D) **Logic-in-Memory** - the memory processes data exploiting full bandwidth. This kind of architecture allows to reduce the amount of memory accesses and power consumption [50] (See Figure [2.31.D]).

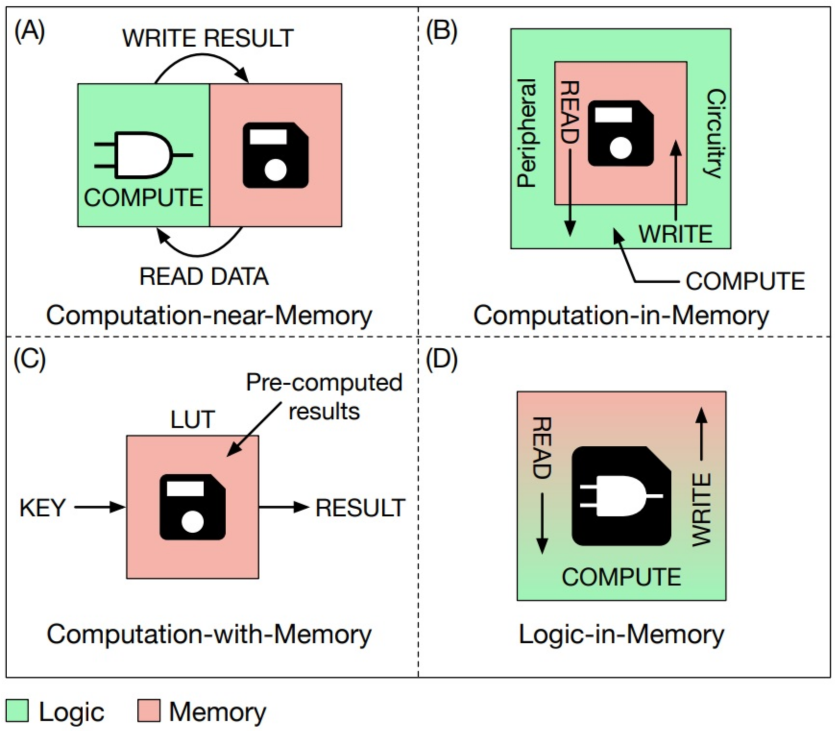

Figure 2.31: (A) Computation-near-Memory (CnM), (B) Computation-in-Memory (CiM), (C) Computation-with-Memory (CwM), (D) Logic-in-Memory (LiM), taken from [20]

2.5.2 Technologies supporting LiM architecture

pNML

In pNML technology, magnets with with perpendicular magnetic anisotropy (PMA) are used [21].

Logic-in-Memory architecture can be implemented thanks to the monolithic 3D integration of pNML [51]. In Figure [2.32] is shown an implementation of a 2-bit adder.

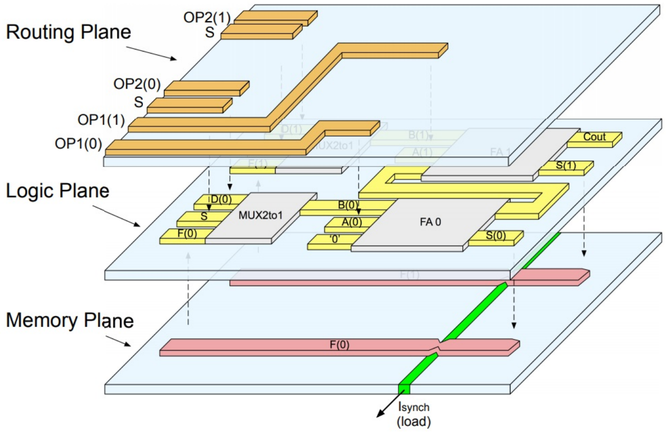

Figure 2.32: Representation of a 2-bit adder exploiting the monolithic 3D integration of pNML technology, taken from [21]

MTJ

A Logic-in-Memory architecture based on the combination between the magnetic tunnel junction (MTJ) and MOS transistors has been proposed in Article [22]. MTJ is able to full exploit the logic-in-memory architecture thanks to its properties such as low access time and small size.

In Figure [2.33] the general structure of this logic-in-memory circuit is described: cross-coupled keeper (CCK) provides binary outputs (z and z'), a dynamic current source (DCS) interrupts the constant current flowing from VDD to GND and a logic circuit tree that can be modified to obtain the logic function desired. Figure [2.34] shows a full adder as possible application of this architecture.

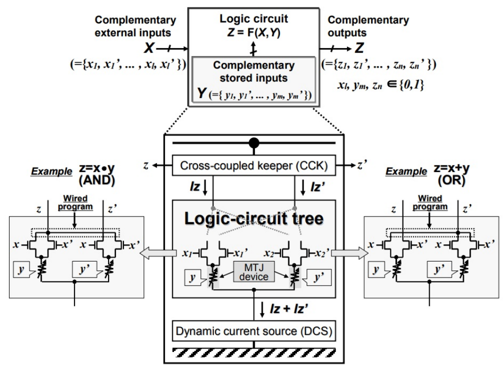

Figure 2.33: General structure of an MTJ-based logic-in-memory circuit, taken from [22]

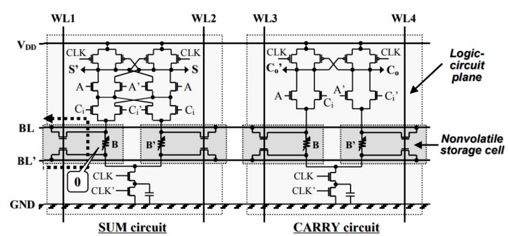

Figure 2.34: Full adder based on MTJ logic-in-memory architecture, taken from [22]

The logic-in-memory technology allows the reduction of static power consumption and chip area. The MTJ write time is one of the most important elements, because it predominates the write energy when updating the inputs. In the Table [2.1] is shown a comparison with a CMOS architecture.

	CMOS	Proposed
Delay	$224ps$	$219ps$
Dynamic power (@500Mhz)	$71.1\mu W$	$16.3\mu W$
Write time	$2ns/bit$	$10ns/bit(2ns/bit)$
Write eneergy	$4pJ/bit$	$20.9pJ/bit(6.8pJ/bit)$
Static power	$0.9nw$	$0.0nW$
Area (Device counts)	$333\mu m^2(42MOS_s)$	$315\mu m^2(43MOS_s + 4MTJ_s)$

Table 2.1: Comparison between CMOS-based and the MTJ-based full-adder architecture, taken from [22]

2.6 Tool : Mumax3

MuMax3 is a micro magnetic simulation program (GPU-accelerated). It calculates the magnetization dynamics in ferromagnets employing a finite difference (FD) discretization [23].

2.6.1 Material Regions

MuMax3 divides the structure with a 3D grid of cells. Volumetric quantities (like the magnetization and effective field) are treated at the center of each cell, while coupling quantities (like the exchange strength) are treated on the surface between the cells (See Figure [2.35])

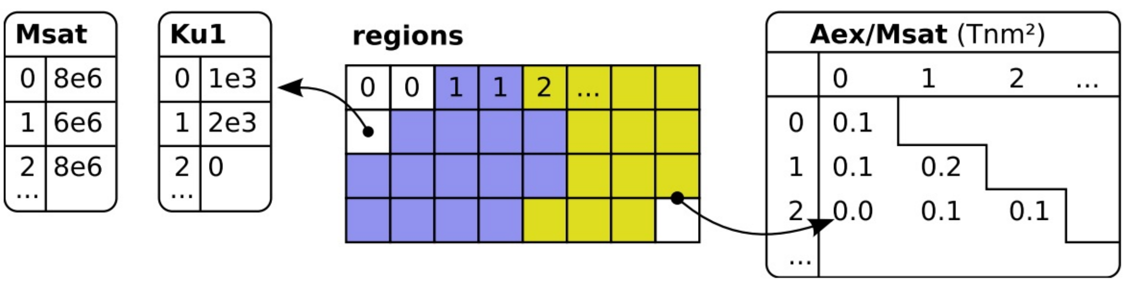

Figure 2.35: Each simulation cell is attributed a region index representing the cell's material type, taken from [23]

2.6.2 Dynamical Terms

MuMax3 estimates the evolution of the reduced magnetization $\vec{m}(\vec{r},t)$. Referring to the derivative time of $\vec{m}$ as the torque $\vec{\tau}$ (units $1/s$):

$$\frac{\delta \vec{m}(\vec{r},t)}{\delta t} = \vec{\tau} \tag{2.14}$$

$\vec{\tau}$ has three contributions:

- Landau-Lifshitz torque $\vec{\tau}_{LL}$

- Zhang-Li spin-transfer torque $\vec{\tau}_{ZL}$
- Slonczewski spin-transfer torque $\vec{\tau}_{SL}$

2.6.3 Energy minimization

MuMax3 offers a relax() function necessary to find the energetic minimum of the system. This function disables the precession term of the Landau-Lifshitz torque equation. This function is like any other energy minimization technique in fact, there is the possibility that the system fall in a saddle point or very flat part of the energy curve.

2.7 Motivation

Skyrmions are great at transporting and storing data thanks to their compact shape and small size.

Unfortunately, skyrmions are not as good as pNML at carrying out logical operations. The ”Majority gate” allows the pNML to carry out complex logic operations.

This is the reason why the two technologies have been hybridized in order to obtain the advantages of both. it is possible by exploiting the versatility and speed of movement of the Skyrmions and the computing power of the pNML.

Skyrmions are used as a seed to construct valid data in pNML.

The starting point of this hybrid system is the structure presented in the article [24] (See Figure [2.36]), where Skyrmions to Domain wall conversion is described (used only for skyrmions duplication otherwise difficult).

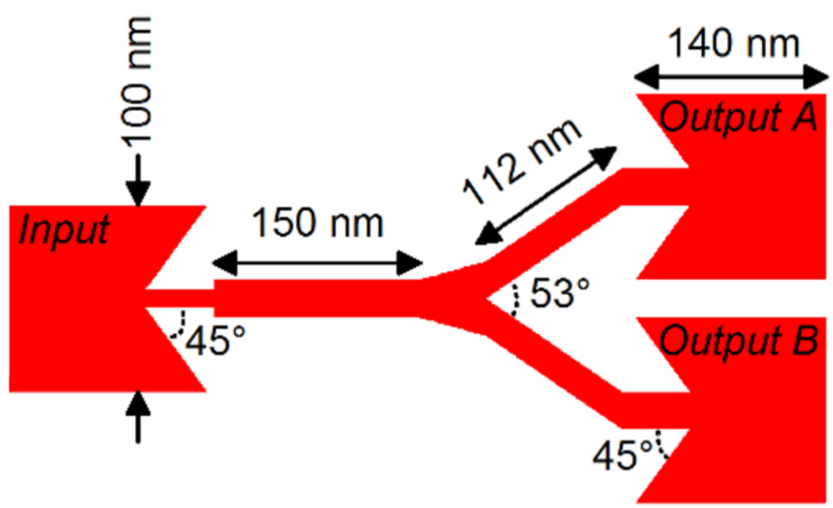

Figure 2.36: Skyrmion duplication block, taken from [24]

The aim is to insert one or more stages of pNML logic between one conversion and the other in order to create a central processing unit as shown in the Figure

[2.37]

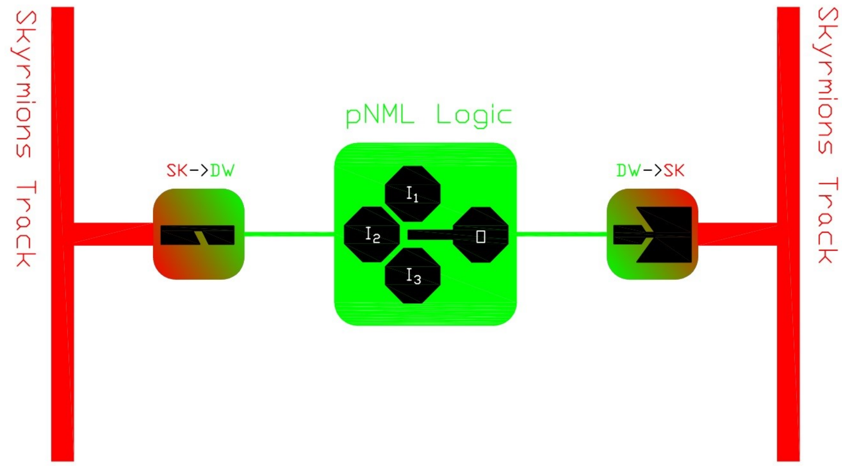

Figure 2.37: Complete hybrid System

In this way it can be inferred of having vertical Skyrmions tracks, which act as interconnections between the processing units and T-shaped intersections that indicate the inputs to the processing units.

Therefore the processing will take place in several steps :

1. The Skyrmion comes along the Skyrmions Track (RED).
2. Skyrmion is converted to Domain Wall pair (RED-GREEN)
3. The Domain Wall pair propagates up to the pNML logic (GREEN)
4. The pNML logic performs the calculations in multiple loops (GREEN)
5. The result is propagated in Domain Wall pair form to the DWtoSK converter(GREEN)
6. The Domain Wall pair is converted to Skyrmion (GREEN-RED)
7. The Skyrmion is again on a Skyrmions track ready to return to the memory or to enter in another processing unit (RED)

2.7.1 Material

To create this type of system, particular attention was given to the different needs of Skyrmions and Domain Wall, in particular the thickness of the material which in this case is a C_oP_t.

The ideal thickness for skyrmions is the Singlelayer of C_oP_t with a total thickness of $1.8nm$. In this way, compact skyrmions are able to move along tracks $50nm$ wide, at about $40m/s$ speed. Otherwise, if materials with a greater number of Layers are used, the Skyrmions maintain stability even with a larger diameter and all the problems that it causes.(See Figure [2.38])

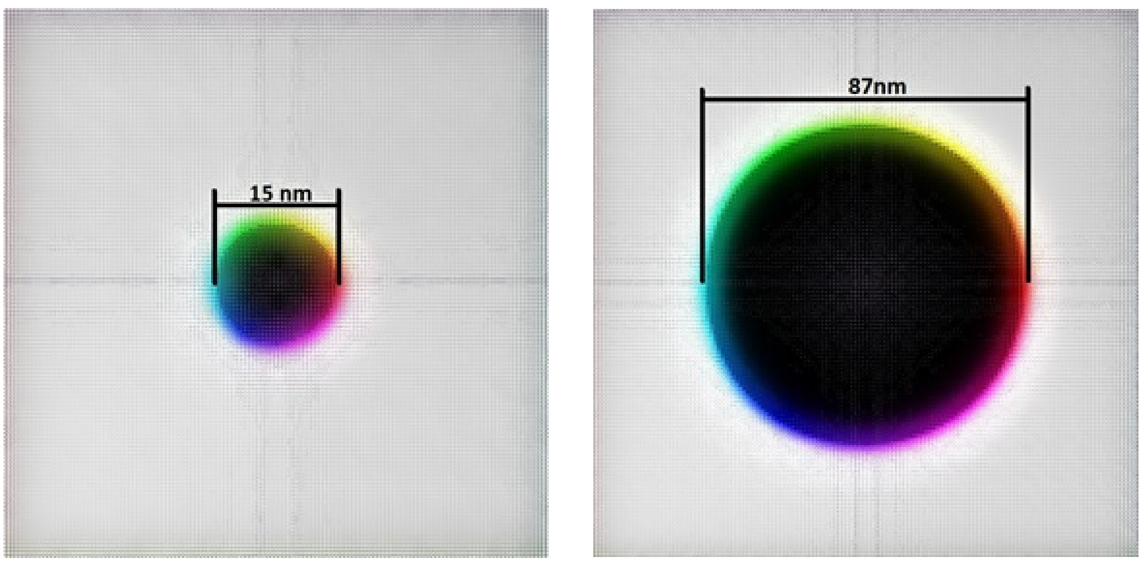

Figure 2.38: On the left a Skyrmions stable on a singlelayer material with a diameter of approx $15nm$, on the right a stable Skyrmions in a Multilayer Material with a diameter of approx $87nm$, result obtained with MuMax3

The pNML works more efficiently in the case of multilayer structures which have an higher saturation magnetization and a much greater coupling field than in the singlelayer case.

Therefore it can be said that the two technologies tend towards opposites (See Figure [2.39]) and a crossroads already shows itself at the beginning:

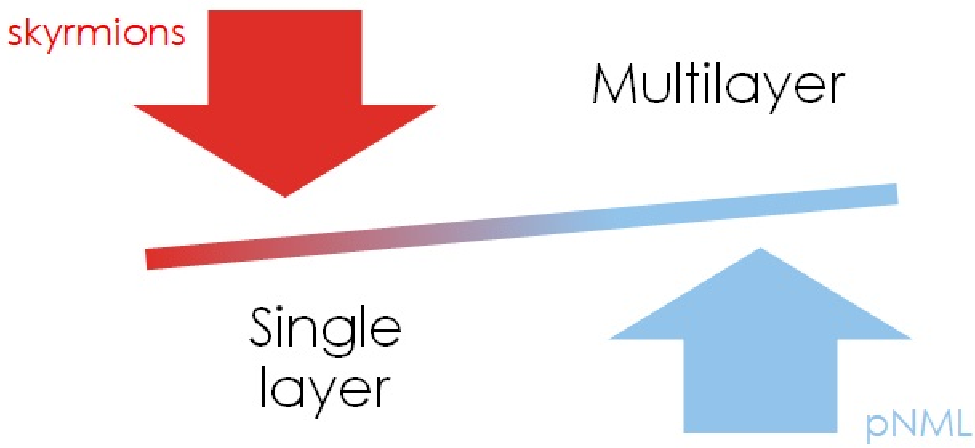

Figure 2.39: Skyrmions & pNML Singlelayer Vs Multilayer

- **Option 1**: find a trade off, therefore a thickness that is acceptable for both technologies and that allows correct operation.
- **Option 2**: making Skyrmions work in Singlelayer and pNML in Multilayer so that both can give their best in all conditions.

The second way has been chosen by studying various methods to make the transition from Singlelayer (on which the Skyrmions will move) to Multilayer (Where the pNML will operate).

Chapter 3

Structure

In this chapter, the main geometries that have been studied are presented.

In particular, the structures which have best returned positive results and finally enabled a complete demonstration structure to be carried out.

All the simulations shown below refer to the Mumax3 simulator and the physical parameters are set as you can see in the table 3.1. All currents are applied

Name	Symbol	Value	Unit
Saturation magnetization	M_{sat}	5.8	$[A/m]$
Exchange stiffness	E_{ex}	1.5e-11	$[J/m]$
Landau-Lifshitz damping constant	α	0.1	
Interfacial Dzyaloshinskii-Moriya strength	D_{ind}	3e-3	$[J/m^2]$
Electrical current polarization	Pol	0.6	
Non-adiabaticity of spin-transfer-torque	Xi	0.35	
Slonczewski Λ parameter	Λ	1	
first order uniaxial anisotropy constant	K_{u1}	6e5	$[J/m^3]$

Table 3.1: Result of Simulation skyrmion under external magnetic field with $T = 0K$

to give a spin current J_s out-of-plane, while the external magnetic field is always applied along Z.

in particular, the structures in this chapter are :

- **3.1 - Input Stage**: the block that allows Skyrmions to Domain Wall Pairs conversion, also identified as $Sk- > DW$.
- **3.2 - Output Stage**: the block that allows Domain Wall Pairs to Skyrmions conversion, also identified as $DW- > Sk$.

- **3.3 - SingleLayer to MultiLayer**: the block that allows to move the Domain Wall from Singlelayer material to Multilayer material.
- **3.4 - MultiLayer to SingleLayer**: the block that allows to move the Domain Wall from Multilayer material to Singlelayer material.
- **3.5 - Inverter**: The most simple pNML logic element tested to ensure that it is fully match with Multilayer-Singlelayer and Multilayer-Singlelayer converters.

3.1 Input Stage

The input stage or conversion stage from Skyrmions to Domain Wall Pairs conversion is very similar to the one realized in the article [24] and visible in the Figure [2.36]. The main difference is that it was reduced in size and adapted to the width of the skyrmions track 50nm wide. Of course, as previously specified, it is tightly a SingleLayer structure (See Figure [3.1])

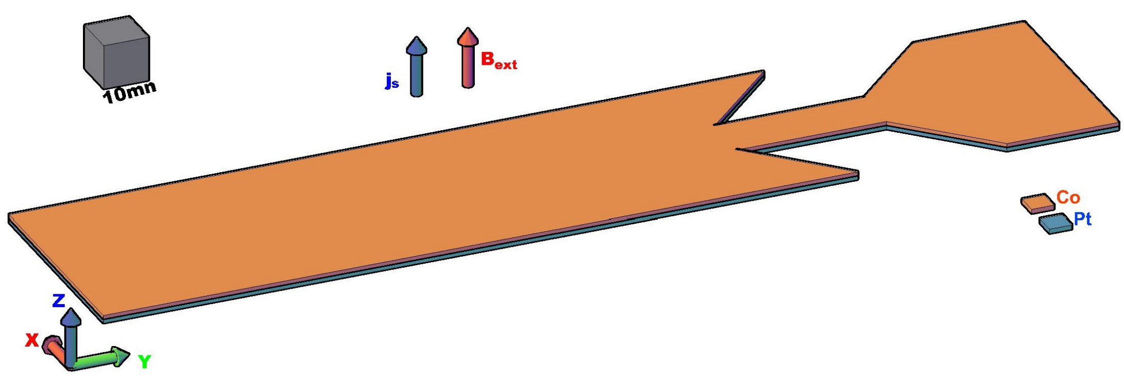

Figure 3.1: Input Stage V1 SingleLayer

The structure is very simple and it can be divided into three parts to make an analysis :

- **First part**: This part of the structure is a simple Skyrmions Track subjected to a constant current density(z axis). It allows the skyrmion to move forward towards the central part, magnetically isolated from the external sinusoidal magnetic field, to avoid to deform the skyrmion(See Figure [3.2.A-C]).

- **Central part**: In this section there is a sharp bottleneck. Once the skyrmion is pushed against this central corridor narrower than the track, it changes its shape and is converted into a DW enclosed in this corridor. It will move out of the central corridor only to the next negative front of the magnetic clock and it will begin to propagate in the third Region of the Structure. The two lateral spaces next to the central corridor are used to erase any possible residue left by the skyrmions after the collision against the central channel to avoid unwanted nucleation(See Figure [3.2.C-E]).

- **Final Part**: Has always the size of the skyrmions track but in this case it is not subjected to constant current density but to the external sinusoidal magnetic field that allows the propagation of DW coming from the Central Region (See Figure [3.2.E-F]).

Then, after careful studies we realized that the skyrmion subjected to a constant current density is helped to move towards one of the two walls. As a result it is preferred to put the bottleneck (where the skyrmions becomes a Domain Wall pair by splitting itself) on one of the side walls Figure [3.3]. This structure works in the same way as the previous one shown in Figure [3.1]. In this case the chance for the skyrmion to hit the bottleneck has increased to 100%, as you can see in the extract of the simulation shown in the Figure [3.4].

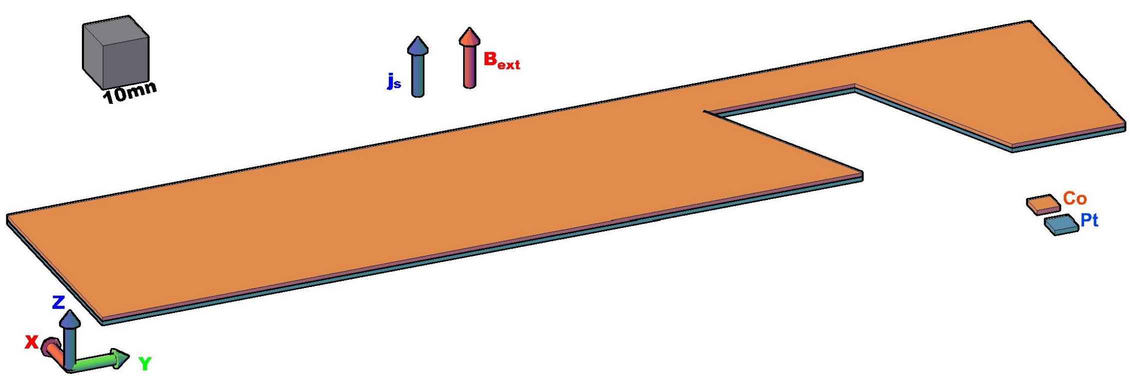

Figure 3.3: Input Stage V2 SingleLayer

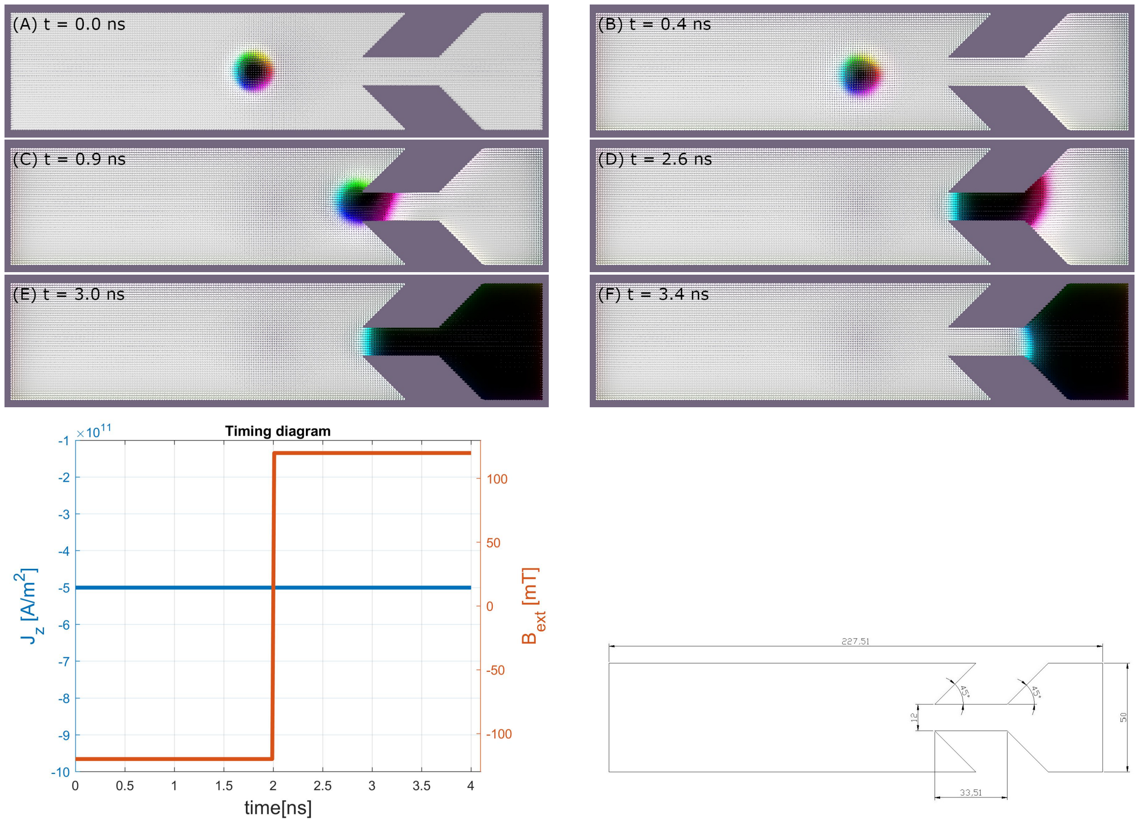

Figure 3.2: Simulation of Input Stage V1, A-C :$J_z = -5e11 A/m^2$, D-E :$B_{ext} = -120 mT$, F :$B_{ext} = 120 mT$, timing diagram (bottom), result obtained with MuMax3

In this way, the problem of centering the skyrmion with the bottleneck has been solved, since it aligns with the new position by itself.

3.1.1 Input Stage with T = 300K

It is possible to introduce in the micromagnetic simulator (MuMax3) a temperature contribution higher than absolute 0, in particular the room temperature T = 27°C (T= 300K). Therefore, it has been decided to carry some simulations out to see how the input stage reacts to the increase of temperature.

Regarding the V1 version (See Figure [3.1]), it has been immediately realized that being able to center the skyrmion, would have been very difficult. In fact, it has a

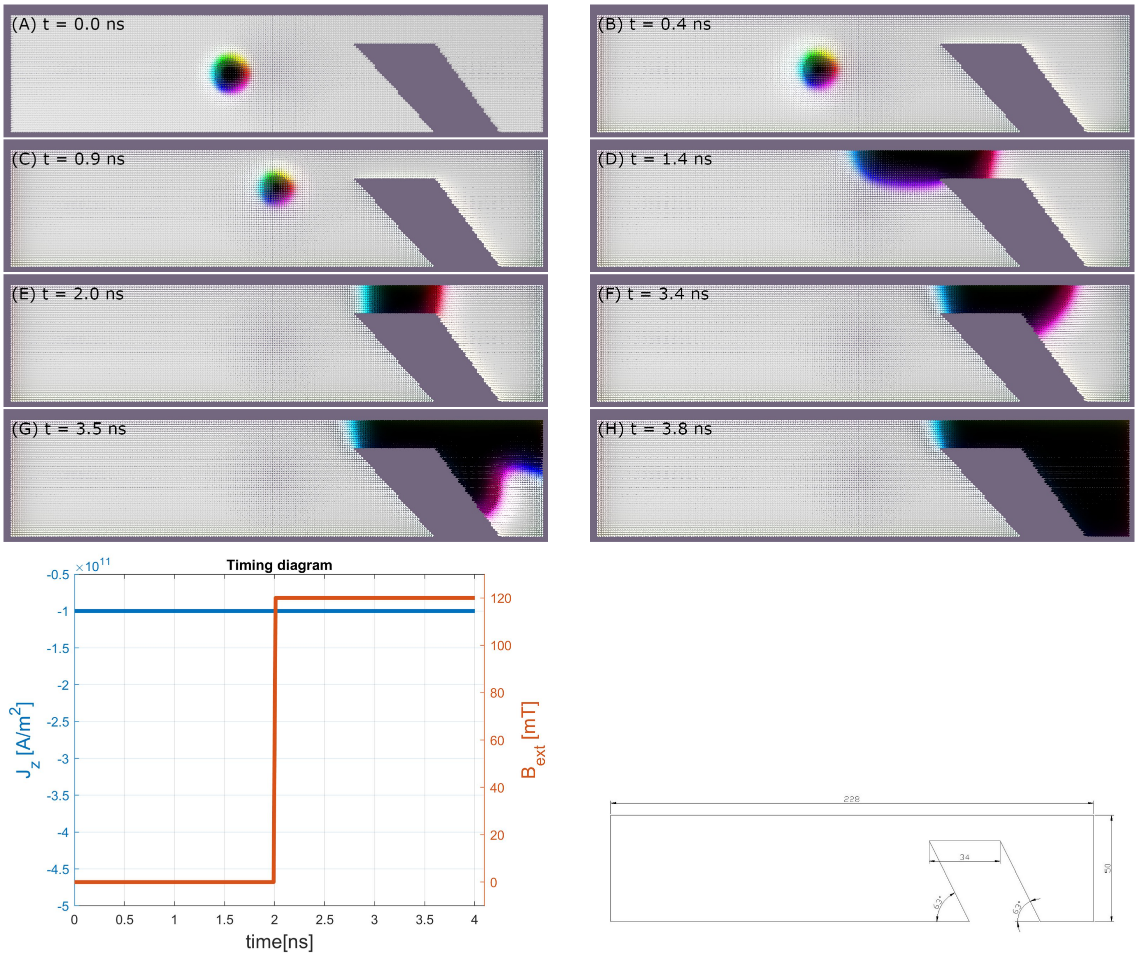

Figure 3.4: Simulation of Input Stage V2,$J_z = 1e11A/m^2$,$B_{ext} = 120mT$, timing diagram (bottom), result obtained with MuMax3

less defined shape and tends to slightly oscillate because of the temperature.

Regarding the structure V2 (See Figure [3.3]), the self-alignment of the skyrmion with the channel allows the conversion also with a higher temperature. So it is possible to make the stage work as you can see in the extract of the simulation shown in the Figure [3.5].

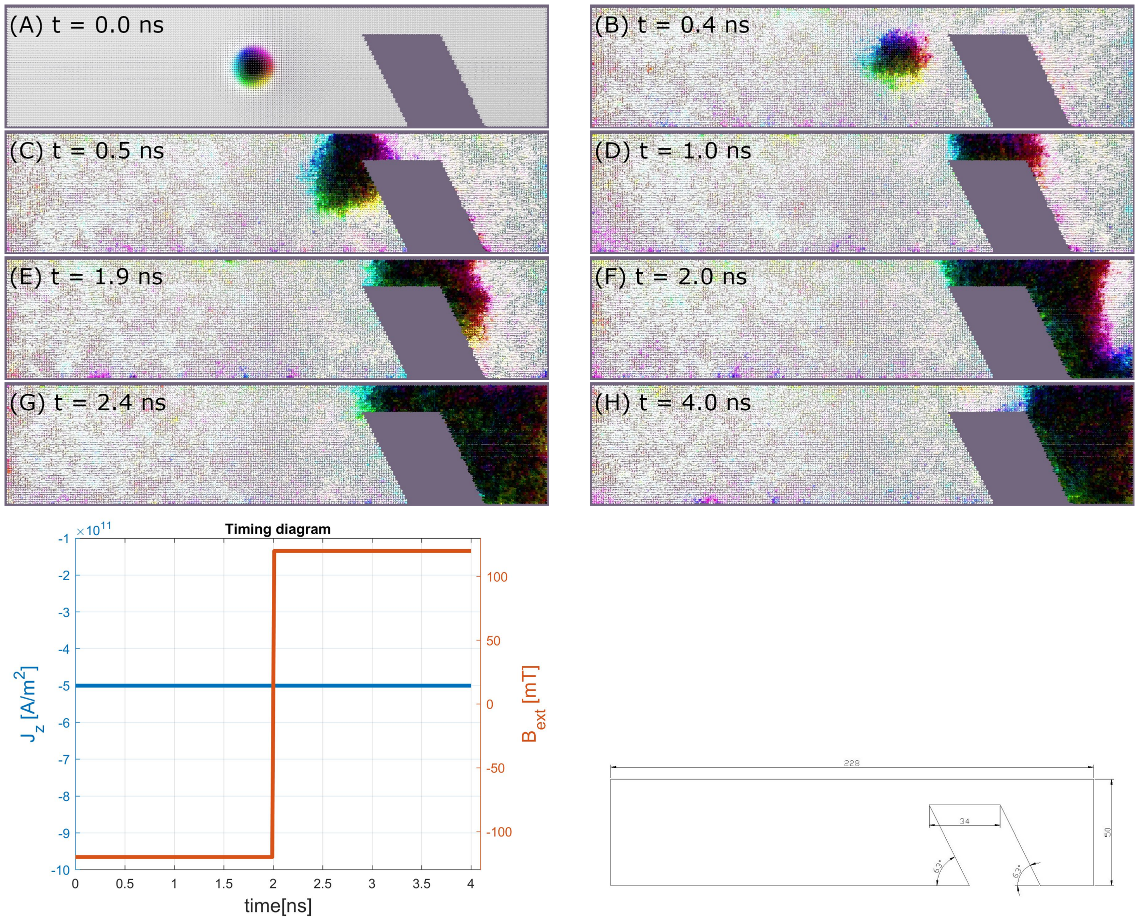

Figure 3.5: Simulation of Input Stage V2, $T = 300K$, A-E $:J = -5e11A/m^2$, F-G $:B_{ext} = -120mT$, H $:B_{ext} = 120mT$, timing diagram (bottom), result obtained with MuMax3

3.1.2 Realistic Input Stage

The structure seen so far as Input stage is very convenient because it can be easily integrated. The aim of these simulations is to test the integration of the structure in a system and how the skyrmion can be directed within the block.

In fact, a T-intersection is required (as shown in the Figure [3.6]) to create a system like the one shown in Figure [2.37] and described in section 2.7.

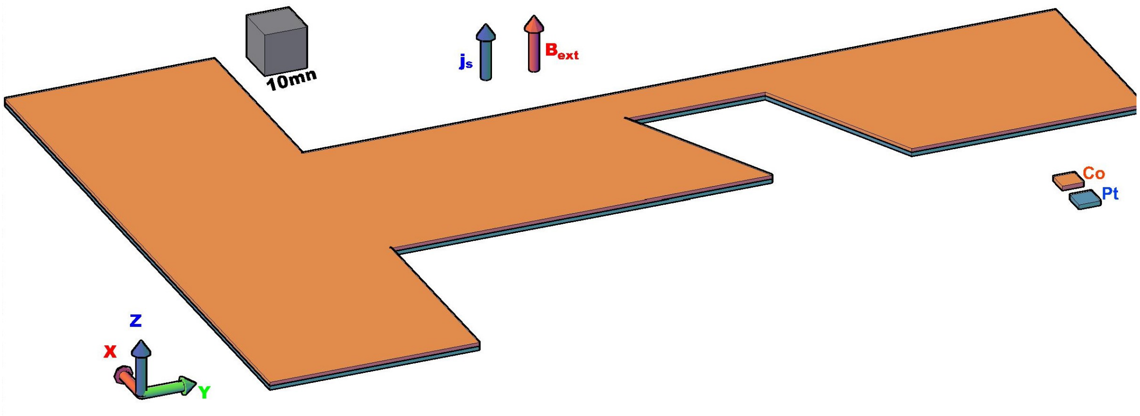

Figure 3.6: T-Type Input Stage SingleLayer

In this case it is also necessary a strategy to decide which skyrmions must enter into the computing unit and which must instead carry on along the skyrmions track to access other inputs. This system is shown in the Figure [3.7] where the chain of skyrmions is subjected to an incoming current density (negative) and tends to move along the line all together. Once passed the T-junction, the direction of the current is inverted (we have a +Z axis spin current) and the skyrmions reverse their course. Thus, the skyrmion closest to the junction tents to enter the corridor of the T. When the current returns to be like in the first stage, the two skyrmions return to move forward but with a difference: the skyrmion in the skyrmions track will proceed again straight while the one that had previously entered in the T-junction you will proceed along it because of the on-board repulsion and eventually it will turn into DW.

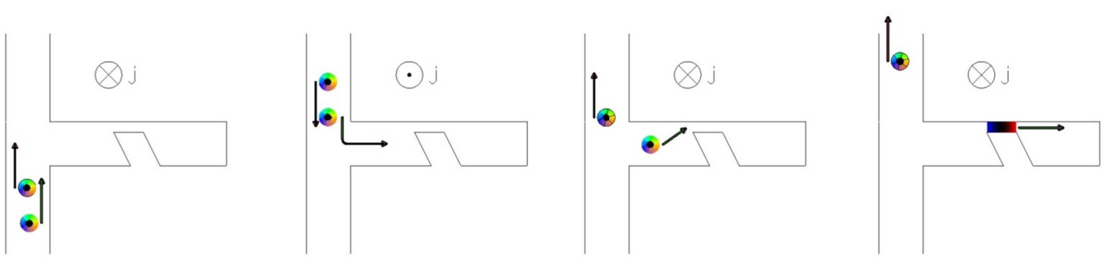

Figure 3.7: T-Type Input Stage SingleLayer principle of operation

So, a correct positioning of the T and a correct timing, make possible to enter countless bits (skyrmions) inside the same elaborative-unit pNML, as shown in the simulation in figure[3.8]

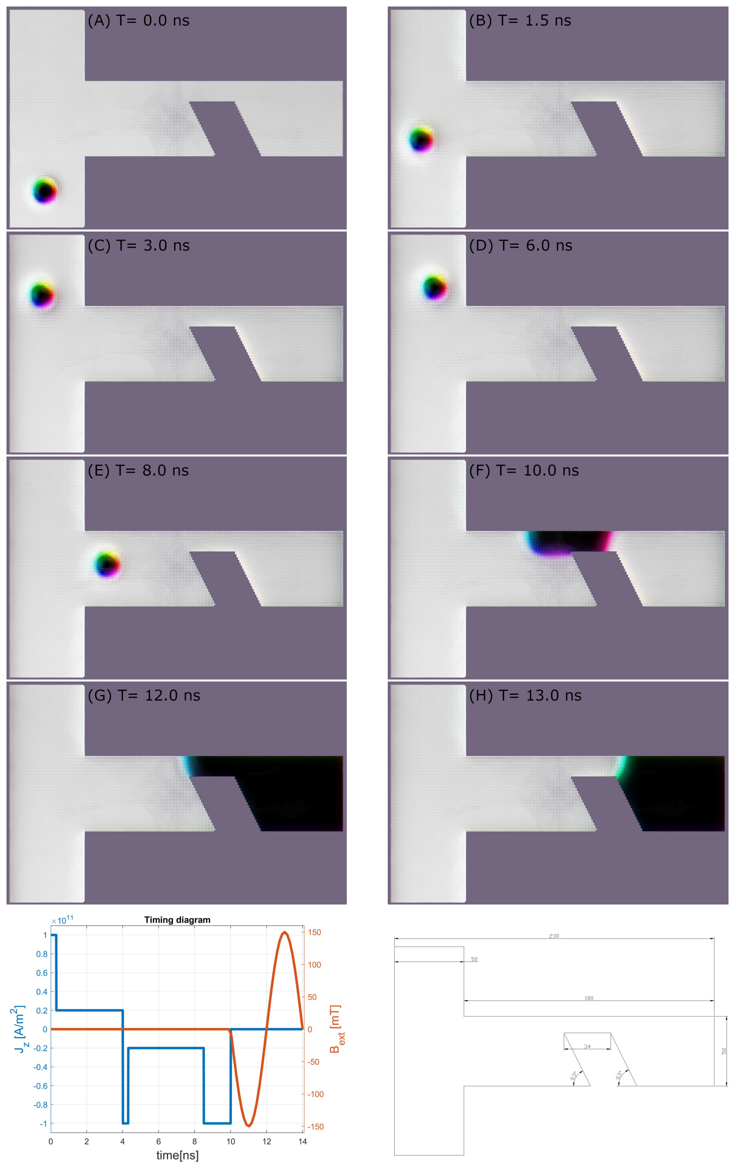

Figure 3.8: Simulation of Realistic Input Stage, A-C : $J = 2e10 A/m^2 B_e xt = 0mT$, D-E : $J = -2e10 A/m^2 B_e xt = 0mT$, E-F : $J = -1e11 A/m^2 B_e xt = 0mT$, G-H : $J = 0A/m^2 B_e xt = -150mT@250MHzSin$, timing diagram (bottom), result obtained with MuMax3

Another useful type of intersection could be the L-junction (See Figure [3.9]), where all skyrmions in the track are converted to DW. In this case the procedure is easier, since it simply needs to push the skyrmions along the track. The edge interactions will bend their trajectory and they will self-align with the bottleneck to be converted into DW. If the skyrmions are pushed too fast against the wall, they risk to overcome the forces of interaction with the edge and explode. A simulation of the L-Type Input Stage is shown in the Figure [3.10].

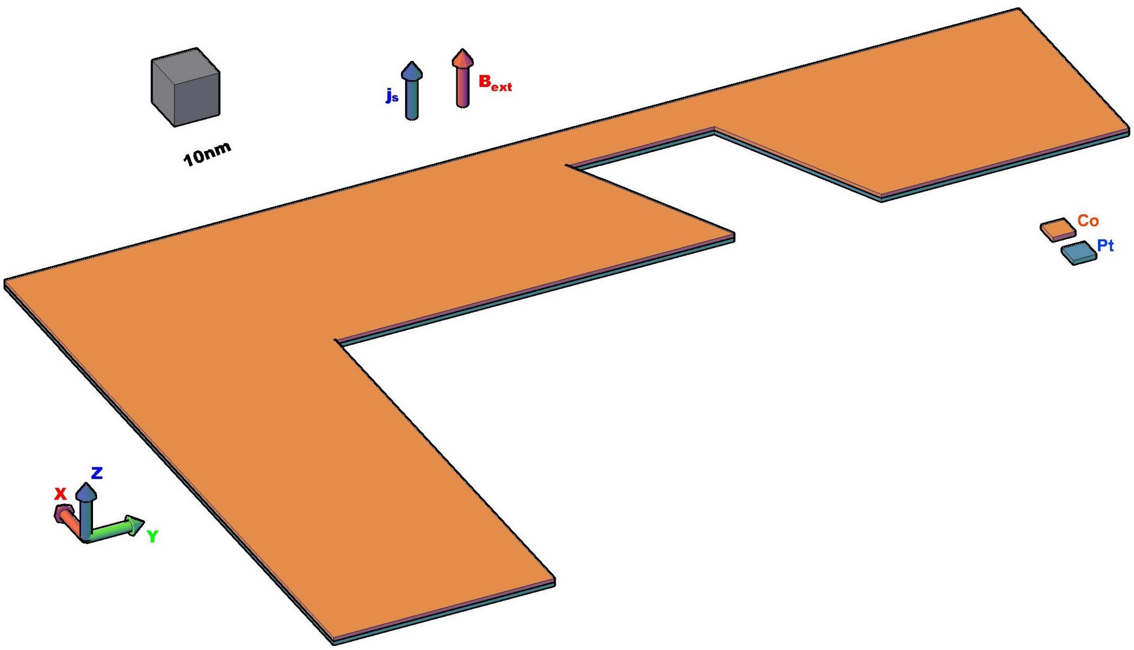

Figure 3.9: L-Type Input Stage SingleLaye

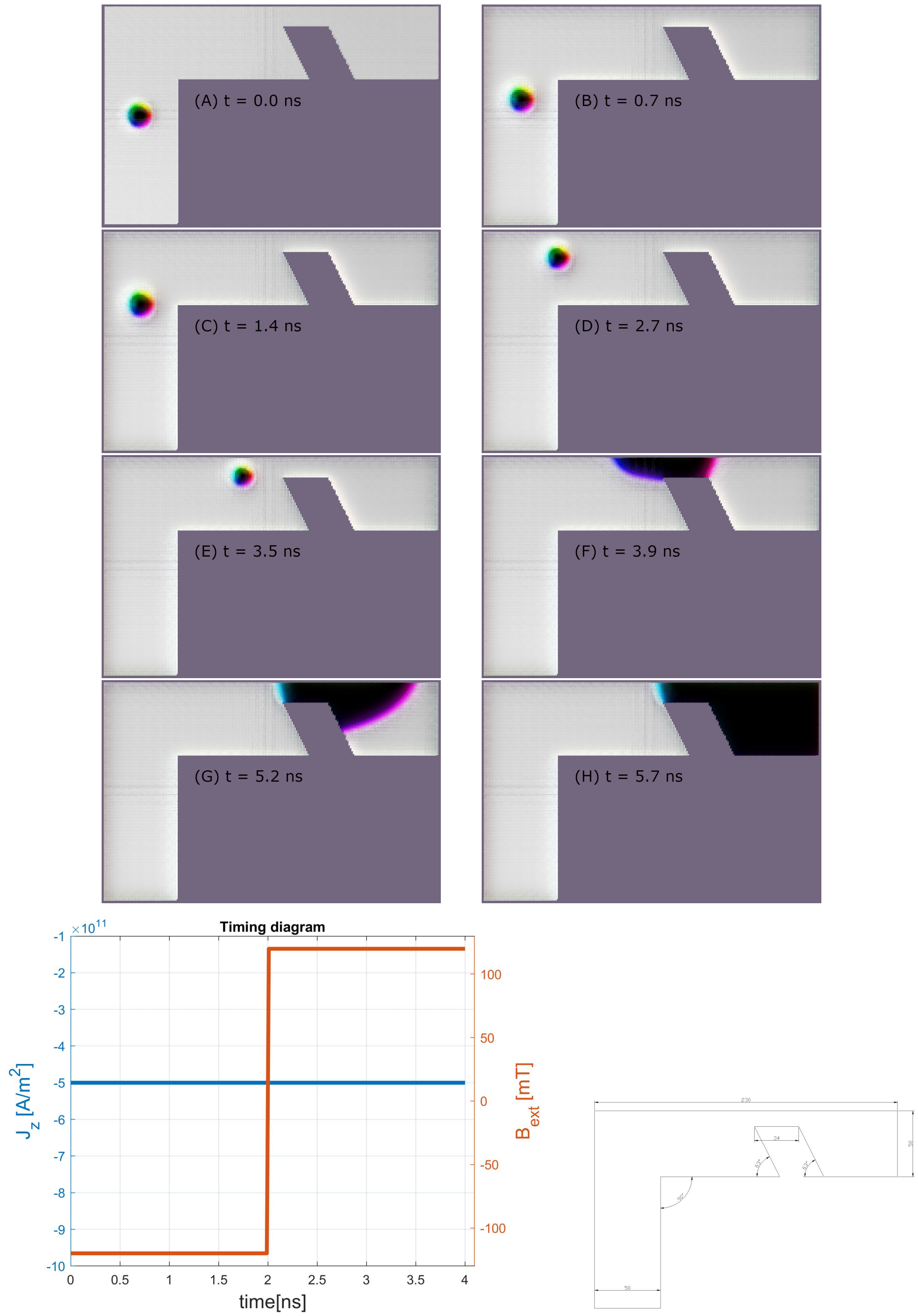

Figure 3.10: Simulation of L -Type Input Stage V2, A-F :$J = -1e11A/m^2$, G :$B_{ext} = 120mT$, H :$B_{ext} = -120mT$, result obtained with MuMax3

3.2 Output Stage

The output stage or Domain Wall to Skyrmions conversion is very similar to the one depicted in the article [24] and shown in the Figure [2.36].The main difference is the dimension: the structure is strictly Singlelayer (See Figure [3.11]).

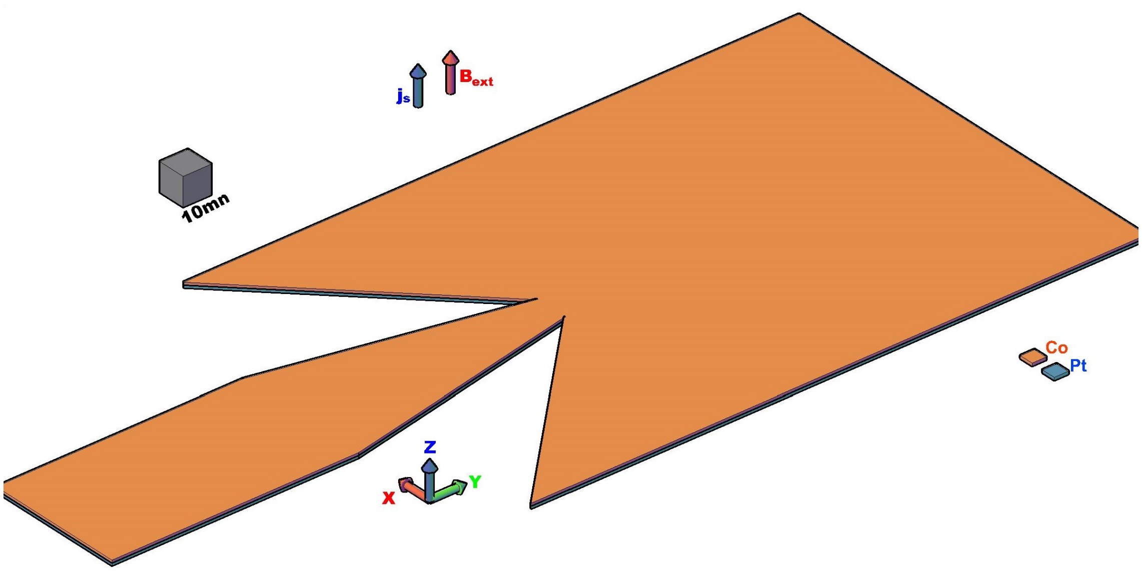

Figure 3.11: Output Stage V1 SingleLayer

The structure is very simple and it can be divided into two parts to make an analysis:

- **First Part**: This part has the same dimension of the skyrmions track but a Domain Wall spreads in it. It will fill the entire region up to the bottleneck. The Domain Wall is subjected to a constant current density comparable to that needed to move the skyrmions along the track.
- **Final Part**: In this second part a very rapid succession of two impulses at a higher current density will succeed each other. The first pulse (about 200ps) allows the DW to cross the wall and spread within the wider region. Therefore, the second pulse (about 30 ps) unplug the DW by the edge and it will tend to close on itself giving rise to a skyrmion.

The main defect of this solution is: having a usually high current density and very short impulses (so high frequencies) that could damage interconnections.

The advantage is that it does not need a timing too precise and because it does not leave the bottleneck, even if during the first phase the DW is subjected to a current comparable to that needed to move the skyrmion (See the extract of simulation in Figure [3.12]).

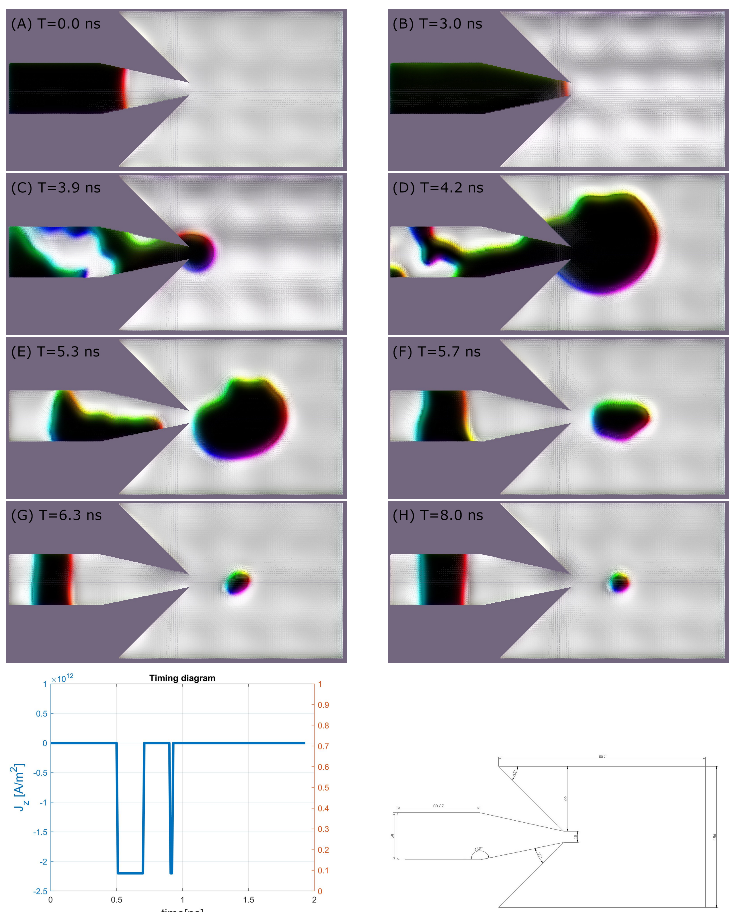

Figure 3.12: Simulation of Out Stage V1, A-B :$J = -5e11A/m^2$, C :$J = -2.2e12A/m^2$, D :$J = 0A/m^2$,E :$J = -2.2e12A/m^2$, F-H :$J = 0A/m^2$, timing diagram (bottom), result obtained with MuMax3

3.2.1 Output Stage with T = 300K

Also for this structure has been carried out a simulation at a room temperature condition ($T = 300K$). After some adjustments the simulation returned the required results as you can see in the simulation shown in the Figure [3.13].

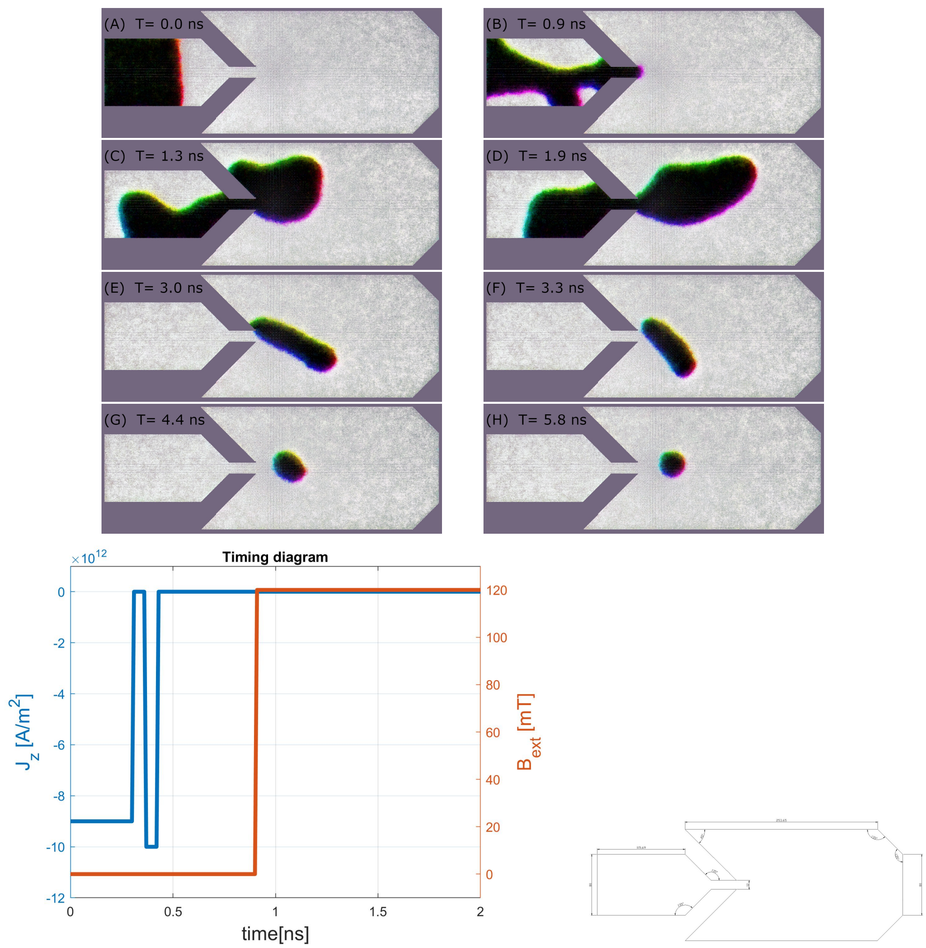

Figure 3.13: Simulation of Out Stage V1 with T =300K, A :$J = -5e11A/m^2$, B :$J = -2.2e12A/m^2$, C-D :$J = 0A/m^2$,E :$J = -2.2e12A/m^2$, F-H :$J = 0A/m^2 B_{ext} = 120mT$, timing diagram (bottom), result obtained with MuMax3

3.2.2 Realistic Output Stage

A further evolution provides an exit for the skyrmion which is generated in such a way that they can easily return to skyrmions track figure [3.14].

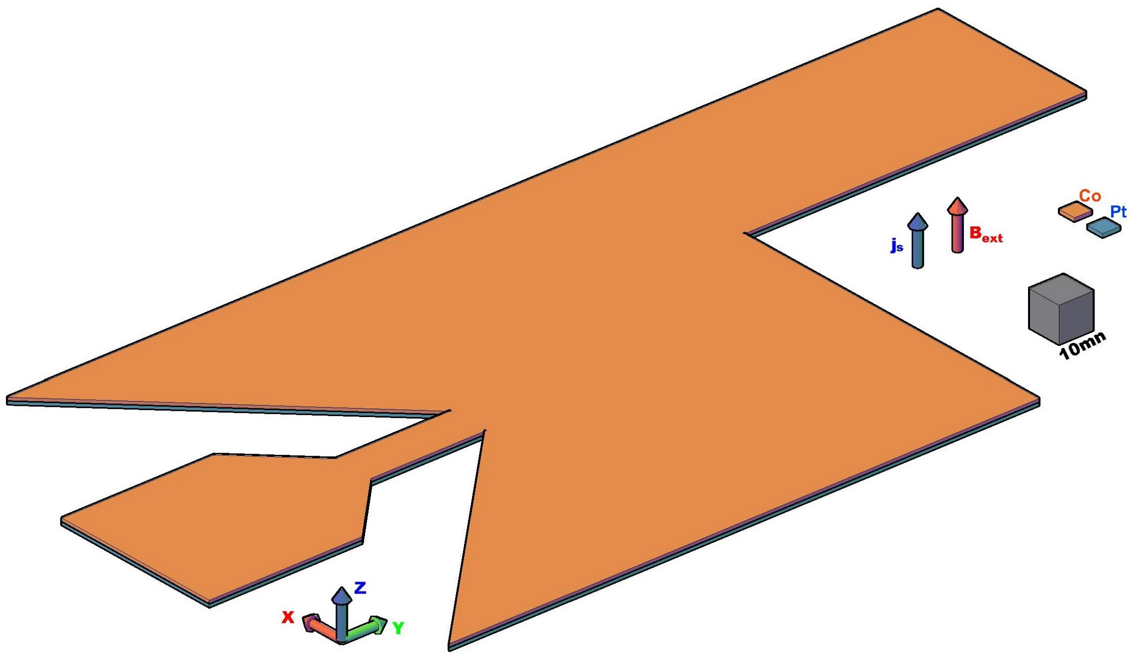

Figure 3.14: Output Stage V2 SingleLayer

During numerous simulations it has been realized that it is possible to create the skyrmion with a right timing of the external magnetic field. The magnetic field is necessary only in the first phase because,the presence of this magnetic field changes only the skyrmion diameter once it is stable.

Below there is a simulation of the realistic output stage that presents both the conversion and the exit of the skyrmion from the stage that returns to the skyrmions track (not present in the simulation shown in Figure [3.15]).

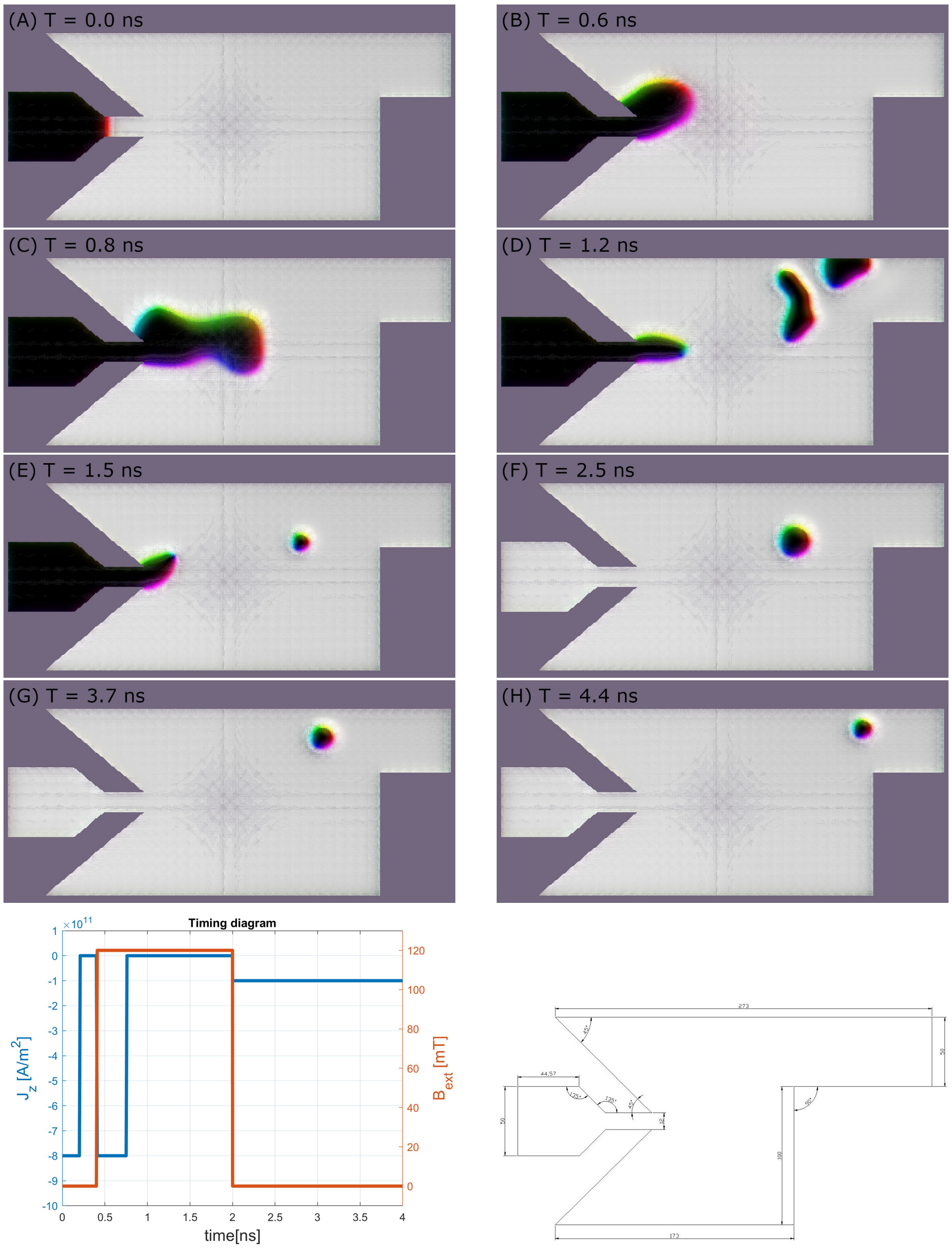

Figure 3.15: Simulation of Out Stage V2,A-E :$J = -8e11A/m^2$, F :$B_{ext} = 120mT$, G-H :$J = -1e11A/m^2$, timing diagram (bottom), result obtained with MuMax3

3.3 Conversion singlelayer to multilayer

To carry out the conversion from a Singlelayer to a Multilayer, different structures (with different qualities and defects) have been studied and realized (at CAD level).

It should be remembered that when referring to a Singlelayer it is talking about a $Co_{0.8}$ layer with a thickness of $0.8nm$ and a Pt_1 layer with a thickness of $1.0nm$ to have a $Co_{0.8}Pt_1$ material with a total thickness of $1.8nm$.

When referring to a Multilayer we are talking about 8 Co layers and 7 Pt layers to have a material $8Co_{0.8}7Pt_1$ for a total thickness of $13.4nm$.

In particular, these structures are:

- **3.3.1 - SingleLayer to MultiLayer V1**: A simple structure which involves the transition from Singlelayer to Multilayer through an identity formed by two strips of CoPt material of different thickness separated by a space (see Figure [3.16]).

- **3.3.2 - SingleLayer to MultiLayer V2**: A structure that provides the transition from a Copt Singlelayer to Multilayer through an horseshoe-shaped inverter (Figure [3.18]).

- **3.3.3 - SingleLayer to MultiLayer V3**: A structure very similar to V2 version but the Singlelayer side raised to reduce the distance between the faces and increase coupling field (Figure [3.22]).

- **3.3.4 - SingleLayer to MultiLayer V4**: it is the last and the best structure tested because of the results obtained. It is based on a ramp in which has been simulated an irradiation in the central region to reduce anisotropy and help nucleation of the DW pair (Figure [3.25]).

3.3.1 Conversion Singlelayer to Multilayer V1

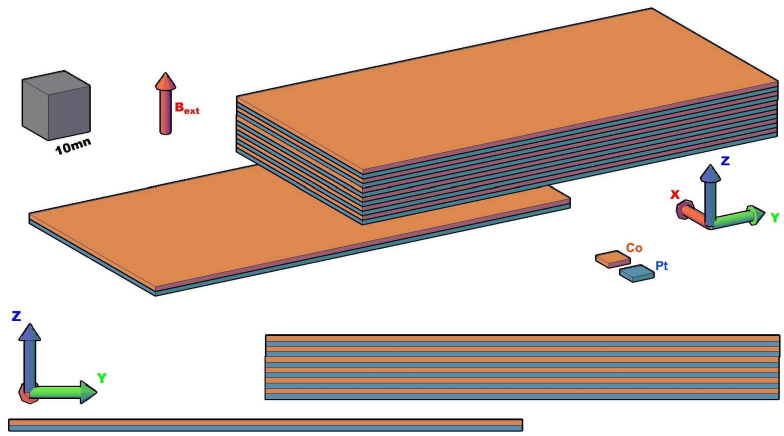

Figure 3.16: Conversion Singlelayer to Multilayer V1

How previously introduced, the Singlelayer to Multilayer conversion Version 1, provides conversion through an identity operator (that is input "1" output "1"). It consists of two strips of CoPt material with different thickness separated by a space (see Figure [3.16]).

To be clear, Input (or IN) stands for the Singlelayer input while Output (or OUT) stands for the Multilayer output.

In this structure there are some interesting points due to the structure: for example the fact that the OUT and the IN overlap for $50nm$ and are spaced of 2 $Co_{0,8}Pt_1$ layers (or 3,6nm). There is an ANC (Artificial Nucleation Center) only in the Multilayer and it can be seen in Figure [3.17].

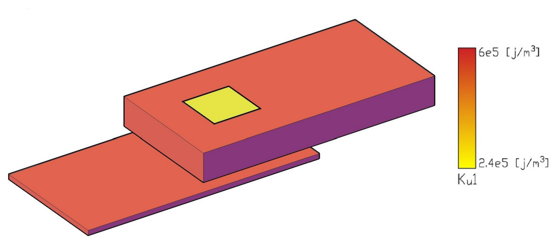

Figure 3.17: Conversion Singlelayer to Multilayer V1 Uniaxial Anisotropy Constant

Result of structure

This structure has been tested by subjecting it to different external magnetic field intensities (from about 100mt to 220mT) oscillating both sinusoidal and square wave.

Unfortunately, it was not possible to make the structure work because there is a partial nucleation of the OUT. It is not completely nucleated because of the coupling field caused by the multilayer that is more intense than the one generated by the Singlelayer. Actually this structure has been reused for inverse conversion where it was more effective (see Section 3.4)

3.3.2 Conversion singlelayer to multilayer V2

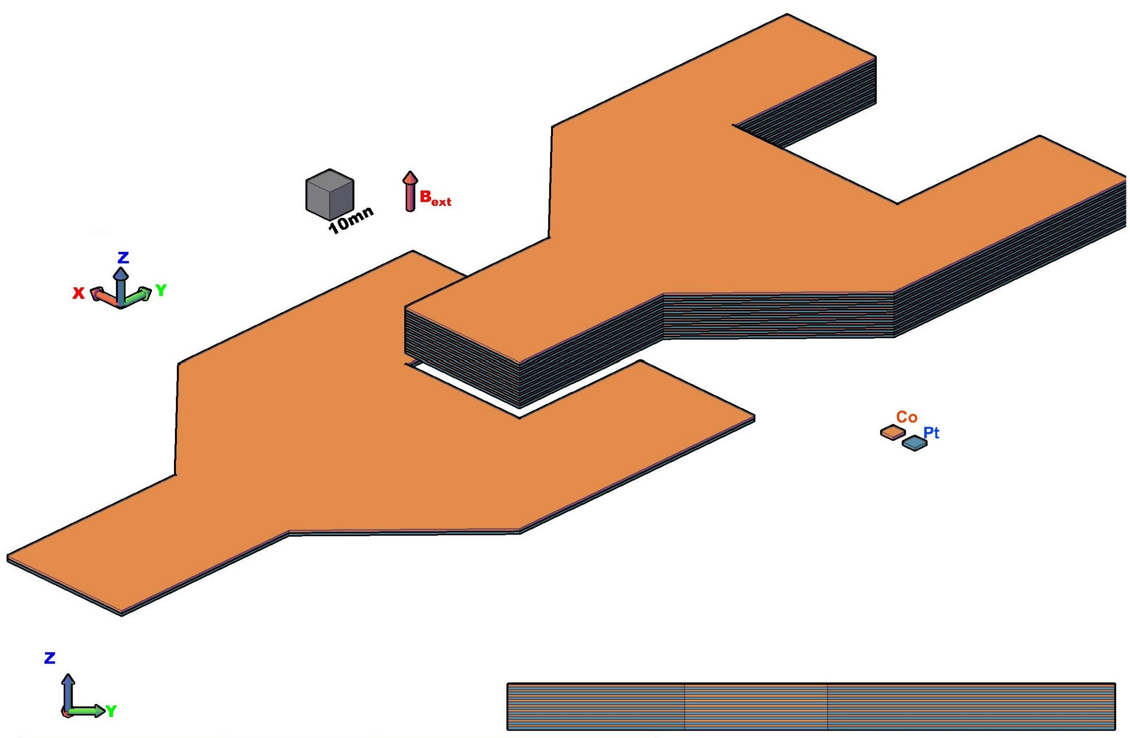

Figure 3.18: Conversion Singlelayer to Multilayer V2

The structure described in this section is the first one based on an inverter in fact, the output of the block is the 'inverse' of the input. It is characterised by a Singlelayer input that looks like a classical pNML horseshoe-shaped inverter and an output stage that looks like another horseshoe-shaped Multilayer inverter, which is elevated by 3,6nm along Z axis (that is 2 Layer of $Co_{0.8}Pt_1$).

To be clear, Input (or IN) stands for the Singlelayer input while Output (or OUT) stands for the Multilayer output.

In the Multilayer part of this structure there is an ANC (See Figure [3.19]) that is necessary to facilitate the nucleation of the OUT.

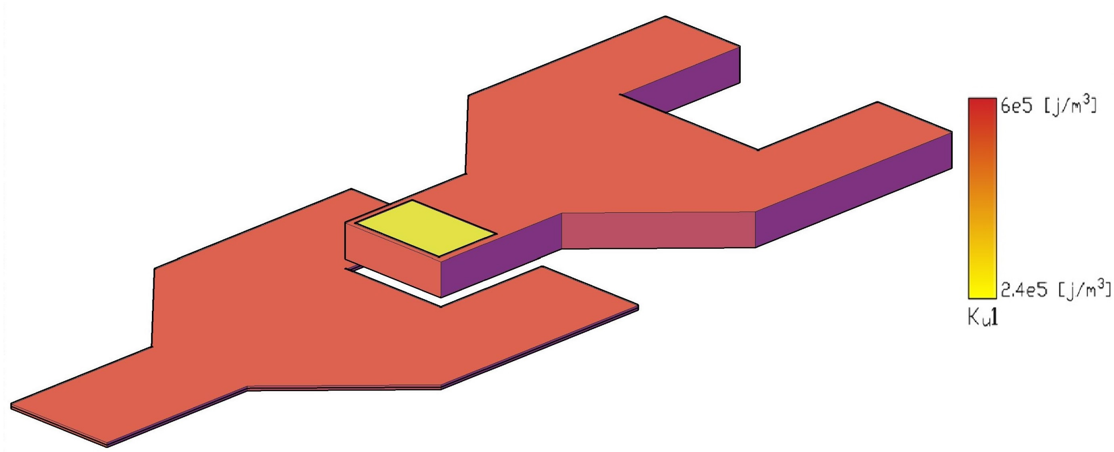

Figure 3.19: Conversion Singlelayer to Multilayer V2 Uniaxial Anisotropy Constant

Result of structure

This structure has been tested by subjecting it to different external magnetic field intensities (from about 200mt to 225mT) oscillating both sinusoidal and square wave.

For some aspects the structure has shown up promising in fact, it resulted to work in an optimal way under certain circumstances. On Table [3.2] are collected the results obtained, sorted by field intensity.

B_ext[mT]	Wave
205	Square Wave
210	Square Wave
215	Square Wave
220	Square Wave
225	Square Wave

Table 3.2: Result of Structure V2 with $T = 0K$

However, in the case with $T = 0K$ it was not possible to make it work with an external sinusoidal magnetic field. A simulation of the case in which $B_{ext} = 210mT$ is shown in Figure [3.20].

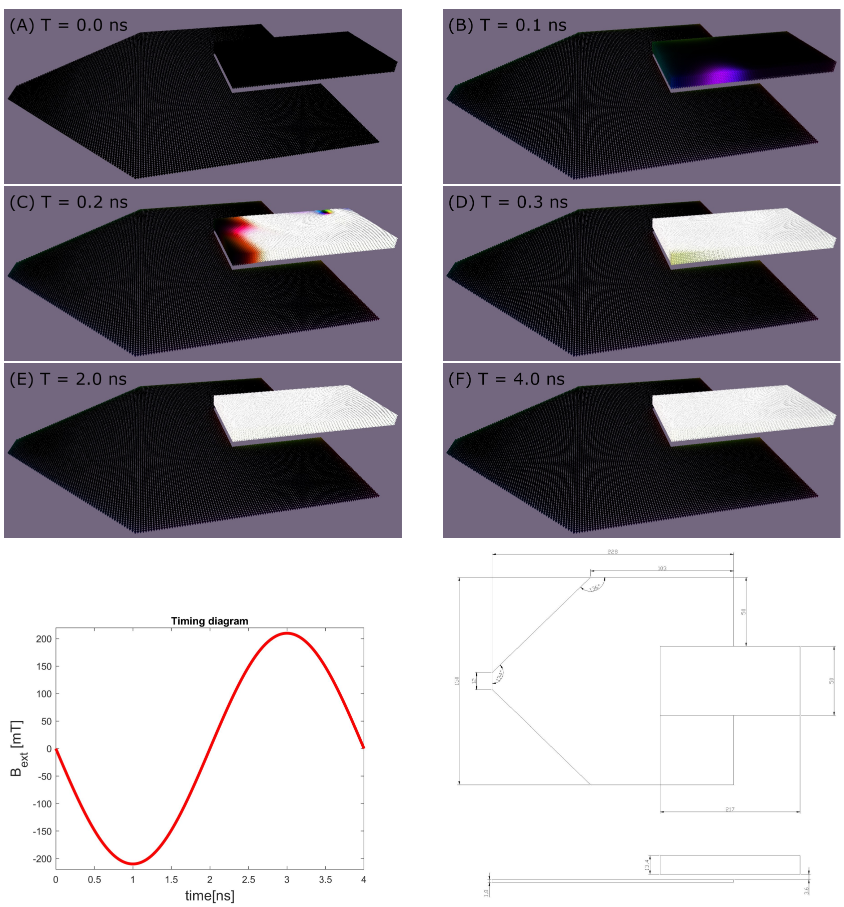

Figure 3.20: Simulation of Conversion Singlelayer to Multilayer V2 with $T = 0K$, $B_ext = -210mT@250MHz$ Sin, timing diagram (bottom), result obtained with MuMax3

To proceed with the simulations it has been added the parameter Temperature and in this case excellent results have been obtained both with an external field of square wave type and with the sinusoidal one, as shown in Table [3.3].

B_ext[mT]	Wave
205	Sin Wave
210	Sin Wave
215	Sin Wave
220	Sin Wave
225	Sin Wave

Table 3.3: Result of Structure V2 with $T = 300K$

Also in this case there is a simulation representing the functioning of Singlelayer to Multilayer V2 conversion block, that you can see in Figure [3.21]. The test conditions are $T = 300K$ e $B_{ext} = 200mT$.

3.3.3 Conversion singlelayer to multilayer V3

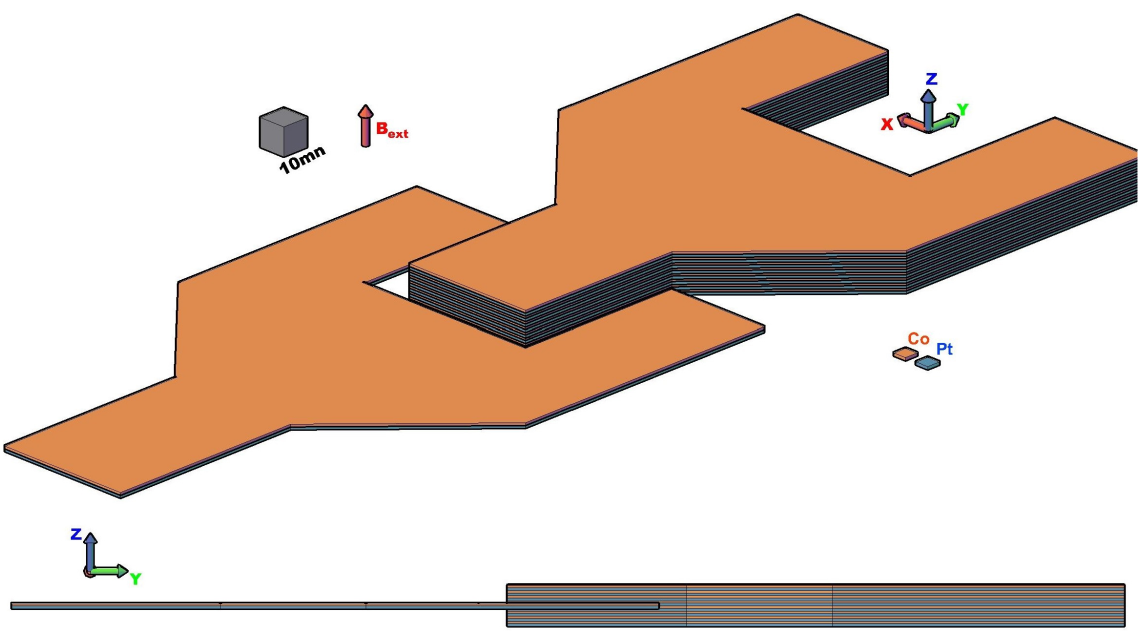

Figure 3.22: Conversion Singlelayer to Multilayer V3

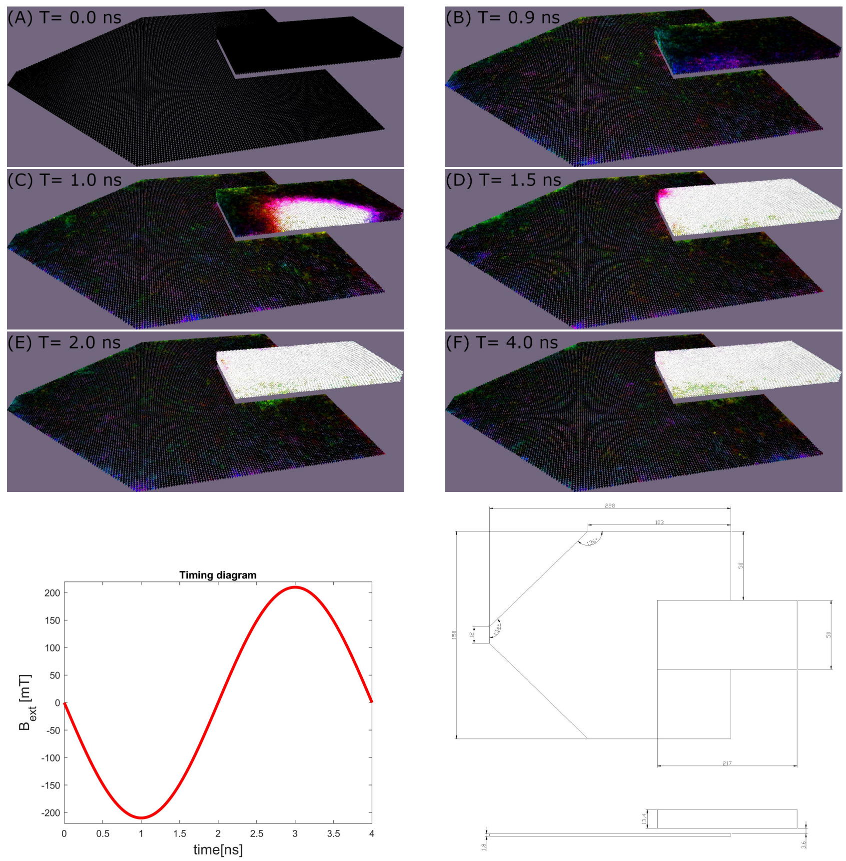

Figure 3.21: Simulation of Conversion Singlelayer to Multilayer V2 with $T = 300K$, $B_ext = -210mT@250MHz$ Sin, timing diagram (bottom), result obtained with MuMax3

The structure described in this section is the second structure based on an inverter in fact, it is very similar to the one seen in the previous section. It is characterised by a Singlelayer input that looks like a classical pNML horseshoe-shaped inverter and an output stage that looks like another horseshoe-shaped Multilayer inverter. In this case the Singlelayer structure is overlapped so it fits with the Multilayer structure at about half its height as you can see in Figure [3.22].

As shown in Figure [3.23] there is also here an Artificial Nucleation Center located in the same place as the previous case.

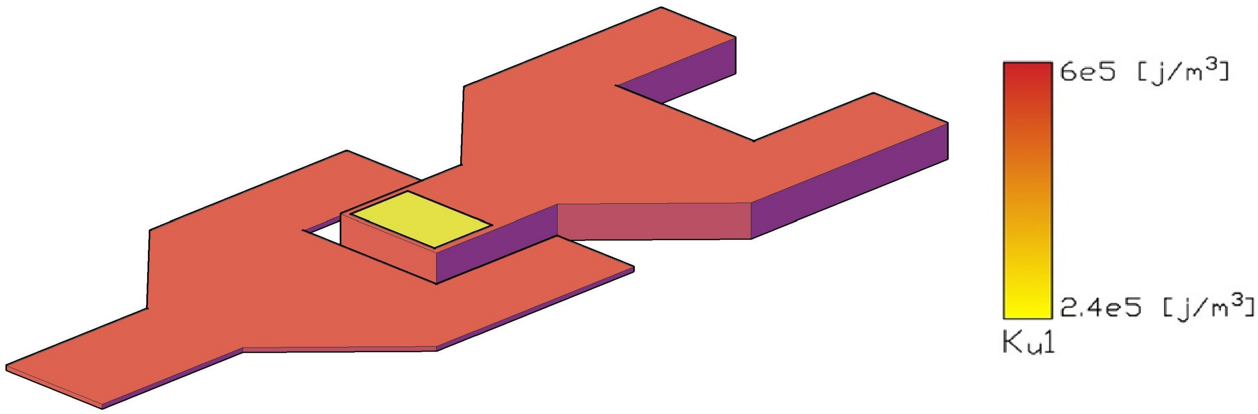

Figure 3.23: Conversion Singlelayer to Multilayer V3 Uniaxial Anisotropy Constant

Result of structure

This structure has been tested by subjecting it to different external magnetic field intensities (from about 100mt to 200mT) oscillating both sinusoidal and square wave.

The structure has shown up promising if subjected to an external magnetic field square wave but not as good for sinusoidal case. Here is a Table [3.4] in which the results obtained are collected according to the field's intensity.

B_ext[mT]	Wave
100	Square Wave
120	Square Wave
140	Square Wave
160	Square Wave
180	Square Wave

Table 3.4: Result of Structure V3 with $T = 0K$

Below, a simulation taken between those shown in Table [3.4] is reported in Figure [3.24], where there is a $B_{ext} = 160mT$. In addition to these simulations, were carried out some at $T = 300k$ but none of them gave the expected results. In fact, there is a partial or total nucleation but during the inversion of the field it overwrite the OUT.

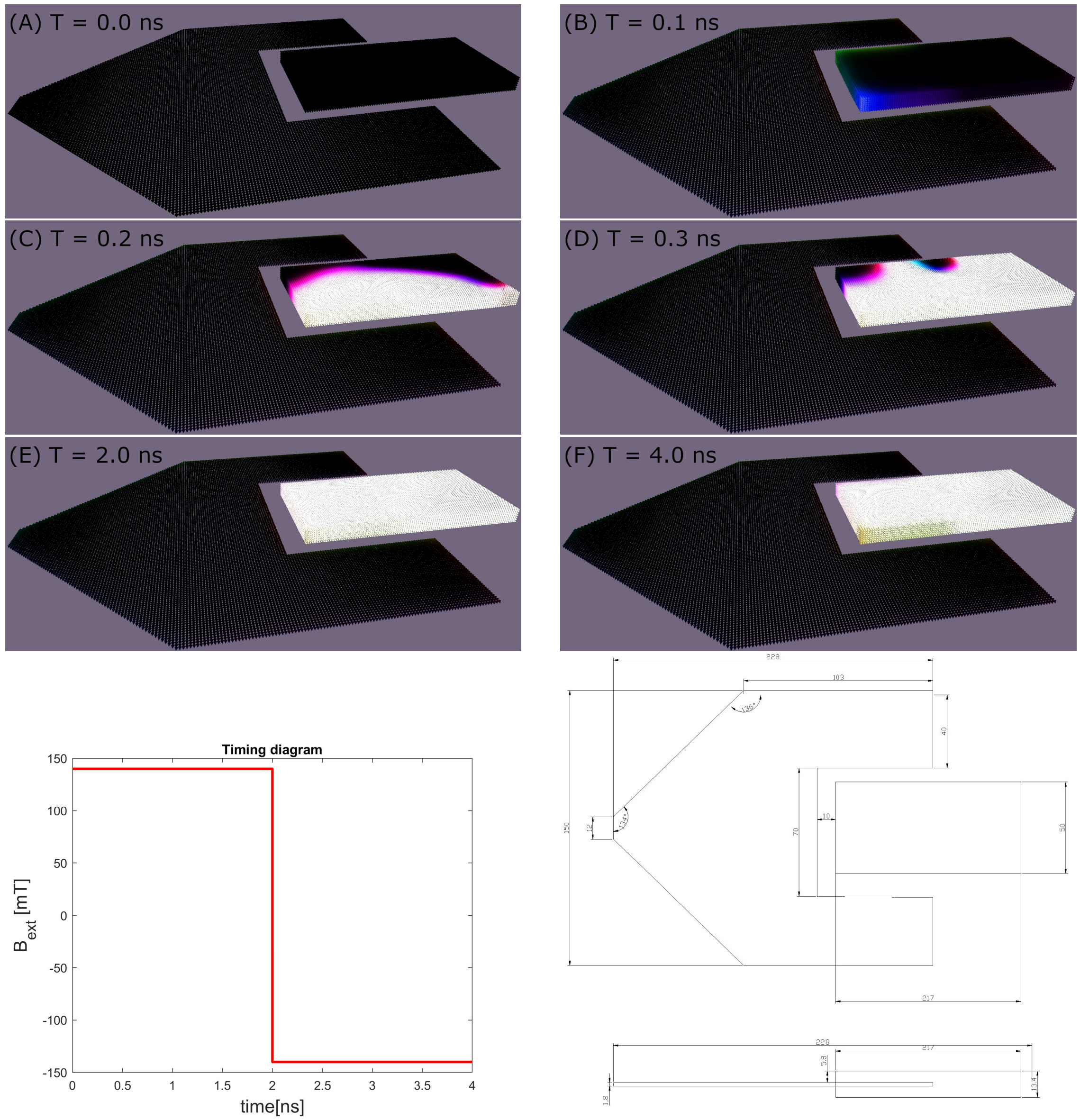

Figure 3.24: Simulation Conversion Singlelayer to Multilayer V3 with $T = 0K$, A-E $:B_{ext} = 140mT$, F $:B_{ext} = -140mT$, timing diagram (bottom), result obtained with MuMax3

3.3.4 Conversion singlelayer to multilayer V4

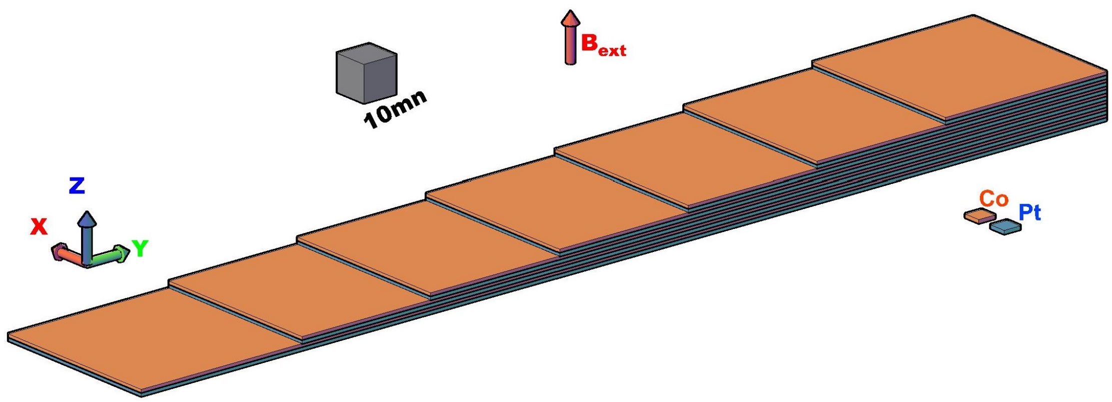

Figure 3.25: Conversion Singlelayer to Multilayer V4

In this structure there is a complete change of philosophy, in fact it is a ramp structure that passes from a $1.8nm$ Singlelayer to a $13.4nm$ Multilayer with a step of $40nm$. Tests were carried out also with steps of $2nm$, $10nm$ e $20nm$ and despite the positive results they are not considered valid, because of the difficult realization of the ramps. Each step of the ramp differs from the previous in thickness of $Co_{0.8}Pt_1$ layer.

To facilitate the propagation of the Domain Wall Pair was simulated an irradiation in the center of the ramp to locally reduce Uniaxial Anisotropy Constant as you can see in Figure [3.26].

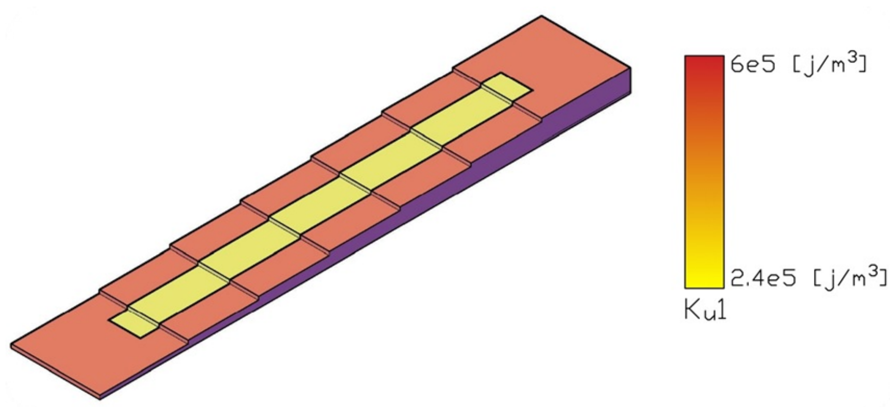

Figure 3.26: Conversion Singlelayer to Multilayer V4 Uniaxial Anisotropy Constant

Result of structure

This structure was tested by subjecting it to different external magnetic field intensities (from about 100mt to 220mt) oscillating both sinusoidal and square wave. In addition, the width of the simulated irradiation has been changed to see which advantages or disadvantages it brought to the block of conversion from Singlelayer a Multilayer.

To simplify, only the results obtained with the reduction of Uniaxial Anisotropy Constant are shown in Figure [3.26]. although the others also gave positive results compatible with those that can be seen in Table [3.5].

B_ext[mT]	Wave @250MHz	B_ext	Wave @250MHz
100	Square Wave	-	Sin Wave
120	Square Wave	-	Sin Wave
140	Square Wave	-	Sin Wave
150	Square Wave	150	Sin Wave
160	Square Wave	160	Sin Wave
170	Square Wave	170	Sin Wave
180	Square Wave	180	Sin Wave
200	Square Wave	200	Sin Wave
210	Square Wave	210	Sin Wave
220	Square Wave	220	Sin Wave

Table 3.5: Result of Structure V4 with $T = 0K$

To give an idea of the functioning of the previously described ramp in Figure [3.27]] is shown the extract of a simulation.

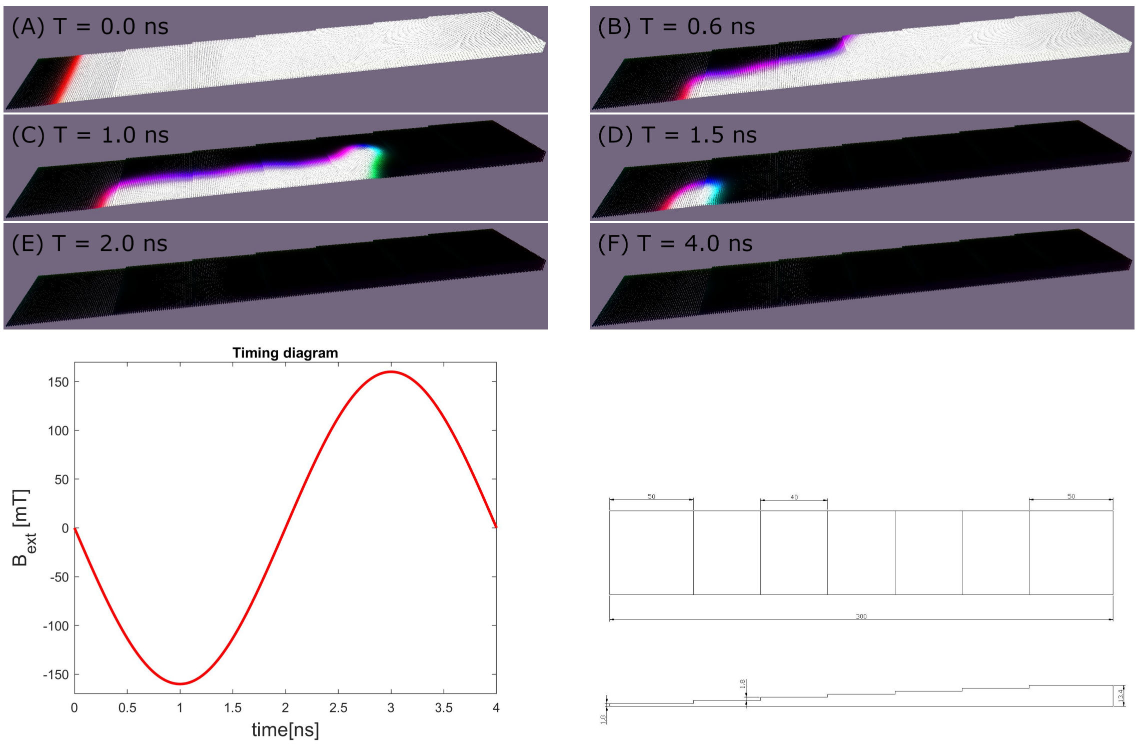

Figure 3.27: Simulation of Conversion Singlelayer to Multilayer V4 with $T = 0K$, $B_ext = -160mT@250MHzSin$, timing diagram (bottom), result obtained with MuMax3

Then the parameter Temperature has been added to proceed with the simulations. In this case, the external magnetic field intensity range has been reduced between $160mT$ and $180mT$ with very positive results as you can see in Table [3.6]. In Figure [3.28] is shown the simulation with sinusoidal external magnetic field $160mT@250MHz$ and $T = 300K$ as conditions.

B_ext[mT]	Wave @250MHz	B_ext	Wave @250MHz
160	Square Wave	160	Sin Wave
170	Square Wave	170	Sin Wave
180	Square Wave	180	Sin Wave

Table 3.6: Result of Structure V4 with $T = 300K$

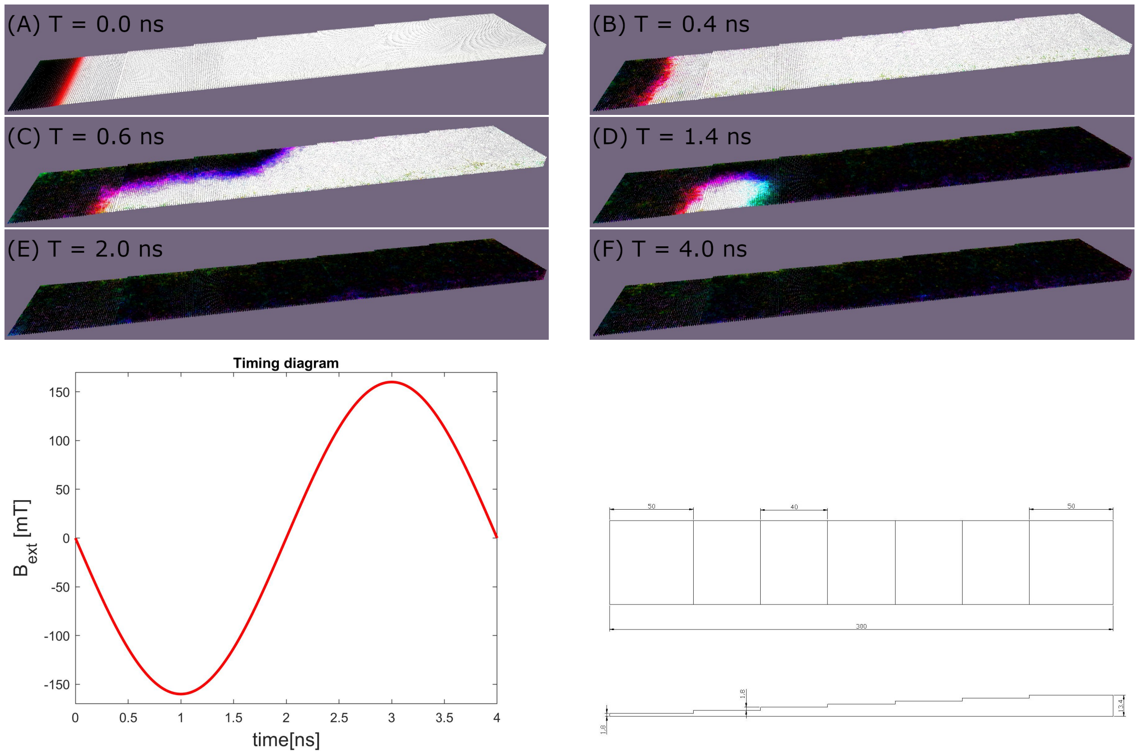

Figure 3.28: Simulation of Conversion Singlelayer to Multilayer V4 with $T = 300K$, $B_ext = -160mT@250MHz$ Sin, timing diagram (bottom), result obtained with MuMax3

3.4 Conversion MultiLayer to SingleLayer

To carry out the conversion from a Multilayer to a Singlelayer different structures, derived from those seen in Section 3.3 have been studied and realized (at CAD level).

It is important to remember that when referring to a Singlelayer it is talking about a $Co_{0.8}$ layer with a thickness of $0.8nm$ and a Pt_1 layer with a thickness of $1.0nm$ to have a $Co_{0.8}Pt_1$ material with a total thickness of $1.8nm$.

When referring to a Multilayer we are talking about 8 Co layers and 7 Pt layers to have a material $8Co_{0.8}7Pt_1$ for a total thickness of $13.4nm$.

in particular, these structures are:

- **3.4.1 - MultiLayer to SingleLayer V1**: the same simple structure of the one discussed in section 3.3.1, which provides the transition from Multilayer to SingleLayer through an identity characterised by two strips of CoPt material with different thickness separated by a space (see Figure [3.29]).

- **3.4.2 - MultiLayer to SingleLayer V2**: this structure switch from a Copt Singlelayer to Multilayer through an horseshoe-shaped inverter (Figure [3.33]); it is the same structure discussed in Section 3.3.2 but Multilayer and Singlelayer are inverted.

- **3.4.3 - MultiLayer to SingleLayer V3**: this structure is the last and the best tested because of the results obtained. It is based on a ramp in which has been simulated an irradiation in the central region to reduce anisotropy and facilitate the nucleation of the DW pair (Figure [3.36]). It is the same ramp discussed in section 3.3.4 but backwards.

3.4.1 Conversion Multilayer to Singlelayer V1

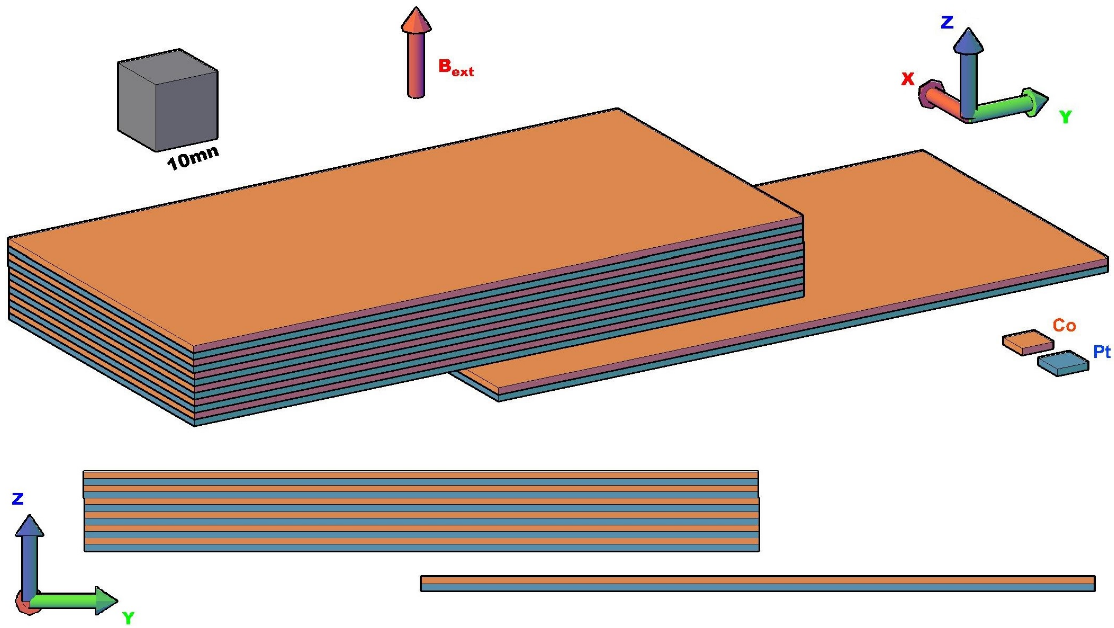

Figure 3.29: Conversion Multilayer to Singlelayer V1

This structure has been largely described in Section 3.3.1. The difference is that the Multilayer side becomes the input and the Singlelayer side becomes the Output (Figure [3.29]).

This structure was founded to make the transition from Singlelayer to Multilayer and vice versa with structures as similar as possible.

To be clear, Input (or IN) stands for the Singlelayer input while Output (or OUT) stands for the Multilayer output.

Only on the output side (singlelayer) of this structure there is an Artificial Nucleation Center as can be seen in Figure [3.30]. This facilitates the nucleation and allows the correct functioning of identity operator.

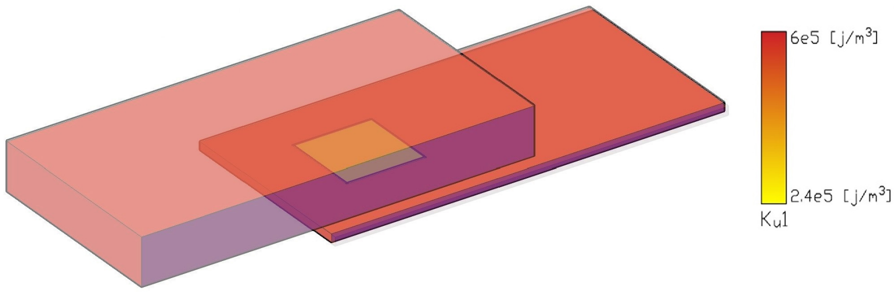

Figure 3.30: Conversion Multilayer to Singlelayer V1 Uniaxial Anisotropy Constant

Result of structure

This structure has been tested by subjecting it to different external magnetic field intensities oscillating both sinusoidal and square wave at different frequencies.

The structure looks promising when subjected to a external sinusoidal magnetic field and at 125 MHz frequencies but not as good when subjected to the square wave with higher frequencies. It is shown on Table [3.7] where the results obtained are collected by intensity field.

B_ext[mT]	Wave @ 125MHz
160	Sin Wave
180	Sin Wave
200	Sin Wave
210	Sin Wave
220	Sin Wave

Table 3.7: Result of Structure V1 with $T = 0K$

To clarify, an extract of a simulation of those listed in the Table [3.7] is shown in Figure [3.31]

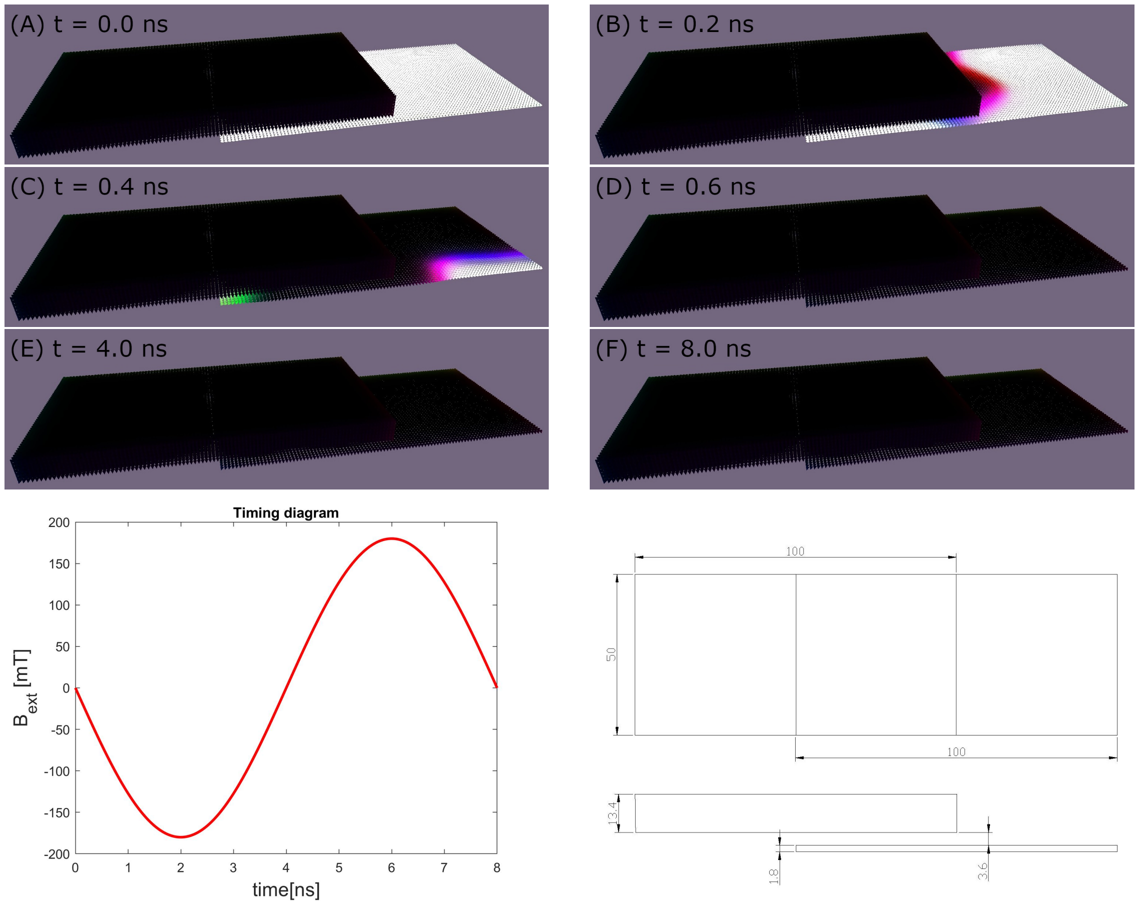

Figure 3.31: Simulation of Conversion Multilayer to Singlelayer V1 with $T = 0K$, $B_ext = -180mT@125MHz$ Sin, timing diagram (bottom), result obtained with MuMax3

For the sake of completeness, simulations were also carried out by adding the temperature factor set to $T = 300K$. In Table [3.8] there is a reference to the simulations made considered the most promising. The extract of one of these simulations below is shown in Figure [3.32].

B_ext[mT]	Wave @ 63MHz
180	Sin Wave
200	Sin Wave
210	Sin Wave
220	Sin Wave
220	Sin Wave

Table 3.8: Result of Structure V1 with $T = 300K$

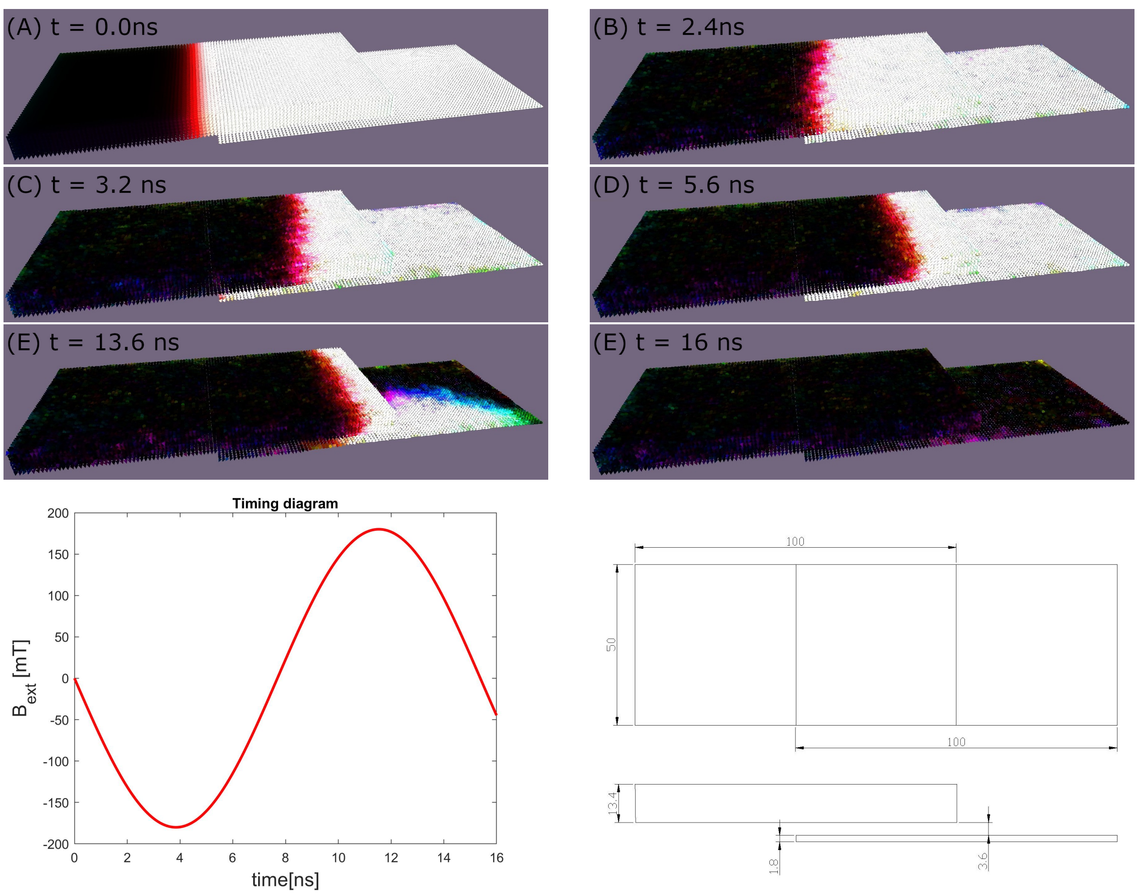

Figure 3.32: Simulation of Conversion Multilayer to Singlelayer V1 with $T = 300K$, $B_e xt = -180 mT@63MHz$ Sin, timing diagram (bottom), result obtained with Mu-Max3

3.4.2 Conversion Multilayer to Singlelayer V2

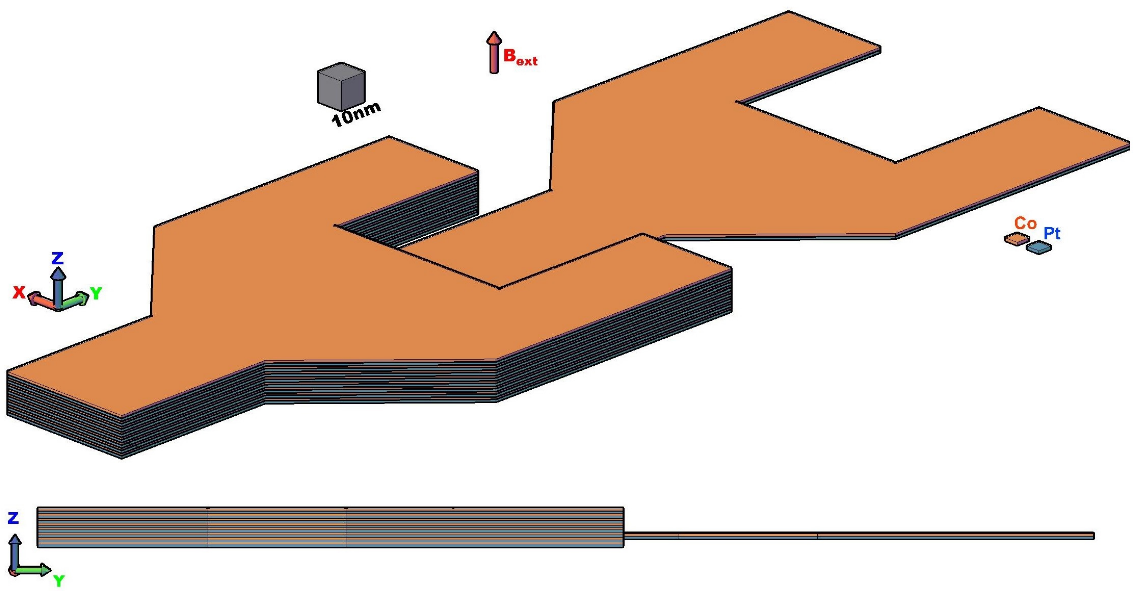

Figure 3.33: Conversion Multilayer to Singlelayer V2

This structure was taken from the one treated in Section 3.3.2, also in this case the input stage is Multilayer and the output side is Singlelayer. The conversion structure Multilayer to Singlelayer can be seen in Figure [3.33].

Only in the output side (singlelayer) of this structure there is an Artificial Nucleation Center as can be seen in Figure [3.34]. It facilitates the nucleation and allows the correct functioning of the inverter operator .

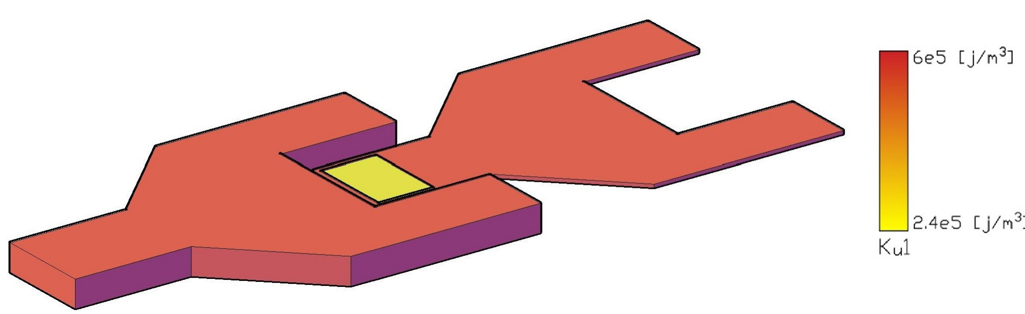

Figure 3.34: Conversion Multilayer to Singlelayer V2 Uniaxial Anisotropy Constant

Result of structure

This structure has been tested by subjecting it to different external magnetic field intensities oscillating both sinusoidal and square wave.

The structure looks promising when subjected to a external sinusoidal and square wave magnetic field.

Innumerable simulations have been carried out by modifying the magnetic field intensity (from $100mT$ to $200mT$). Unfortunately, the only positive result has been obtained using a square weave $B_{ext} = 184mT$ as can be seen in Figure [3.35].

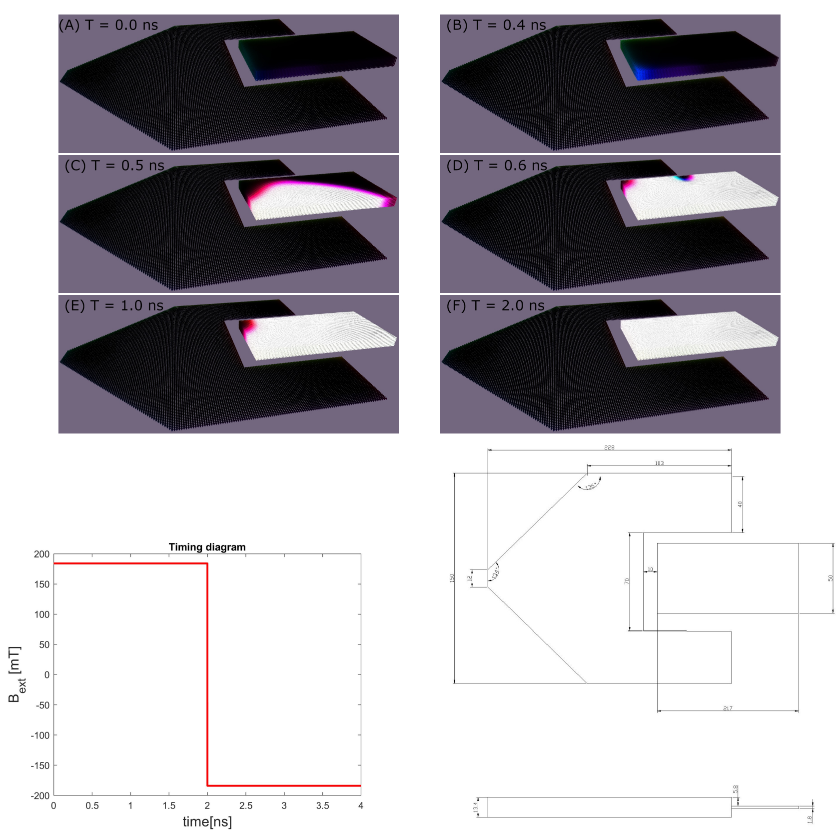

Figure 3.35: Simulation of Conversion Multilayer to Singlelayer V2 with $T = 0K$, A-F : $B_{ext} = 184mT$, G : $B_{ext} = -184mT$, timing diagram (bottom), result obtained with MuMax3

Because of the low amount of positive results at $T = 0K$ temperature, no simulations have been performed at $T = 300K$.

3.4.3 Conversion Multilayer to Singlelayer V3

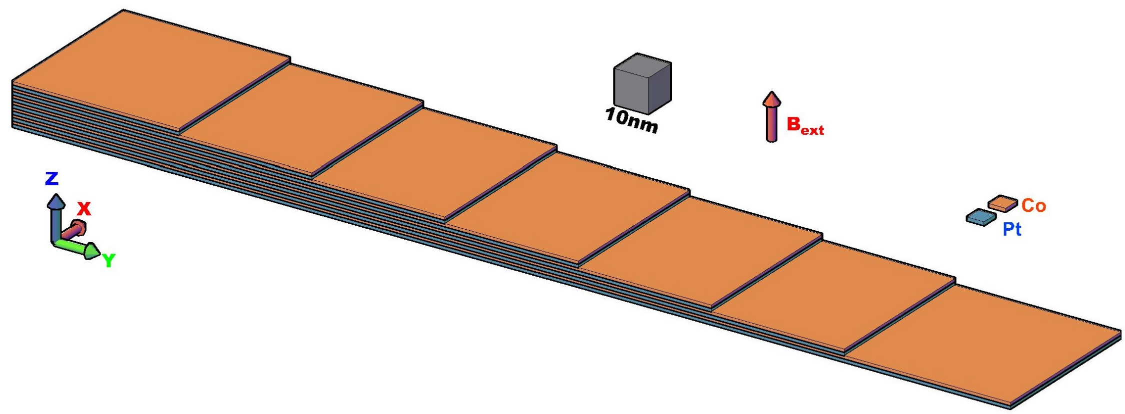

Figure 3.36: Conversion Multilayer to Singlelayer V3

This structure has been largely described in Section 3.3.4. It is characterized by the the same ramp but it is run in the opposite direction. Referring to other details the two structures are identical as can be seen in Figure [3.36].

This structure was born from the idea of making the transition from SingleLayer to MultiLayer and vice versa with similar structures as far as possible.

To be clear, Input (or IN) stands for the Singlelayer input while Output (or OUT) stands for the Multilayer output.

To facilitate the propagation of the Domain Wall Pair was simulated an irradiation in the center of the ramp to locally reduce Uniaxial Anisotropy Constant as you can see in Figure [3.37].

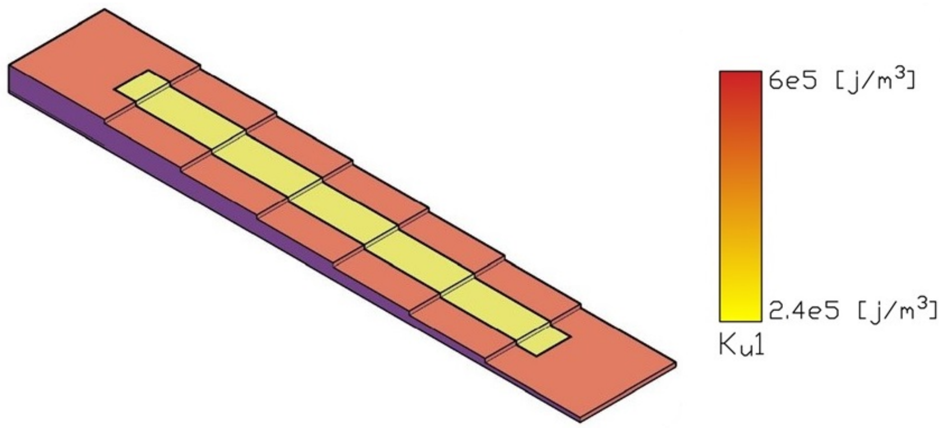

Figure 3.37: Conversion Multilayer to Singlelayer V3 Uniaxial Anisotropy Constant

Result of structure

This structure has been tested by subjecting it to different intensities of external magnetic field oscillating both sinusoidal and square wave at different frequencies.

The structure is promising when subjected to both external sinusoidal magnetic and square wave. In the table [3.9]are collected the obtained results ordered by intensity field.

B_ext[mT]	Wave @250MHz	B_ext	Wave @250MHz
100	Square Wave	100	Sin Wave
120	Square Wave	120	Sin Wave
140	Square Wave	140	Sin Wave
150	Square Wave	150	Sin Wave
160	Square Wave	160	Sin Wave
170	Square Wave	170	Sin Wave
180	Square Wave	180	Sin Wave
200	Square Wave	200	Sin Wave
210	Square Wave	210	Sin Wave
220	Square Wave	220	Sin Wave

Table 3.9: Result of Structure V4 with $T = 0K$

To be clear an extract from a simulation of those listed in the table is shown in Figure [3.38] below.

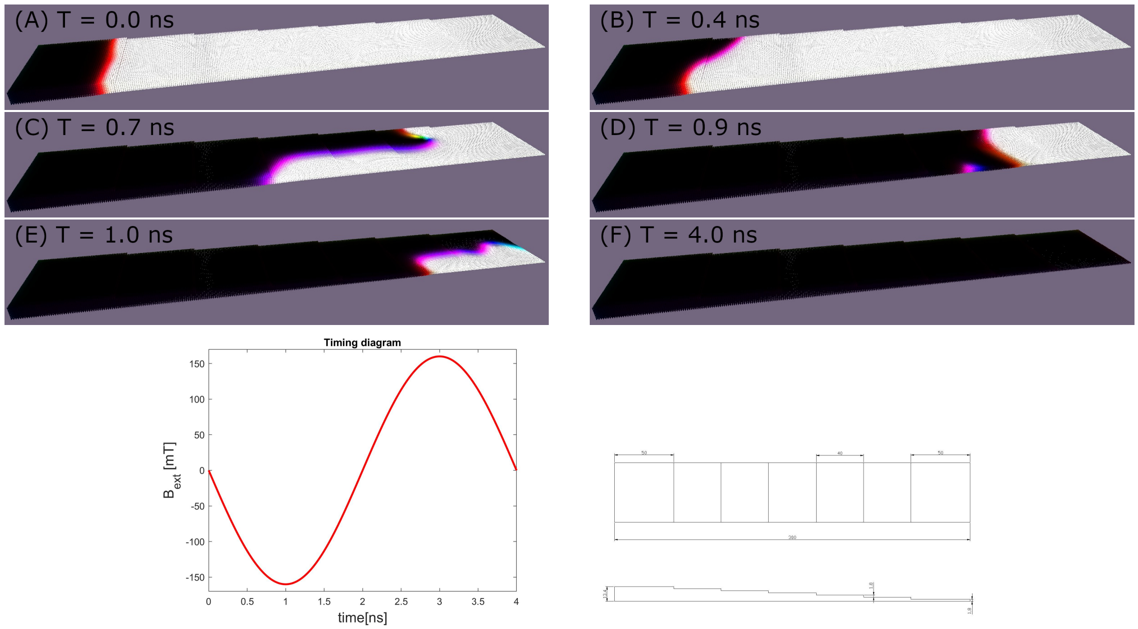

Figure 3.38: Simulation of Conversion Multilayer to Singlelayer V3 with $T = 0K$, $B_ext = -160mT@250MHz$ Sin, timing diagram (bottom), result obtained with MuMax3

For the sake of completeness, simulations have been also carried out by adding the temperature set to $T = 300K$. In table [3.10] are shown simulations performed considered promising. The extract of one of these simulations can be seen in Figure [3.39]

B_ext[mT]	Wave @250MHz	B_ext	Wave @250MHz
100	Square Wave	100	Sin Wave
120	Square Wave	120	Sin Wave
140	Square Wave	140	Sin Wave
150	Square Wave	150	Sin Wave
160	Square Wave	160	Sin Wave
170	Square Wave	170	Sin Wave
180	Square Wave	180	Sin Wave
200	Square Wave	200	Sin Wave
210	Square Wave	210	Sin Wave
220	Square Wave	220	Sin Wave

Table 3.10: Result of Structure V4 with $T = 300K$

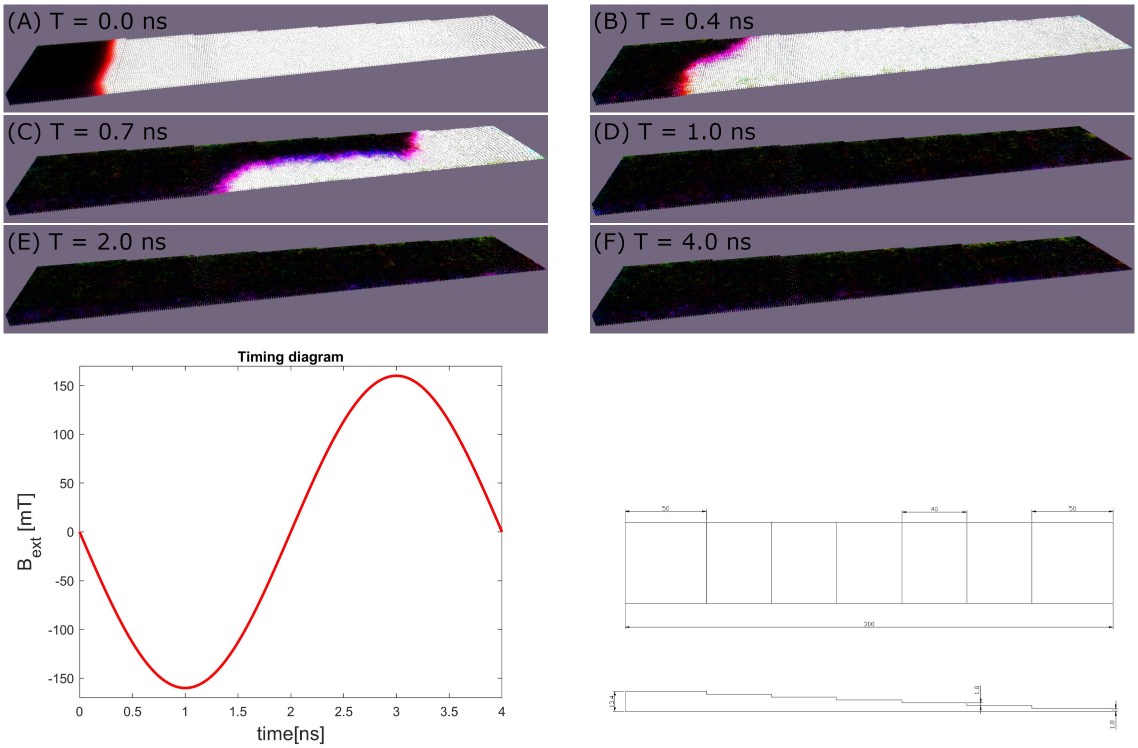

Figure 3.39: Simulation of Conversion Multilayer to Singlelayer V3 with $T = 300K$, $B_ext = -160mT@250Mhz$ Sin, timing diagram (bottom), result obtained with MuMax3

3.5 pNML Stage (inverter)

The pNML stage was studied as a horseshoe-shaped inverter because the inverter is the simplest operator that can be made at simulative level.

Once the correct functioning of this operator is established it is possible to make also more complex operators(majority voter) thanks to studies and deepening.

In this chapter we will see two different types of inverters:

- **3.5.1 - Inverter SingleLayer**: it reiterates the attempt to make Skyrmions and pNML technology work together on a singlelayer platform.
- **3.5.2 - Inverter MultiLayer**: it represents the second part of the studies where it was decided to use each technology on the appropriate thickness of *CoPt* material using converters from SingleLayer to Multilayer (Section 3.3) and vice versa (Section 3.4)

3.5.1 Inverter SingleLayer

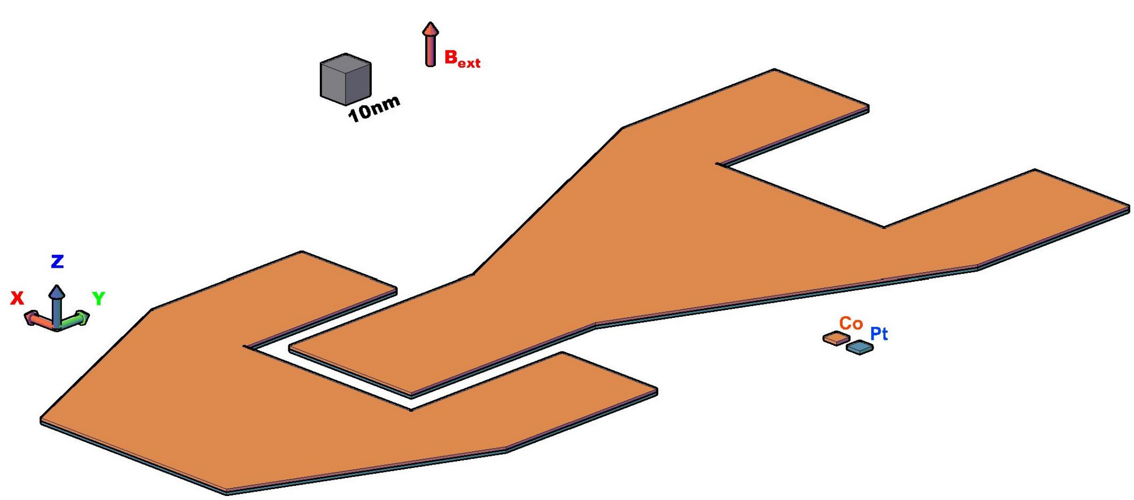

Figure 3.40: Inverter SingleLayer

During this first phase the dimensions and distances of the inverter structure are taken from the state of art. The results can be seen in Figure [3.40].

During simulations, different positions of the Artificial Nucleation Center have been tested and the parameter that varied between a simulation and the other was the distance between the two magnets (Input magnet and Output magnet) and the external magnetic field, such for which the commutation happened.

In Figure [3.41] the inverter is shown with a representation of the variation of the Uniaxial Anisotropy Constant (ANC).

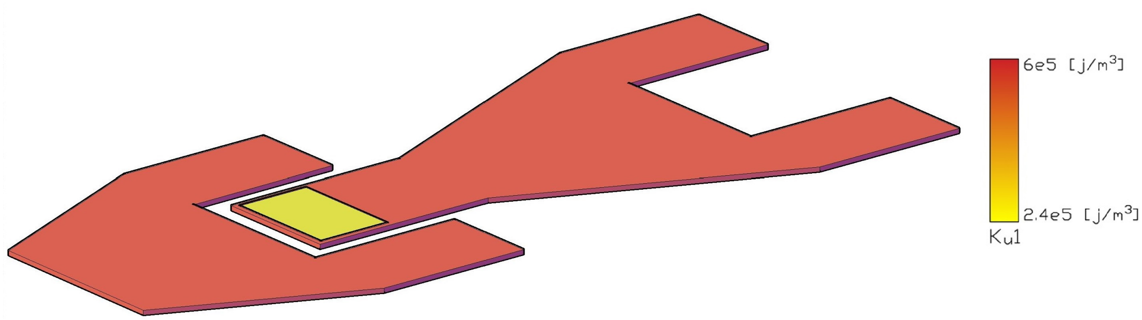

Figure 3.41: Inverter SingleLayer Uniaxial Anisotropy Constant

Below is shown a graph (See Figure [3.42]) which summarizes the simulations: by varying the distance d (distance between two magnets) and by varying the reduction of the ANC.

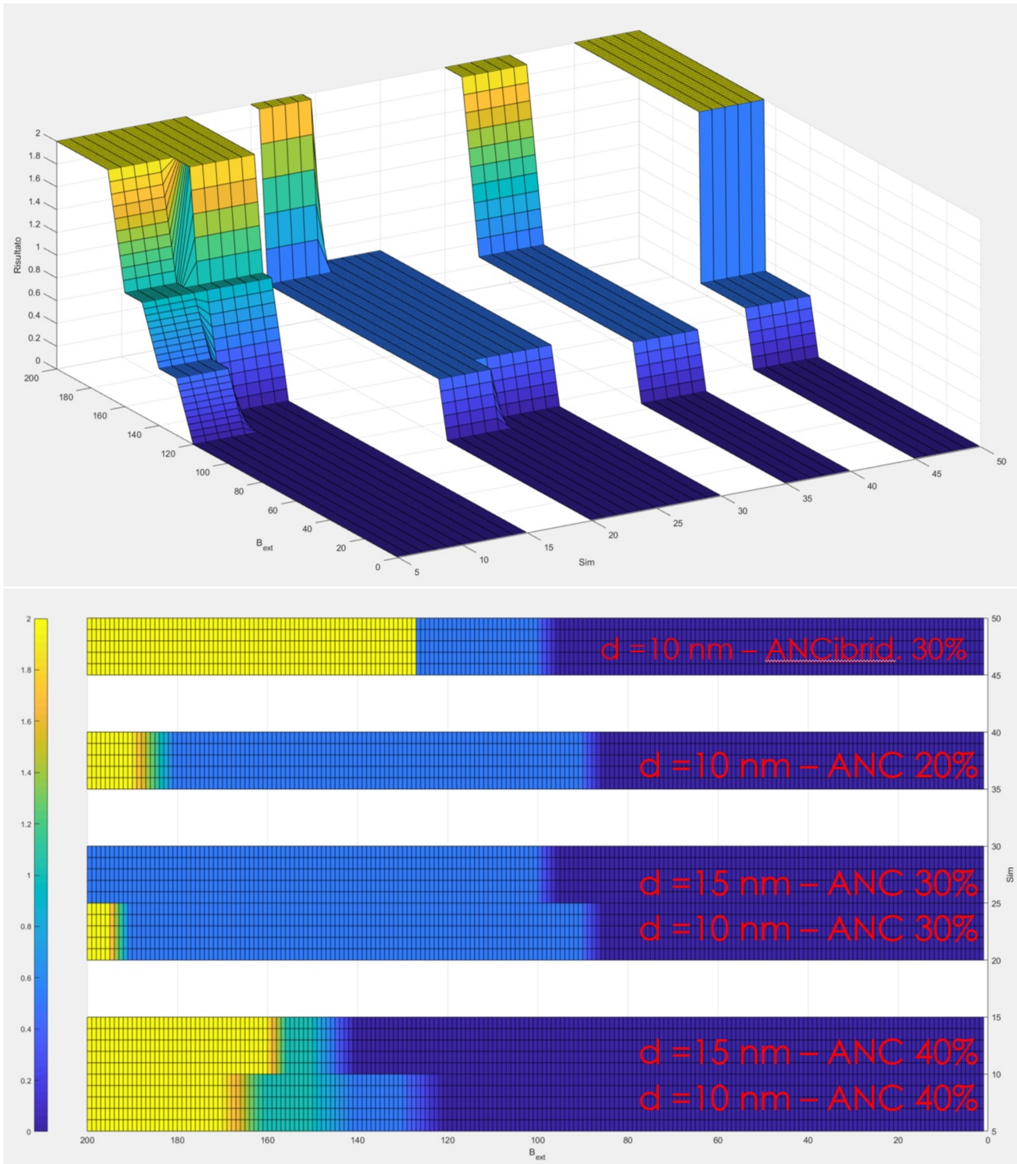

Figure 3.42: Result of Inverter SingleLayer, were 0(Blue) insufficient magnetic field - 0.5(Heavenly) partial nucleation - 1(Green) correct nucleation - 2(Yellow) Excessive magnetic field

An extract of a simulation of the SingleLayer inverter is shown in Figure [3.43] below.

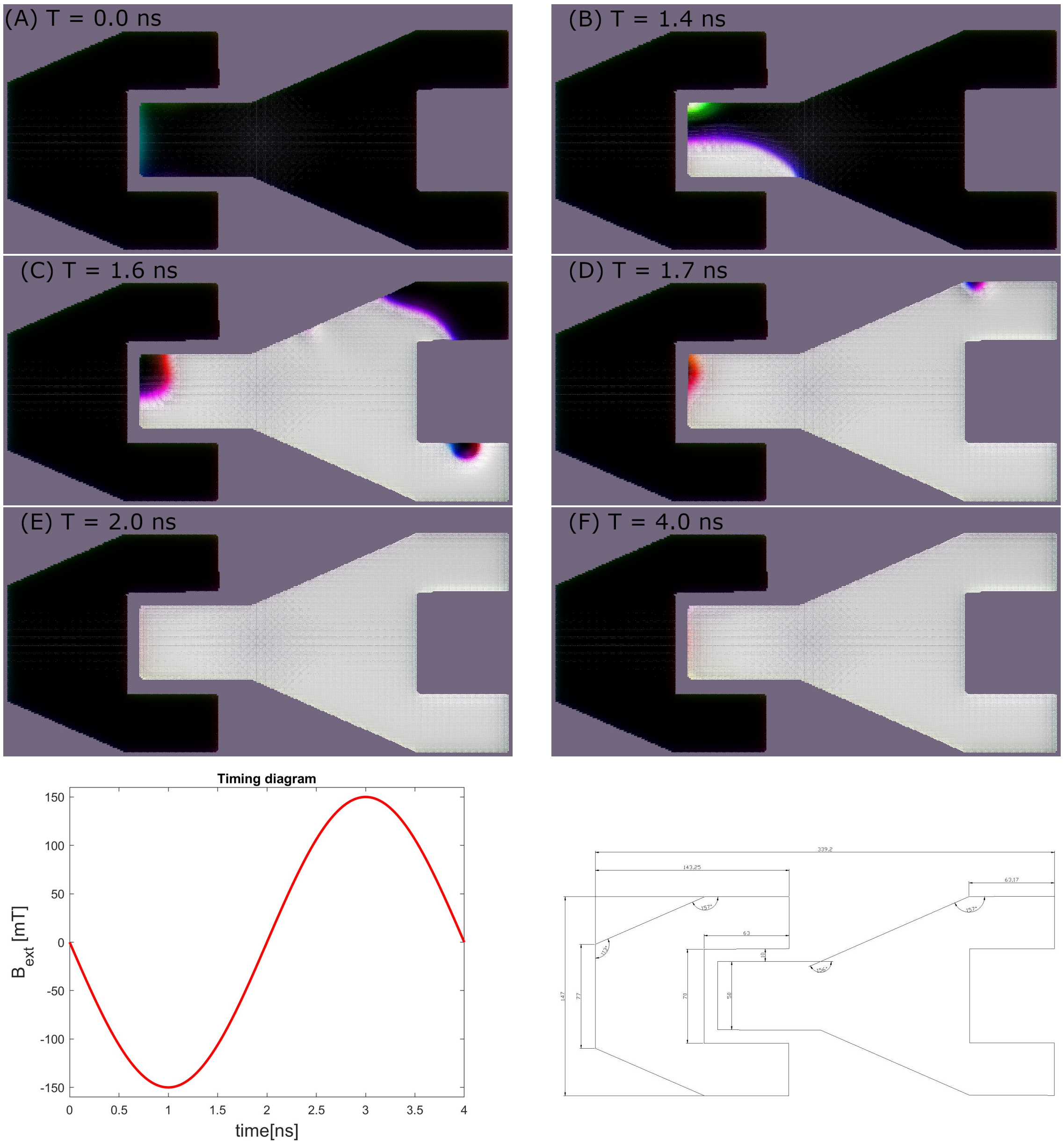

Figure 3.43: Simulation Inverter SingleLayer with $T = 0K$, $B_{ext} = -150mT@250MHz$ Sin, timing diagram (bottom), result obtained with MuMax3

As can be seen Figure [3.42] the results obtained were not the best and consequently was decided to deepen the study through a script MatLab in order to calculate the coupling field:

This script is based on the presence of a template like that shown in Figure [3.44.A] which represents the standard horseshoe-shaped of the parameterized inverter. Once all the values necessary to define it have been entered, it is divided into meshes. Then, the contribution of each square of the horseshoe mesh is calculated to each square of the output mesh. In particular what is shown in Figure [3.44.B] is the coupling field of the output.

In this way it has been ascertained that the problem was the fact of having a material too thin and to improve the performance and the efficiency of the inverter, it was necessary to make it multilayer.

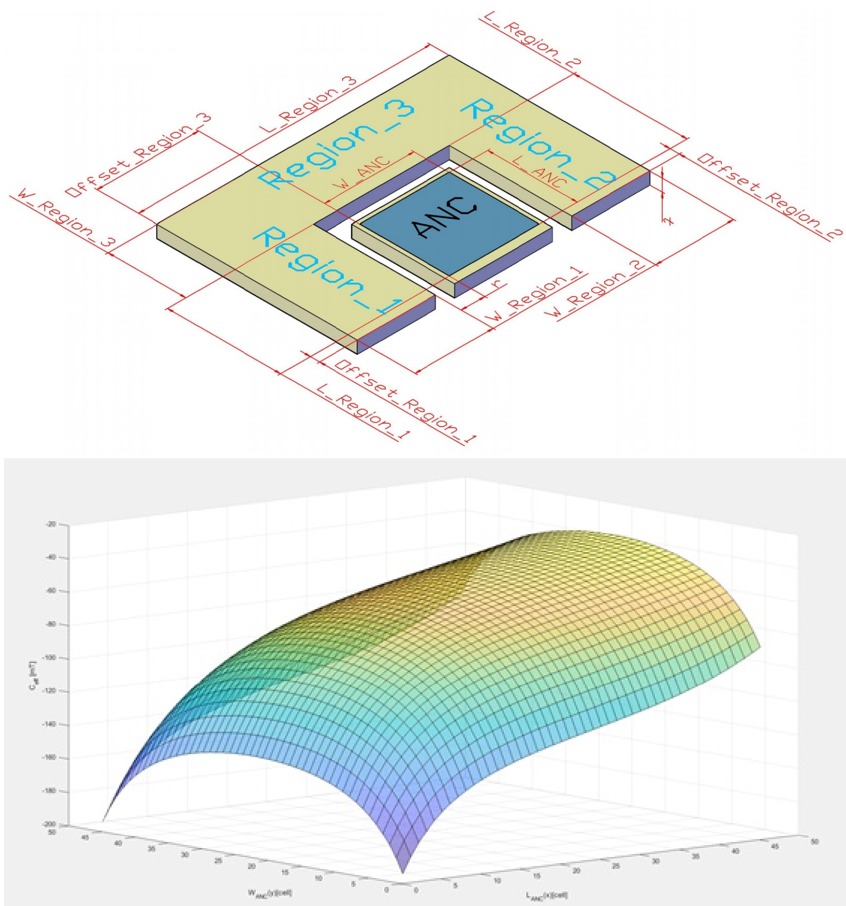

Figure 3.44: Inverter SingleLayer Coupling field

Once these calculations are carried out has been decided to continue to see how the probability of nucleation varies in the case of Singlelayer structure (thickness $=1.8nm$).

To do this, an additional MatLab script was needed that implemented the calculations described in [52] below:

$$P_{nuc}(t) = 1 - exp\left[-N(t)t_{clock}f_0 \cdot exp\left(-\frac{E_{0,ANC} \cdot (1-\frac{H_{eff}(t)}{H_{0,ANC}})^2}{K_bT}\right)\right] \tag{3.1}$$

$$E_{0,ANC} = K_{eff,ANC} \cdot V_{ANC} \tag{3.2}$$

$$H_{0,ANC} = \frac{2 * K_{eff,ANC}}{\mu 0 \cdot M_s} \tag{3.3}$$

with $H_{eff} = H_{ck} + H_{couplingfield}$ and $N(t) \in [0,1]$ evaluate the actual duration of the current field pulse. The results of this analysis are shown in Figure [3.45], while in section 3.5.2 you can see how varies the probability of nucleation in the case of Multilayer inverters.

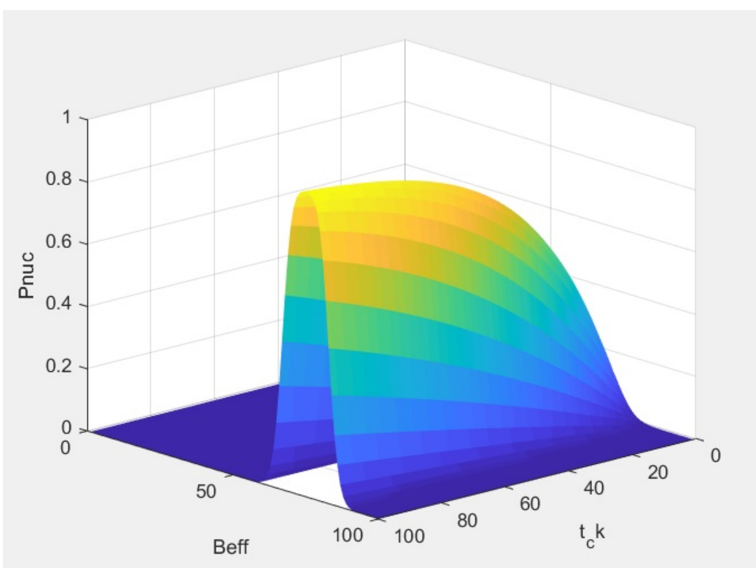

Figure 3.45: Inverter SingleLayer P_{nuc}

3.5.2 Inverter MultiLayer

the Multilayer inverter (thickness = 13.4nm) unlike the Singlelayer (thickness = 1.8nm) has been widely used in literature in fact, it is better thanks to the major coupling field that can be obtained thanks to the thickest structure (13,4nm versus 1.8nm of the singlelayer structure).

In fact, also in this case has been extracted using the same method shown in the previous Section (Section 3.5.1) the probability nucleation shown in figure [3.46] and it's immediately noticed a curve more flat than in the singlelayer case (thickness =1.8nm).

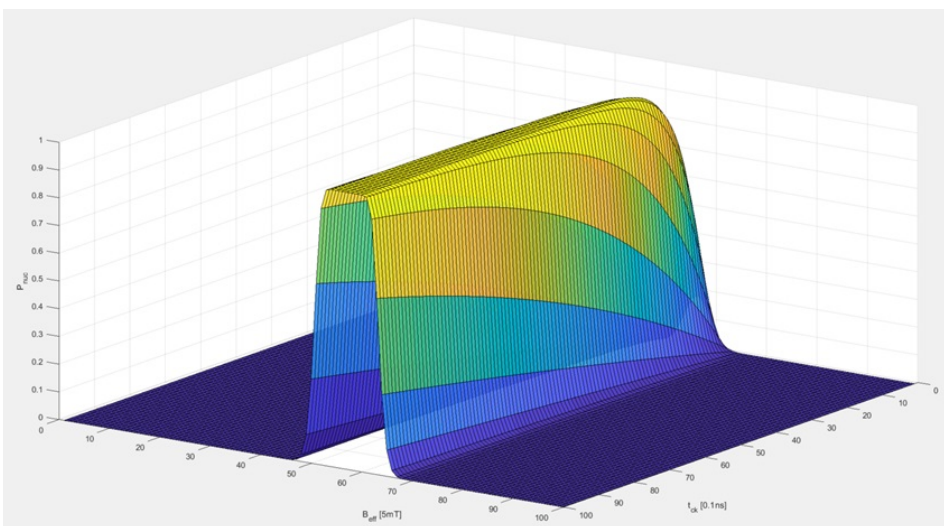

Figure 3.46: Inverter MultiLayer P_{nuc}

Also in this case simulations have been made to vary the distance d between the two magnets. The results are shown in the Figure 3.47 and it can be noticed a visible improvement both on the variation of the distance and on the variation of the external magnetic field.

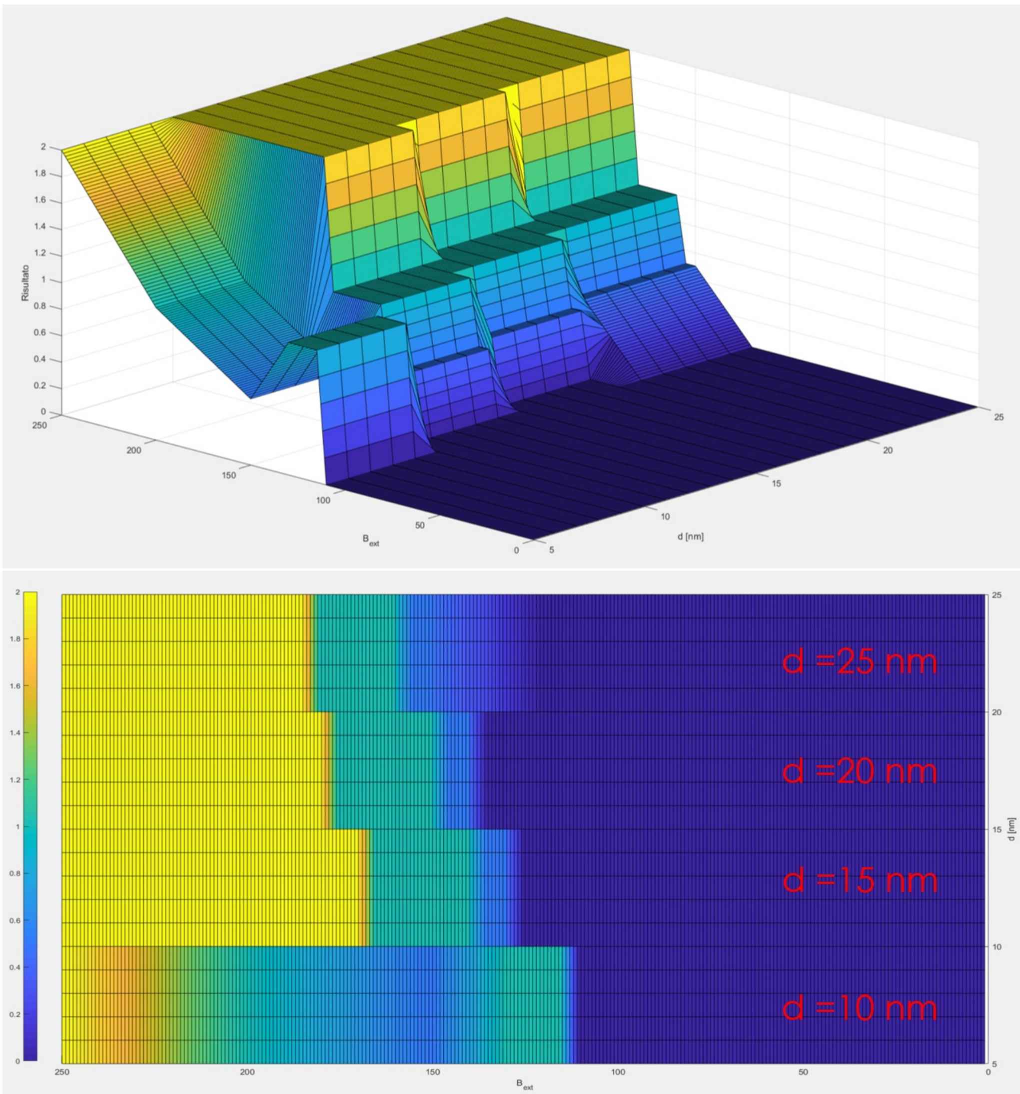

Figure 3.47: Result of Inverter MultiLayer, were 0(Blue) insufficent magnetic field - 0.5(Heavenly) partial nucleation - 1(Green) correct nucleation - 2(Yellow) Excessive magnetic field

Finally we report a simulation for a Multilayer inverter with a $d = 10nm$ distance and subjected to an external magnetic field of $160mT$ in Figure [3.48].

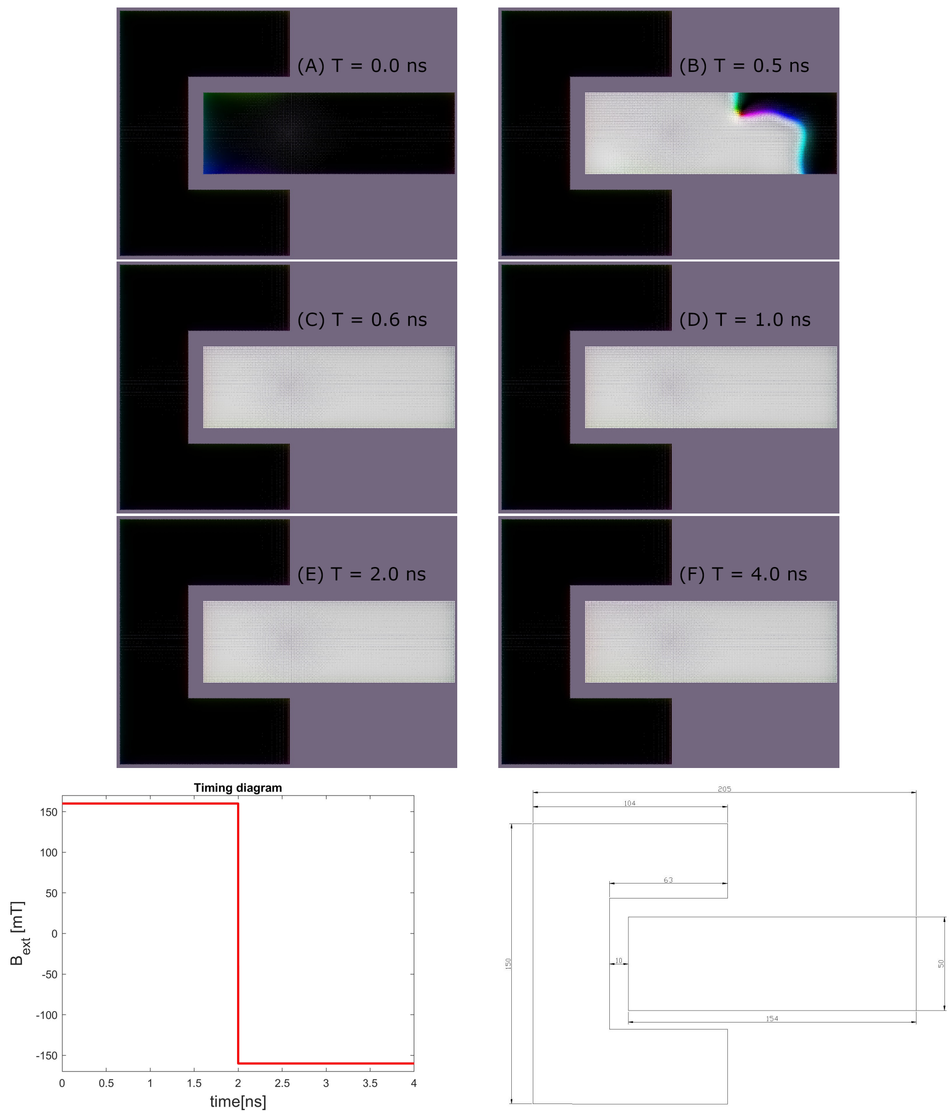

Figure 3.48: Simulation of Inverter SingleLayer with $T = 0K$, A-E :$B_{ext} = 160mT$, F :$B_{ext} = -160mT$, timing diagram (bottom), result obtained with MuMax3

Inverter MultiLayer T =300K

As regards room temperature tests, no tests were carried out for the Multilayer inverter since the results at T =0K were more than positive. However it refers to structures that are already widely studied and described in other articles, to deepen this aspect has been considered not necessary.

Chapter 4

Characterization

While studying the behavior of skyrmions and pNML at a structural and functional level it has been decided to make a complete characterization of skyrmions to be able to predict their behaviour when subjected to particular situations.

The most interesting physical and behavioral aspects studied are listed below :

- 4.1 - **Track width for skyrmions**: this study consists of putting a skyrmion within a track and gradually reducing its width to see if after the phase of energetic Relax() it survives to find the minimum track width.
- 4.2 - **Skyrmion Density**: a study similar to the previous one but in this case more skyrmions are put to find the maximum density of skyrmions as a function of the path width without loss of information.
- 4.3 - **Skyrmion velocity**: this study uses a long track to know the speed with which skyrmions travel it according to the density of current to which the track is subjected.
- 4.4 - **skyrmion under external magnetic field**: this study wants to understand the behaviour of skyrmions when subjected to an external magnetic field and in particular till which values it can be pushed before causing the extinction of the skyrmions
- 4.5 - **skyrmions's movements**: in this system skyrmions brings the 1/0 binary information, so it is important to check that in case of different Word the skyrmions behave the same way.
- 4.6 - **skyrmion stability**: it studies the stability of both skyrmions and pNML to decree in which of the two formats the information resists longer.

- **4.7 - static power and energy consideration**: static power consumption in a skyrmions system based on the current running through the track. It studied the energy contribution of various conversion blocks sk-Dw and vice versa.

Finally, we have also carried out a characterization of a ”Low Power” inverter subjected to an external magnetic field at much lower frequency in such a way the energy contribution of the external magnetic field is lower.

- **4.8 - Inverter low energy**: the inverter has the same structure of the one studied in the previous chapters but subjected to an external magnetic field oscillating at much lower frequencies to be able to use external magnetic fields at lower intensity and consequently save energy.

4.1 Track width for skyrmions

To carry out this characterization has been used a piece of track at first of $100nm \times 100nm \times 1.8nm$ dimension and a skyrmion with diameter of $14nm$ has been inserted at its central point.

Then, to relax the skyrmion a period of time of 1 ns passes and it is possible to notice how the interactions with the edges modified it.

This operation has been carried out several times by changing the width of the track from $100nm$ to $20nm$. This has been done excluding the parameter Temperature (See Section 4.1.1) and considering a room temperature $T = 300K$ (See Section 4.1.2)

4.1.1 Track width with T = 0K

The report of the simulations is shown in Figure [4.1] and the data about the skyrmions diameter are reported in Table [4.1].

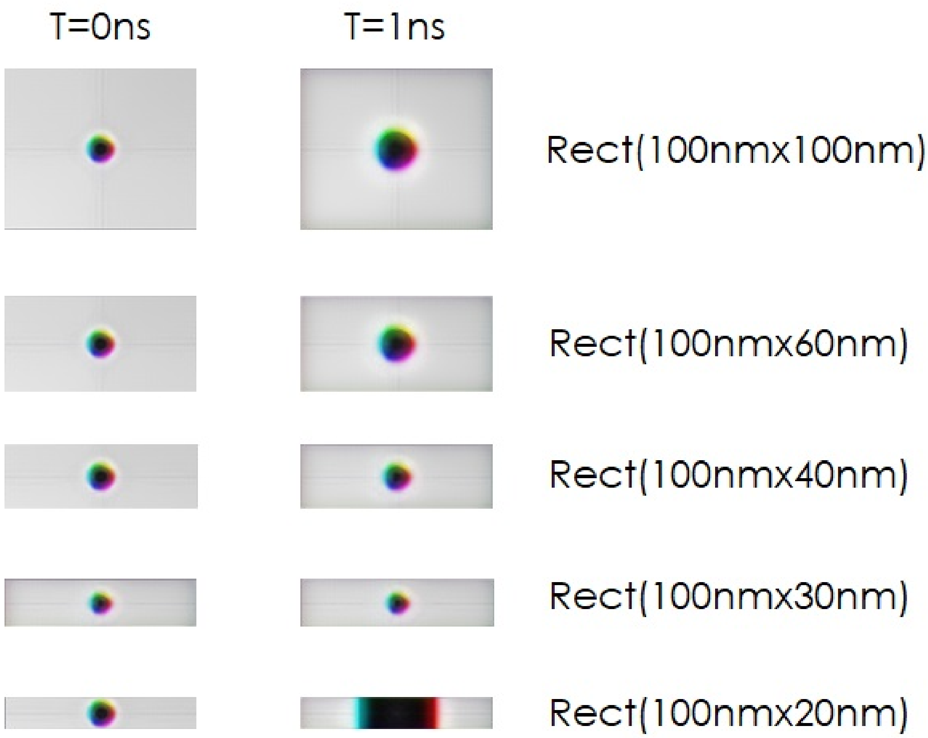

Figure 4.1: Simulation of track width with $T = 0K$, result obtained with MuMax3

Track Width	Skyrmion diameter	
	t = 0ns	t=1ns
$100nm$	$14nm$	$22nm$
$60nm$	$14nm$	$18nm$
$40nm$	$14nm$	$14nm$
$30nm$	$14nm$	$10nm$
$20nm$	$14nm$	/

Table 4.1: skyrmions diameter for different track width with $T = 0K$

In this case as you can see in Figure [4.1] up to a width of $40nm$ the skyrmions do not produce any variation due to the on-board effects. The situation changes reducing further the width of the line in fact, in a $100nm \times 30nm$ line the skyrmions are clearly flattened by the edges and consequently reduce their diameter. As can be seen in the skyrmion's velocity tests (See Section 4.3) the skyrmions in a 30nm wide track are much more sensitive and they cannot be pushed beyond certain velocities, otherwise it risks to make it explode against the edge and to lose information. Finally in the case of a $100nm \times 20nm$ track it is so small that it does not allow the skyrmion to exist and consequently turns into a Domain Wall pair.

4.1.2 Track width with T = 300K

The simulations report is shown in Figure [4.2] and the data about the skyrmions diameter are reported in Table [4.2].

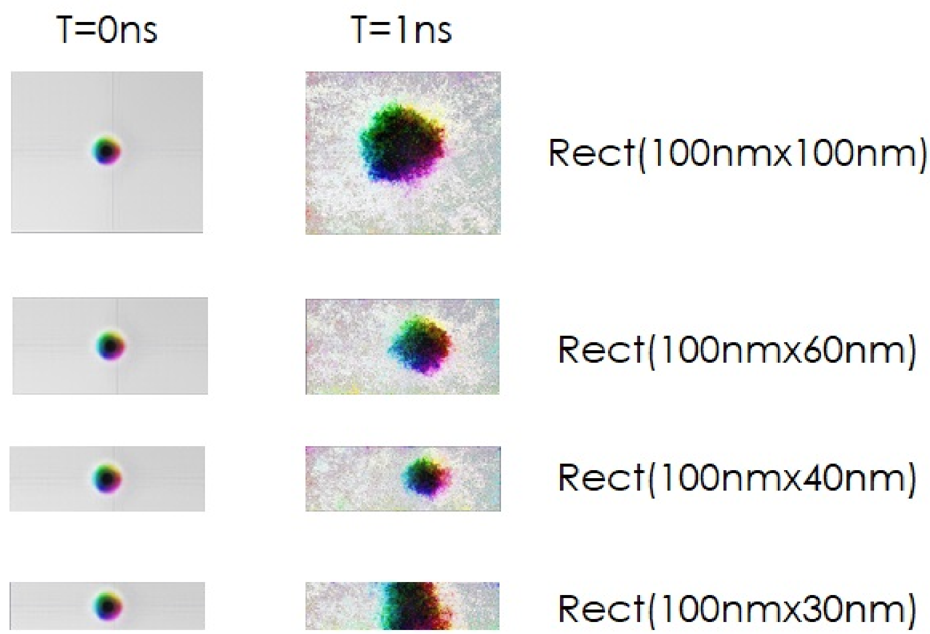

Figure 4.2: Simulation of track width with $T = 300K$, result obtained with MuMax3

Track Width	Skyrmion diameter	
	t = 0ns	t=1ns
$100nm$	$14nm$	$46nm$
$60nm$	$14nm$	$28nm$
$40nm$	$14nm$	$22nm$
$30nm$	$14nm$	/

Table 4.2: skyrmions diameter for different track width with $T = 300K$

The effect of temperature can be seen in fact, the edges of skyrmions are imprecise and develop micromovements. In this case as you can see in Figure [4.2] up to a width of 60nm the skyrmions do not produce any variation due to the on-board effects. It changes further reducing the width of the line in fact in the case of $100nm \times 40nm$ line the skyrmions are clearly flattened by the edges and consequently they reduce their diameter. In the case of $100nm \times 30nm$ track unlike the previous case (See Section 4.1.1), the skyrmion does not exist and it is converted into a domain wall pair because of the addition of thermal noise.

4.2 Skyrmion Density

To make this characterization a rectangular track piece 400nm length is used. Three skyrmions at regular distance (at first 30nm distant) are inserted into it to see after the energetic relaxation at what distance they settle because of the repulsion effects between skyrmions. For this reason we waited a period of 1ns to relax energetically the skyrmions and it showed how the interactions with the edges and between them modified their positions.

This operation has been performed several times by varying the track width from $70nm$ to $30nm$.This has been done excluding the parameter Temperature (See Section 4.2.1) and considering a room temperature $T = 300K$ (See Section 4.2.2)

4.2.1 Density with T = 0K

In the case of temperature = 0K the simulation report is shown in Figure [4.3]

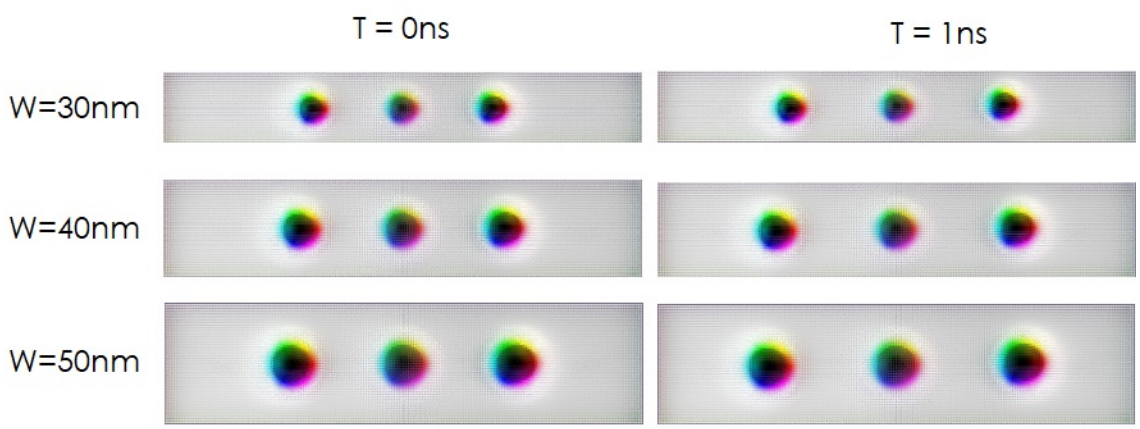

Figure 4.3: Simulation for Density with $T = 0K$, result obtained with MuMax3

In this case as can be seen in Figure [4.3] basing on the width of the line, the skyrmions have a slightly different diameter. This varies the forces of repulsion Skyrmions-Skyrmions and as a result are positioned slightly more distant from each other. Once they reach this position, they maintain this distance.

The distances can be seen in Figure [4.3] and are collected in Table [4.3].

Track Width [nm]	skyrmions diameter [nm]	skyrmions distance [nm]	
		t = 0 ns	t = 1 ns
30	11	38	44
40	14	42	52
50	17	47	54

Table 4.3: skyrmion diameter and distance for Density simulation with $T = 0K$

4.2.2 Density with T = 300K

In the case of temperature T= 300K the simulation report is shown in Figure [4.4]

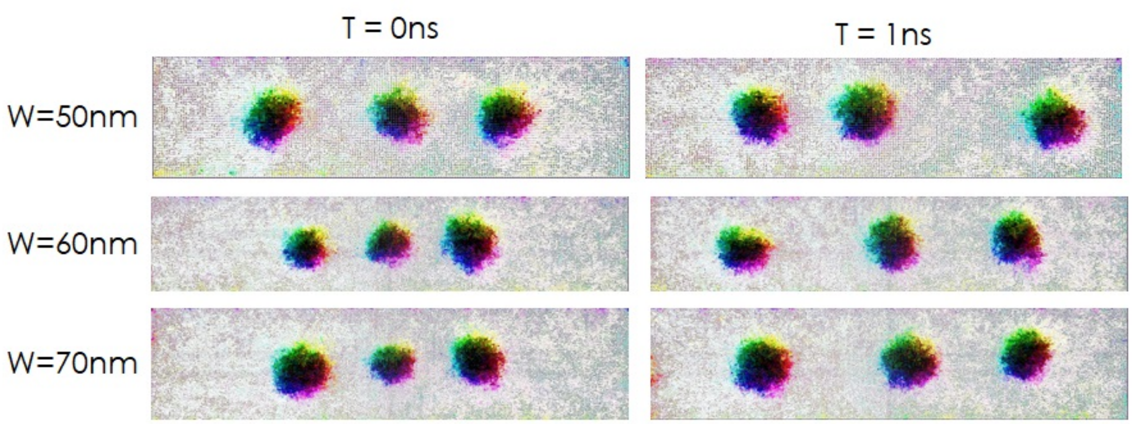

Figure 4.4: Simulation for Density with $T = 300K$, result obtained with MuMax3

In this case as can be seen in Figure [4.4] basing on the width of the line, the skyrmions have a slightly different diameter. This varies the forces of repulsion Skyrmions-Skyrmions and as a result they are positioned slightly more distant one another. Once reached this position they maintain this distance.

Can also be seen that the distances are not homogeneous because when subjected to a temperature $> 0K$ they tend to slightly move.

The distances can be seen in figure [4.4] and are collected in Table [4.4].

Track Width [nm]	skyrmions diameter [nm]	skyrmions distance [nm]	
		t = 0 ns	t = 1 ns
50	20	48.5nm	44nm - 79nm
60	25	52nm	77nm - 93nm
70	30	59nm	73nm - 92nm

Table 4.4: skyrmion diameter and distance for Density simulation with $T = 300K$

4.3 Skyrmion velocity

To carry out this characterization a piece of track has been used. At first, it was $100nm \times 60nm \times 1.8nm$ and a skyrmion was inserted, then a constant current density was applied to the whole simulation.

To extract the data about the average speed from the simulations, a graphic tool (GIMP) was used. It allows the comparison of two images representing different time instants of our simulation. In this way, knowing exactly the time that elapses between the two images and calculating the displacement of the skyrmion through the graphic tool, it is possible to calculate the average speed as $Velocity = \frac{Space}{Time}$.

This operation has been carried out several times by changing the width of the track from $70nm$ to $30nm$, and the density of current j for each track width. Simulations have been made excluding the parameter Temperature (See Section 4.3.1) and considering an ambient temperature $T = 300K$ (See Section 4.3.2)

4.3.1 Skyrmions velocity with T = 0K

In the case of temperature T = 0K the results obtained through the method described in the Section 4.3 are shown in the graph in Figure [4.5].

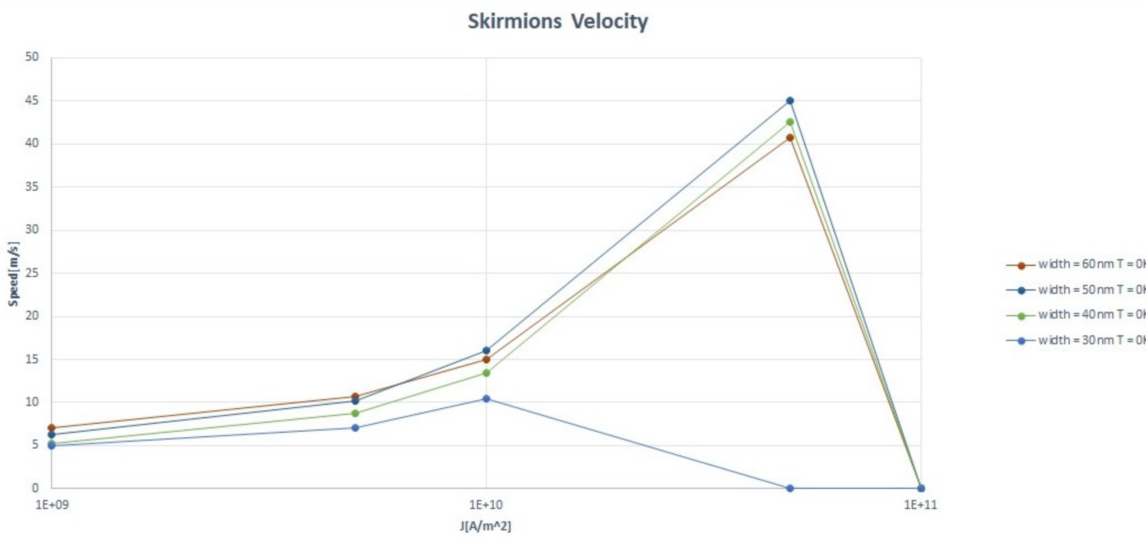

Figure 4.5: Simulation of skyrmions velocity with $T = 0K$, result obtained with MuMax3

In Figure [4.5] can be observed that the average speed of skyrmions increases at the increasing of the density of current. In fact, there is a peak of speed at superficial density of current of $j = 5e10[\frac{A}{m^2}]$. This is valid for all the track widths superior than 30nm. In the case of a track 30nm wide it can be seen that the speed curve follows the other ones. When the values of current density are higher than $j = 1e10[\frac{A}{m^2}]$, the skyrmions overcome the repulsion of the board and crashes against. This happens because the skyrmions travel along a small track and become much more sensitive than in the previous cases and therefore it is easier to extinguish them.

the data reported in the graph of figure [4.5] are collected in Table [4.5].

4.3.2 Skyrmions velocity with T = 300K

In the case of temperature T = 300K the results obtained through the method described in the Section 4.3 are shown in the graph in Figure [4.6].

Current density $[\frac{A}{m^2}]$	Track Width			
	30 nm	40 nm	50 nm	60 nm
1e9	5 m\s	5.2 m\s	6.25 m\s	7 m\s
5e9	7 m\s	8.75 m\s	10.25 m\s	10.75 m\s
1e10	10.5 m\s	13.5 m\s	16 m\s	15.05 m\s
5e10	0 m\s	42.55 m\s	45 m\s	40.75 m\s
1e11	0 m\s	0 m\s	0 m\s	0 m\s

Table 4.5: skyrmion velocity of different track width subjected to different current density with $T = 0K$

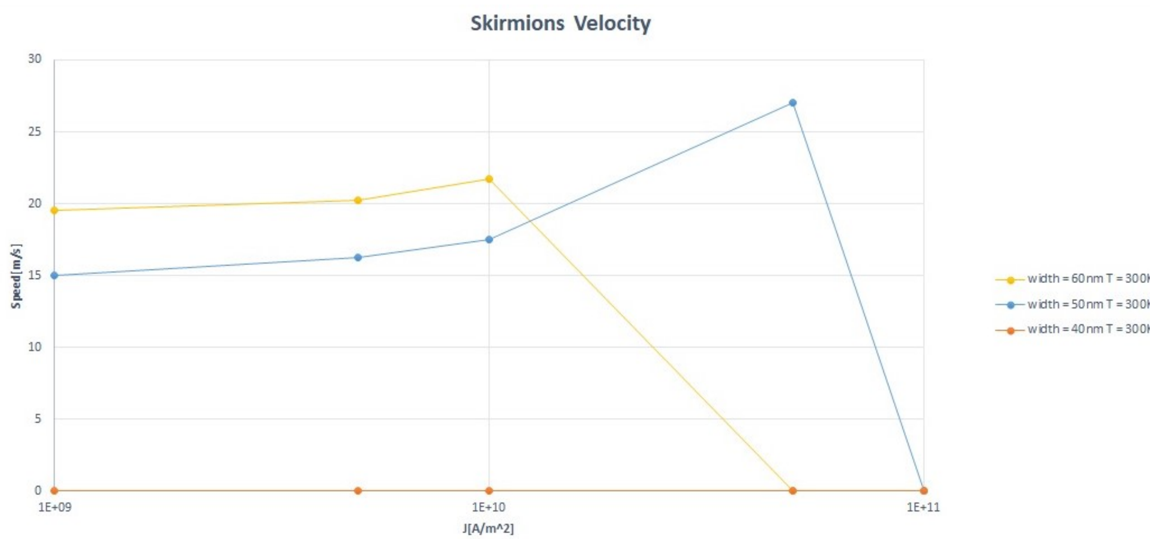

Figure 4.6: Simulation of skyrmions velocity with $T = 300K$, result obtained with MuMax3

In this case as can be seen in Figure [4.6]can be observed that the average speed of skyrmions increases at the increasing of the density of current. In fact, there is a peak of speed at superficial density of current of $j = 5e10[\frac{A}{m^2}]$. In a track 40nm wide it is possible to insert a skyrmion but as soon as it is subjected to a current density, it impacts against the edge and as a consequence a larger track is required to allow the skyrmions to move without risk its elimination.

The data shown in the graph in Figure [4.6] are collected in Table [4.6].

Current density $[\frac{A}{m^2}]$	Track Width		
	40 nm	50 nm	60 nm
1e9	0 m\s	15 m\s	19.5 m\s
5e9	0 m\s	16.27 m\s	20.25 m\s
1e10	0 m\s	17.5 m\s	21.75 m\s
5e10	0 m\s	27 m\s	0 m\s
1e11	0 m\s	0 m\s	0 m\s

Table 4.6: skyrmion velocity of different track width subjected to different current density with $T = 300K$

4.3.3 Skyrmions velocity combined

This section compare how the average speed of a skyrmion varies from simulations with temperature T=0K to those with a temperature T=300K, as can be seen in the graph in Figure [4.7].

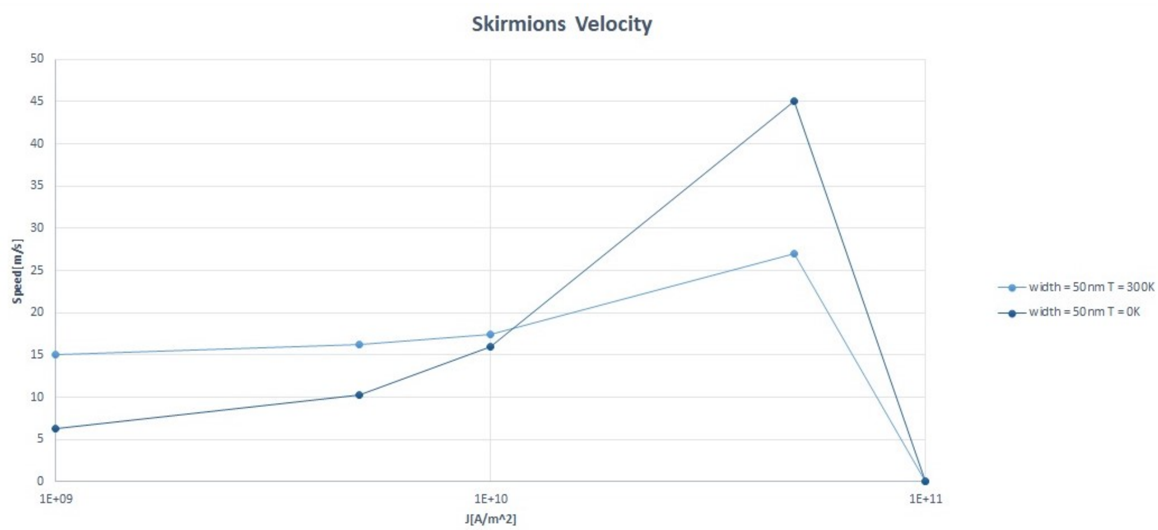

Figure 4.7: Comparative of Skyrmions velocity with $T = 0K$ versus $T = 300K$, result obtained with MuMax3

In the case taken into account there is a track 50nm wide, as can be seen in the graph in Figure [4.7]. At lower densities of current $j < 1e10[\frac{A}{m^2}]$ the equal current speed is bigger at T=300K. In contrast at current density greater than $j = 1e10[\frac{A}{m^2}]$, the slope of the curve speed - current density changes in favor of the case with T=0K and in fact the speed peak is $45\frac{m}{s}$ for case T=0K and $27\frac{m}{s}$ for the case T=300K.

4.4 Skyrmion under external magnetic field

To carry out this characterization has been used a piece of track at first with $50nm \times 50nm \times 1.8nm$ dimensions and a skyrmion has been inserted into the central part.

Then an constant external magnetic field has been applied, whose intensity varies from one simulation to another. The diameter of skyrmion has been measured through a graphic tool after 1ns.

This operation has been carried out several times by changing the size of the track in three variants:

- $50nm \times 50nm \times 1.8nm$
- $40nm \times 40nm \times 1.8nm$
- $30nm \times 30nm \times 1.8nm$

The external magnetic field has been changed from $-200mT$ to $+200mT$, and simulations have been made both by excluding the parameter Temperature (See Section 4.4.1) and considering an ambient temperature $T = 300K$ (See Section 4.4.2)

4.4.1 skyrmion under external magnetic field with T = 0K

In the graph shown in Figure [4.8] can be seen how the diameter of skyrmions subjected to external magnetic field varies. The results have been obtained following the procedure described in Section 4.4.

As can be notice in the graph, the diameter of skyrmion grows linearly with the size of the track if not subjected to an external magnetic field of 0mT. This happens because in the case of a $50nm \times 50nm$ track, the on-board repulsion effects are significantly lower than in a smaller track.

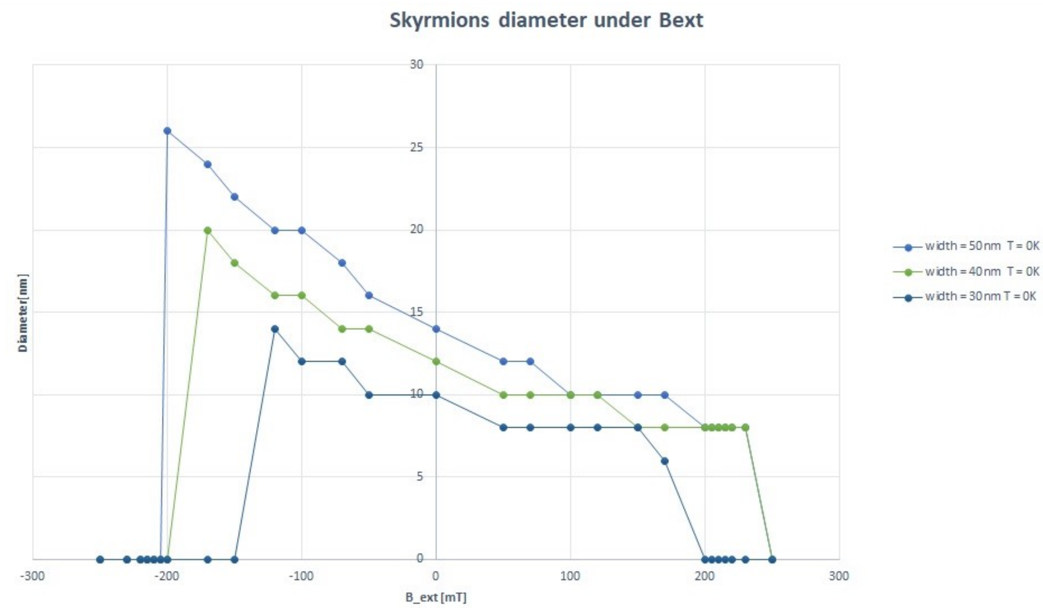

Figure 4.8: Skyrmion under external magnetic field with $T = 0K$, result obtained with MuMax3

Taking as a reference the track 50nm wide can be seen how the skyrmion can withstand magnetic fields ranging from $-200mT$ at $+200mT$. The skyrmion changes its diameter in 26nm when the external magnetic field is -200mT and in 8nm when the external magnetic field is 200mT.

Another important aspect consists of reduction the tolerance of the skyrmion through the reduction of the size of the track subjected to a negative magnetic field. To observe in a more detailed way the data, the graphic in Figure [4.8] and Table [4.7] can be consulted.

External Magnetic field [mT]	Track Width		
	50nm	40nm	30nm
-200	26 nm	0 nm	0 nm
-150	22 nm	18 nm	0 nm
-100	20 nm	16 nm	12 nm
-50	16 nm	14 nm	10 nm
0	14 nm	12 nm	10 nm
50	12 nm	10 nm	8 nm
100	10 nm	10 nm	8 nm
150	10 nm	10 nm	8 nm
200	8 nm	8 nm	0 nm

Table 4.7: diameter of skyrmion subjected to external magnetic field with $T = 0K$

4.4.2 Skyrmion under external magnetic field with T = 300K

In the graph shown in Figure [4.9] can be seen how the diameter of skyrmions subjected to external magnetic field varies. The results have been obtained following the procedure described in Section 4.4.

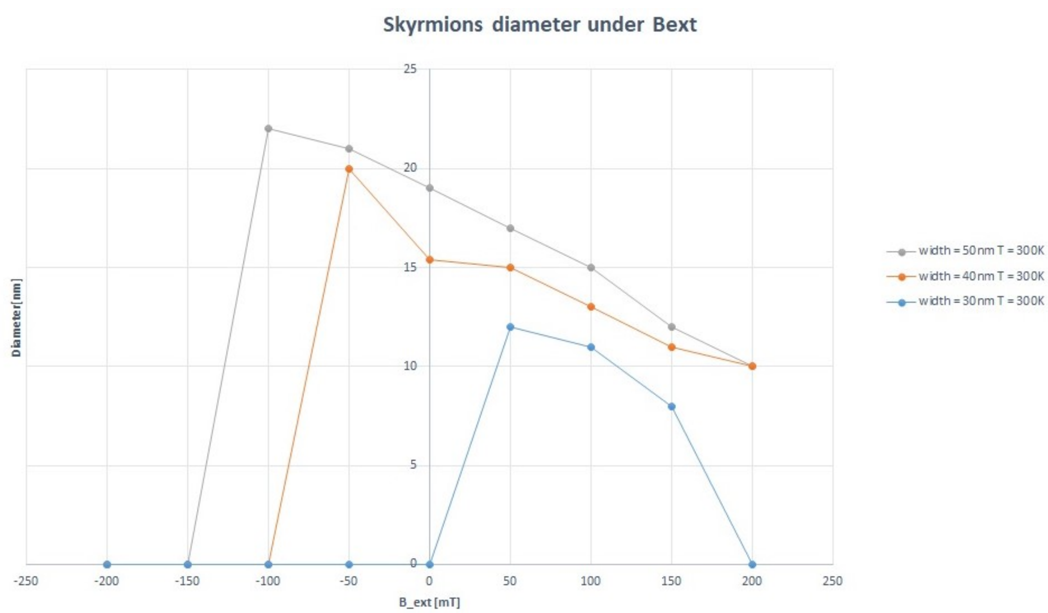

Figure 4.9: Skyrmion under external magnetic field with $T = 300K$, result obtained with MuMax3

The graph in Figure [4.9] confirms what is shown in Section 4.1.2:a skyrmion in

30nm track subjected to an external magnetic field of 0mT, it does not resist and turns into a Domain Wall Pair.

Regarding the simulations with the other track dimensions it can be noticed that even in the 50nm track, the maximum negative that can be withstand is -100mT while the positive case is not a problem.

This happens because the addition of the temperature factor makes sure that the dimensions of the skyrmions are slightly larger and consequently are more sensitive to the negative external magnetic field which tends to increase further the diameter.

To observe in more detail the data from which is extracted the graphic in Figure [4.9] you can see the Table [4.8].

External Magnetic field [mT]	Track Width		
	50nm	40nm	30nm
-200	0 nm	0 nm	0 nm
-150	0 nm	0 nm	0 nm
-100	22 nm	0 nm	0 nm
-50	21 nm	20 nm	0 nm
0	19 nm	15.4 nm	0 nm
50	17 nm	15 nm	12 nm
100	15 nm	13 nm	11 nm
150	12 nm	11 nm	8 nm
200	10 nm	10 nm	0 nm

Table 4.8: diameter of skyrmion subjected to external magnetic field with $T = 300K$

4.4.3 Skyrmion under external magnetic field Combined

This section compares how the diameter of a skyrmion varies switching from a simulation with temperature T=0K to another with temperature T=300K, as it can be seen in the graph in Figure [4.10].

In the case taken into account there is a track 50nm wide and as you can see from the graph in Figure [4.10] the skyrmion with T=300K has a larger diameter when subjected to the same external magnetic field.

Also the larger size of the skyrmions make it more sensitive to negative magnetic fields and consequently less sensitive to positive magnetic fields. In fact, we pass from having a tolerance to magnetic fields from [-200mT - +200mT](case of T = 0K) to [-100mT - +200mT](case of T = 300K).

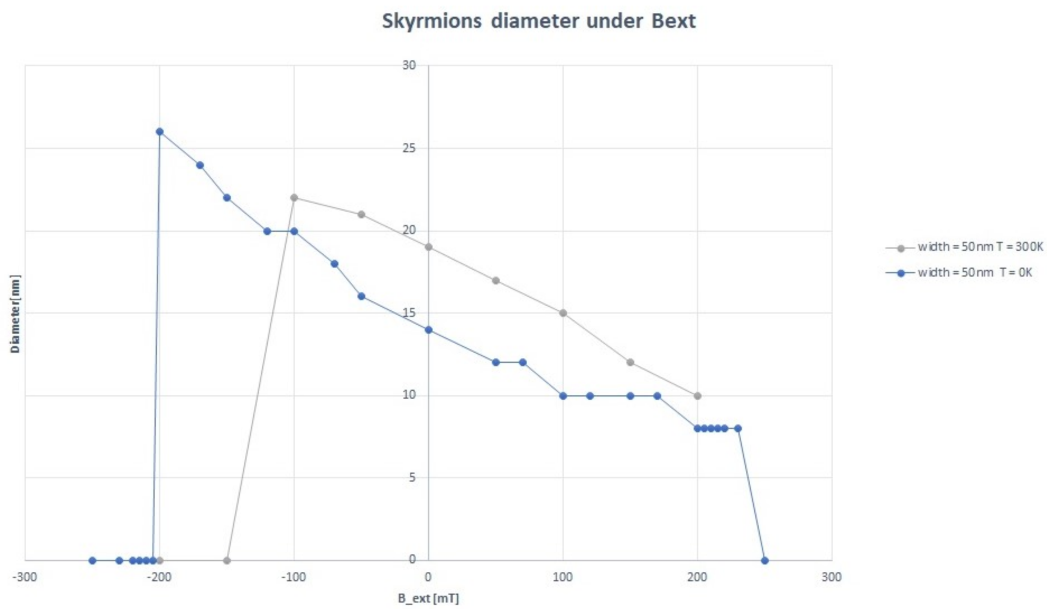

Figure 4.10: skyrmion under external magnetic field with $T = 0K$ versus $T = 300K$, result obtained with MuMax3

4.5 skyrmions movement

An essential quality to make sure that skyrmions are used as a medium for data transport is to be able to move 1 (presence of skyrmions) or 0 (absence of skyrmions) equally.

In fact, simulations have been made to verify if this feature is functional. Simulations have been made both excluding the parameter Temperature (See Section 4.5.1) considering an room temperature $T = 300K$ (See Section 4.5.2)

4.5.1 skyrmion movement with T = 0K

To confirm the correct functioning of this quality, a pair of simulations are necessary. These simulations are based on a skyrmions track 400nm long and 50nm wide where the skyrmions (with a 17nm diameter and 60nm distant from each other) moves in shape of two different words.

In the first simulation there is the word ”111”, while in the second one the word ”101”. So, through a time synchronization of the two simulations the first ”1” and the second ”1” must be in the same place after a certain period of time. An extract of the simulations is shown in Figure [4.11].

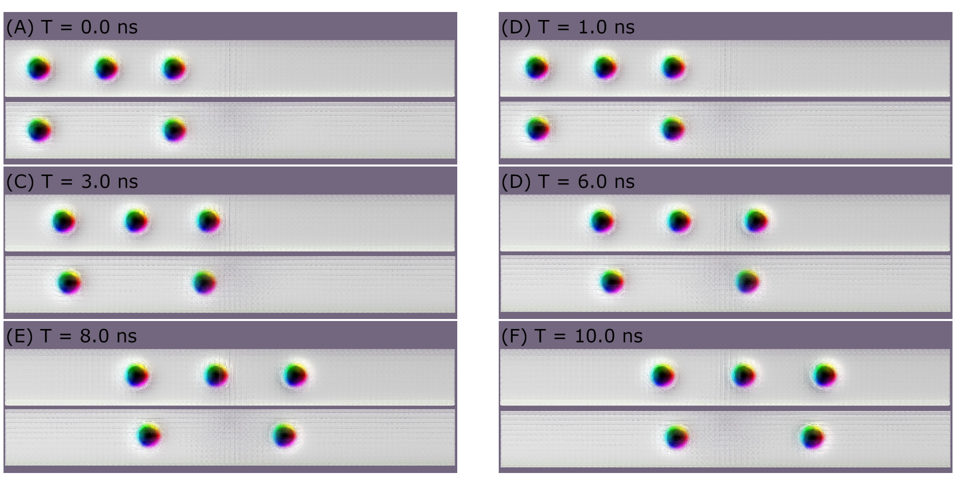

Figure 4.11: Skyrmion’s movements with $T = 0K$, $J = -1e10A/m^2$, result obtained with MuMax3

4.5.2 skyrmion movement with T = 300K

For the sake of completeness, simulations were also made with T=300K but in this case it is more difficult to ensure this behaviour because of the skyrmions micro-movements due to the temperature.

These simulations are based on a skyrmions track 400nm long and 50nm wide where the skyrmions (with a 20nm diameter and 67nm distant from each other) moves in shape of two different words, "111" and "110". An extract of the simulations is shown in Figure [4.12].

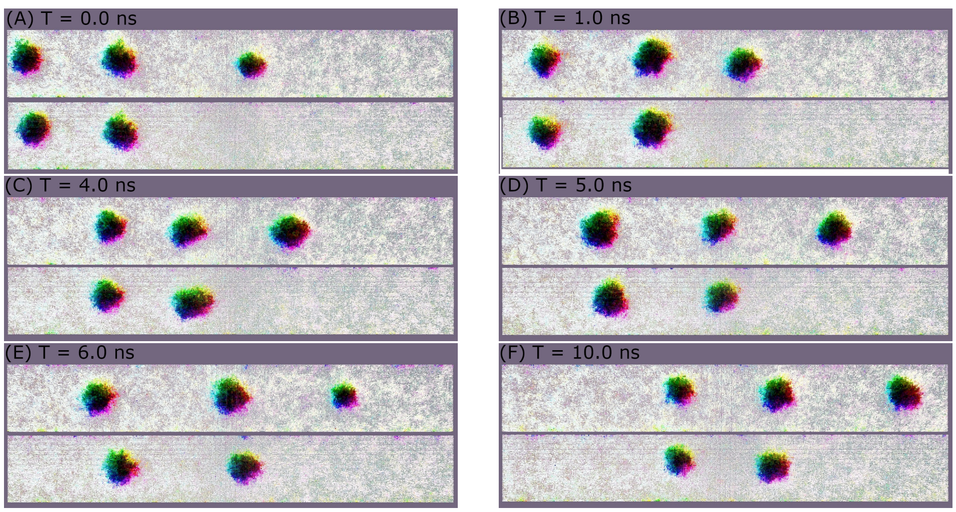

Figure 4.12: Skyrmion's movements with $T = 300K$, $J = -1e10A/m^2$, result obtained with MuMax3

4.6 skyrmion stability

The comparison of the stability between skyrmions and pNML, is based on four simulations made to compare the four possible states :

- Magnetized magnet +1
- Magnetized magnet -1
- Magnetized magnet +1
- Magnet with Skyrmion

from each of these simulations, information regarding the energy components: $E_{exchange}$, E_{ani}, E_{Zeeman} and E_{demag} which added together give the total energy (E_{total}).

It is calculated the variation of energy between the two different magnetic states (”+1” ”-1” and ”+1” ”sk”) finding ΔE. subsequently the *Stability* is calculated through the following formula :

$$\Delta E_{pNML} = E_{+1} - E_{-1} \tag{4.1}$$

$$Stability_{pNML} = \frac{\Delta E_{pNML}}{K_b T} \tag{4.2}$$

$$\Delta E_{Sk} = E_{+1} - E_{sk} \tag{4.3}$$

$$Stability_{Sk} = \frac{\Delta E_{Sk}}{K_b T} \tag{4.4}$$

This procedure and these calculations are repeated for a series of structures by comparing Skyrmions and pNML on different sizes of magnets $50nm \times 50nm$ (where the skyrmion have a diameter of $20nm$), $60nm \times 60nm$ (where the skyrmion have a diameter of $25nm$) e $70nm \times 70nm$ (where the skyrmion have a diameter of $30nm$).

Simulations were made with the pNML both on multilayer and singlelayer magnets and the skyrmion on singlelayer magnets. The results of these simulations are collected in the bar chart in Figure [4.13].

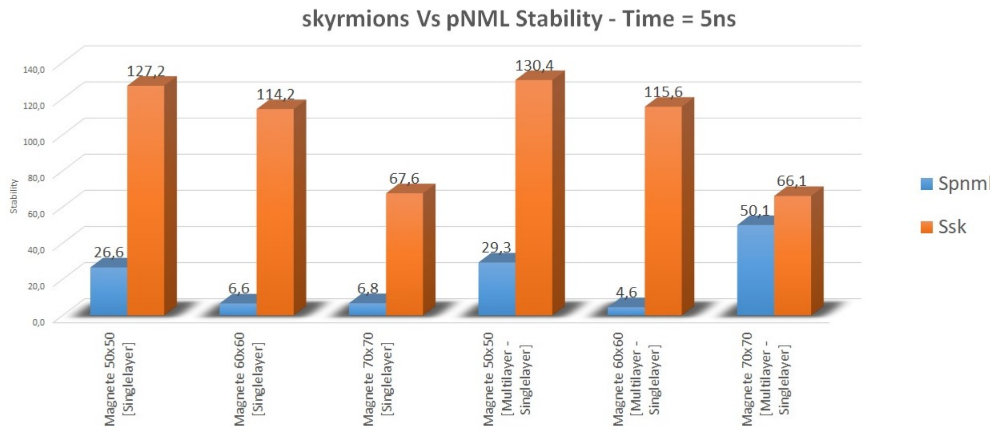

Figure 4.13: Skyrmion Versus pNML Stability - Time 5ns, result obtained with MuMax3

From the simulations can be noticed that the skyrmions tend always to be better than the pNML in terms of stability, regardless the size and the thickness of the magnet.

4.7 Static power and energy consideration

Some considerations about the power and the energy of skyrmions line, start by describing the line's shape and its resistivity. In fact we considered the track as a resistive line that can be seen in Figure [4.14].

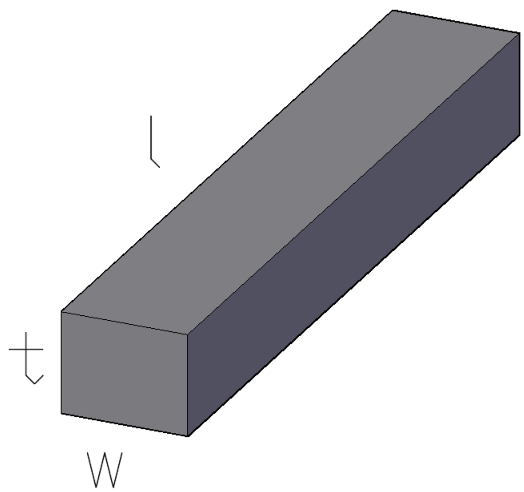

Figure 4.14: skyrmion track as resistive line

Considering a line with $t = 2nm$ (thickness), $w = 50nm$ (width), $\rho = 3.10e - 7$ (resistivity) and 10 long. The static power of this line depends on the current density that varies from $1e9A/m^2$ to $5e10A/m^2$ as shown in the Table [4.9].

Current density $[A/m^2]$	$P_{10\mu m}[W]$
1e9	3.10e-10
1e10	3.10e-8
2e10	1.24e-7
3e10	2.79e-7
4e10	4.96e-7
5e10	7.75e-7

Table 4.9: static power of skyrmions track for different current density value

Once these calculations were made, it was decided to increase the complexity and make considerations regarding the energy component necessary to travel the line and to carry out the Sk to DW conversions and vice versa :

- **4.7.1 - Energy Track Consideration**
- **4.7.2 - Energy Conversion Dw - Sk Consideration**
- **4.7.3 - Energy Conversion Sk - Dw Consideration**

4.7.1 Energy Track Consideration

To make some considerations about the track, a MatLab script is used to model it as resistive line by exploiting a template shown in Figure [4.15].

Figure 4.15: Energy Track Consideration MatLab template

The first part of the script calculates, the number of skyrmions that can be inserted in to a track $100\mu m$ long (data extracted from Section 4.2). 1852 skyrmions may exist in shape of a word and if the track is used as a skyrmions accumulator (when the important thing is the skyrmions presence or absence and not their position), they can be 5556.

In the second part of the script, considerations were made on the energy needed to allow a skyrmion to travel the entire line. By using the speed data obtained in the Section 4.3 the travel times have been calculated.

The results obtained are collected in the Table [4.10] where the variation of energy as function of current density can be noticed.

Current density $[A/m^2]$	$E_{10\mu m}[J]$
1e9	4.96e-14
5e9	7.56e-13
1e10	1.94e-12
5e10	1.72e-11

Table 4.10: Result of energetic consideration for skyrmions track

4.7.2 Energy Conversion Dw - Sk Consideration

To make an approximate analysis of the energy input necessary to make the conversion from Domain Wall to Skyrmions, we have referred to some simulations discussed in the Section 3.1. All calculations were performed through a MatLab script that uses the template shown in Figure [4.16].

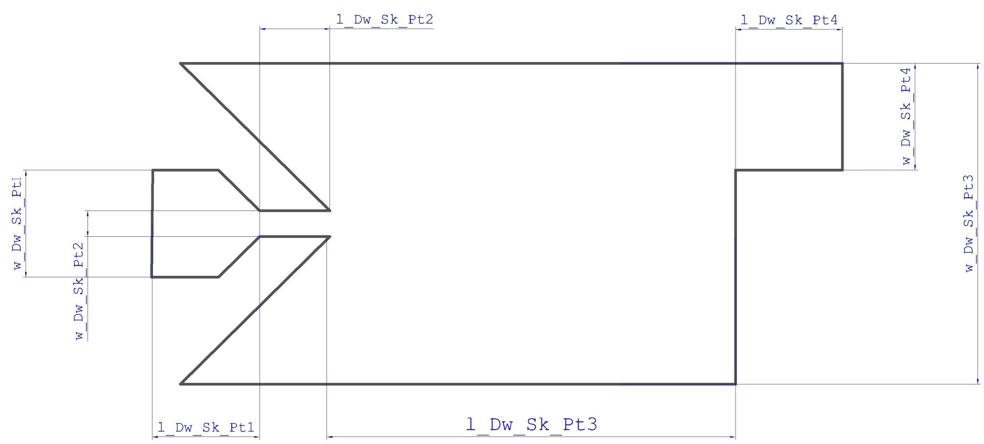

Figure 4.16: Energy DW to SK Consideration MatLab template

The script calculates the amount of the energy of the two pulses necessary to complete the transition Dw-Sk. The transition last 550ps and the energy necessary to complete it is $3.34e-15J$.

4.7.3 Energy Conversion Sk - Dw Consideration

To make an approximate analysis of the energy input necessary to make the conversion from Skyrmions to Domain Wall, some simulations already dealt with in the

Section 3.1. All the calculations were performed through a MatLab script that uses a template shown in Figure[4.17].

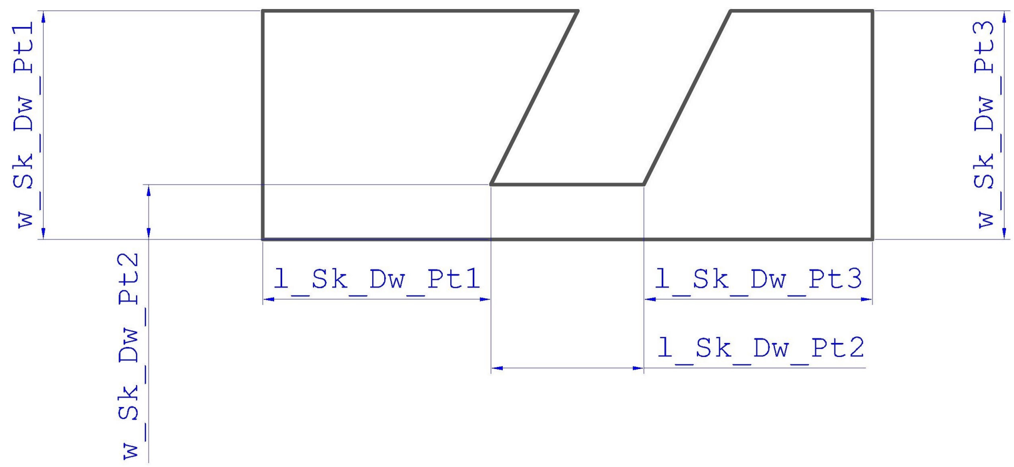

Figure 4.17: Energy SK to DW Consideration MatLab template

The script calculates the amount of the energy of the pulses necessary to complete the transition Sk-DW. The transition last 2ns and the energy necessary to complete it is $1.55e - 16J$.

4.8 Inverter low energy

The low power inverter arises from the necessity to verify the possibility of making the system work at a lower frequency in order to be able to consume less energy. The energy consumption is strongly dependent on the clock frequency of the external magnetic field.

From this idea, the need to test the inverters at a frequency of 25MHz, that is a frequency ten times lower than the frequency tested for the inverters discussed in Section 3.5 which all work at 250MHz.

The horseshoe shape inverter structure is shown in Figure [4.18].

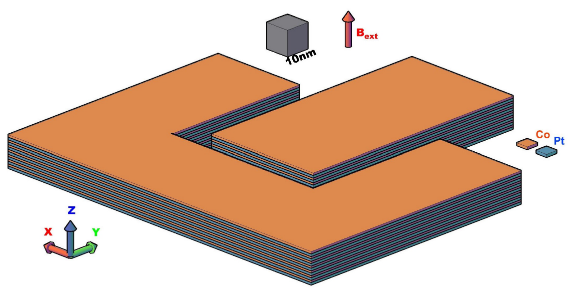

Figure 4.18: Inverter Low Power

In Figure [4.19] is shown the ANC that serves to facilitate the switching of the output.

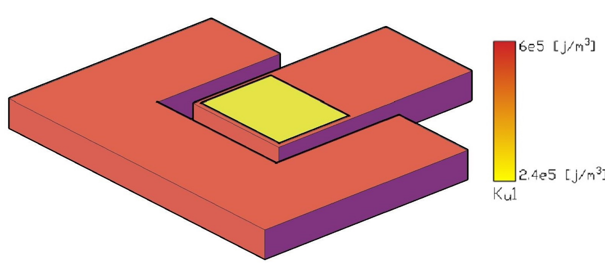

Figure 4.19: Inverter Low Power Ku

Several simulations were carried out to characterize this inverter and their results were compared with those related to the high frequency inverter. This comparison is shown in Figure [4.20].

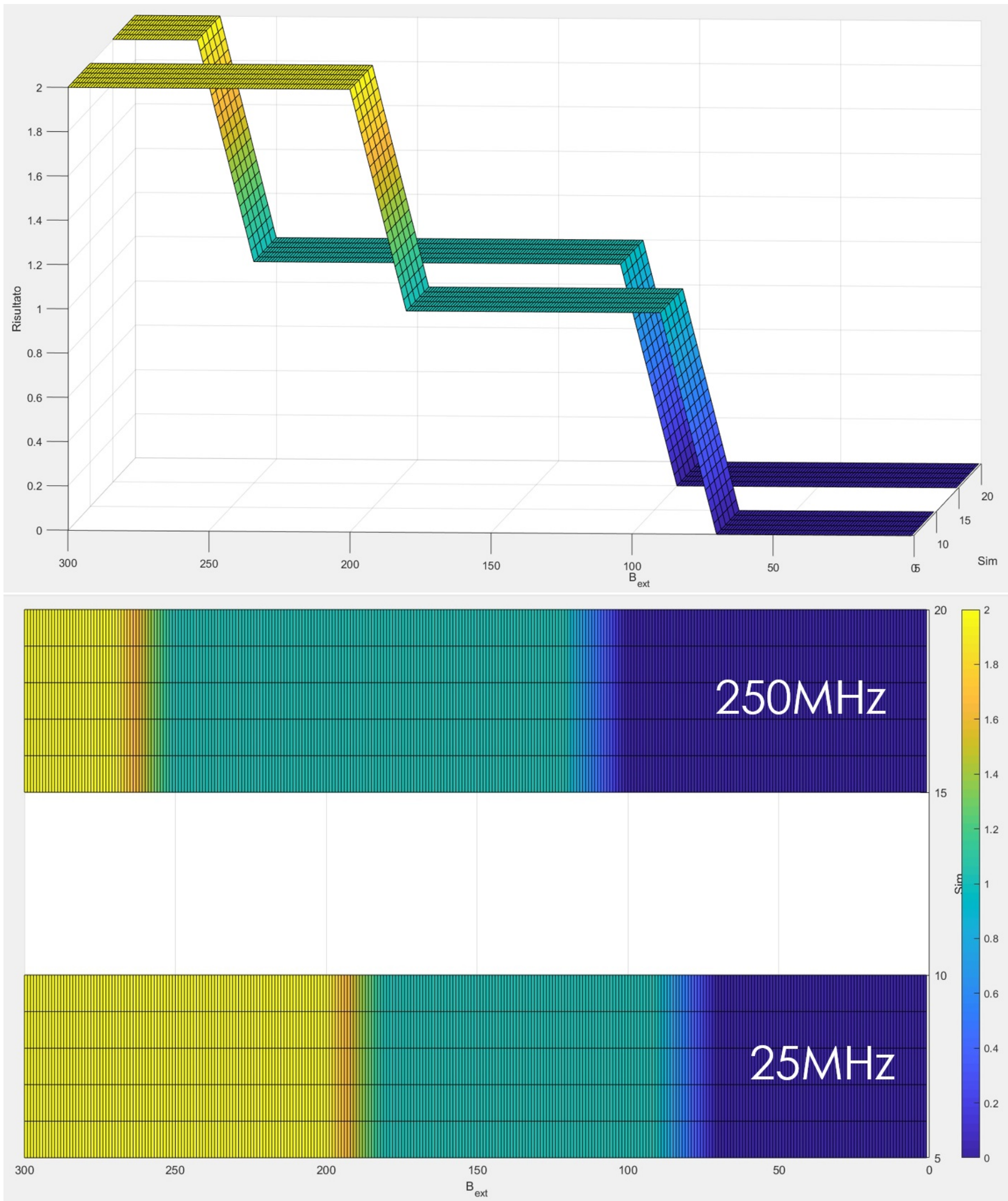

Figure 4.20: Result of Inverter Low Power Vs Inverter High Frequency, were 0(Blue) insufficient magnetic field - 0.5(Heavenly) partial nucleation - 1(Green) correct nucleation - 2(Yellow) Excessive magnetic field

As can be seen from the graph in Figure [4.20], it is also possible to reduce the range of the field intensity with which the inverter works by reducing the frequency. In fact, it passes from a range of (120mT - 250mT) to a range of (90mT - 190mT).

Below there is an extract of a simulation of a low power inverter Figure [4.21].

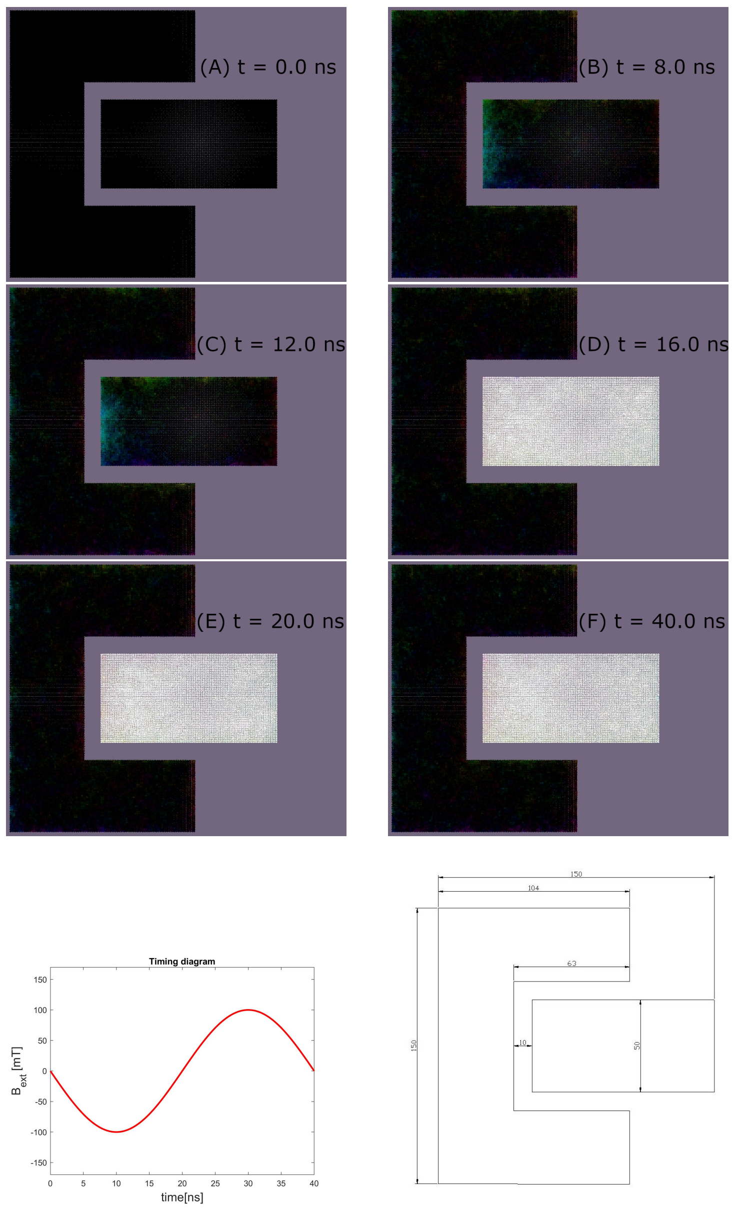

Figure 4.21: Simulation of inverter Low Power with $T = 0K$, $B_ext = 100mT@25MHz$ Sin, timing diagram (bottom), result obtained with MuMax3

Chapter 5

Complete Structure

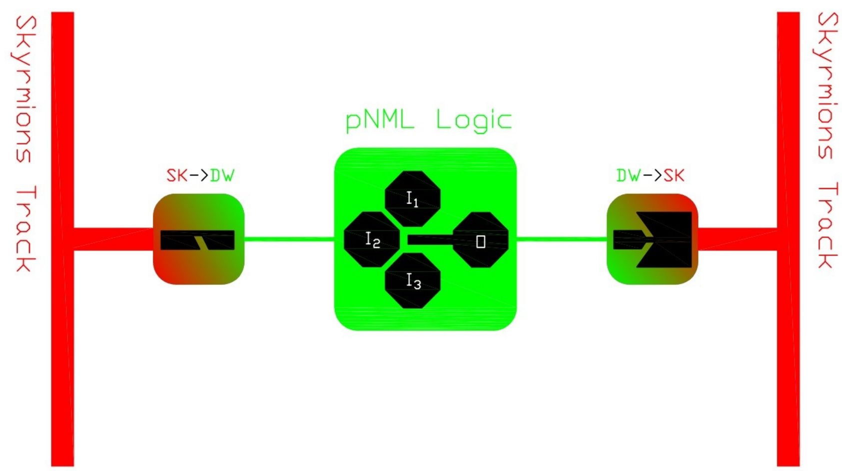

Figure 5.1: Complete System

The working of a complete structure as the one you can see in Figure [5.1] is composed by several phases described below :

it starts by picking up the skyrmion from a skyrmion's memory and putting it in a skyrmions track, then it is converted in Domain wall pair through the conversion block $Sk- > DW$. After that, the data is elaborated by pNML (in this case an inverter),during which it can be easily duplicated. Later it can be converted back to skyrmion through the conversion block $DW- > Sk$ and finally the skyrmion outgoing can be re-stored in memory or sent to another elaborative unit.

5.1 Complete structure example

Actually, there is not a single option in order to realize a complete structure, in fact all the base blocks that can be used, have already been extensively described in the previous sections.

In this section we will see only some examples of how complete conversion structures could be implemented :

- **5.1.1 - Complete Structure with Ramp**
- **5.1.2 - Complete Structure with Identity**
- **5.1.2 - Complete Structure with Inverter**

5.1.1 Complete Structure with Ramp

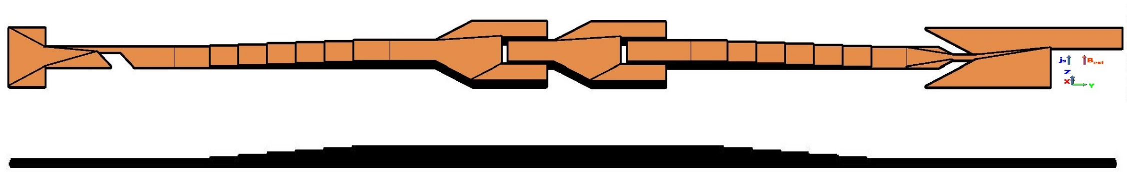

Figure 5.2: Complete Structure with Ramp

In the structure shown in Figure [5.2] you may notice that an Input T-Type Stage discussed in Section 3.1.2 has been used. Subsequently, to convert from Singlelayer to Multilayer has been used a ramp structure discussed in Section 3.3.4. Later there is a Multilayer inverter discussed in Section 3.5.2. After the pNML processing stage, a ramp (Section 3.4.3) is used again to return from Multilayer to Singlelayer. Finally to convert again from Domain Wall to skyrmion the output Stage discussed in Section 3.2.2 has been used.

5.1.2 Complete Structure with Identity

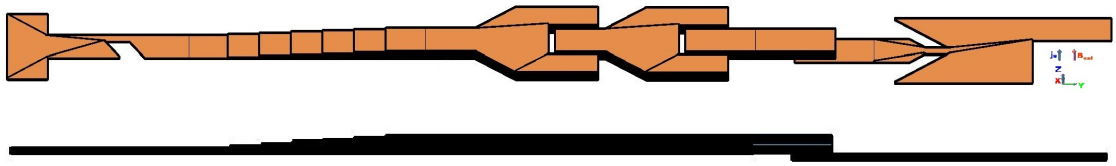

Figure 5.3: Complete Structure with Identity

In the structure shown in Figure [5.3] you may notice that an Input T-Type Stage discussed in Section 3.1.2has been used. Subsequently, to convert from Singlelayer to Multilayer has been used a ramp structure discussed in Section 3.3.4. Later there is a Multilayer inverter (Section 3.5.2) and, after the pNML processing stage, the identity operator discussed in Section 3.4.1 has been used to return from Multilayer to Singlelayer. Finally to convert again from Domain Wall to skyrmion the output Stage discussed in Section 3.2.2 has been used.

5.1.3 Complete Structure with Inverter

Figure 5.4: Complete Structure with Inverter

In the structure shown in Figure[5.4] you may notice that an Input T-Type Stage discussed in Section 3.1.2. Subsequently, to convert from Singlelayer to Multilayer has been used a ramp structure discussed in Section 3.3.4. Later there is a Multilayer inverter (Section 3.5.2) and, after the pNML processing stage, the inverter operator discussed in Section 3.4.2 has been used to return from Multilayer to Singlelayer.

Finally to convert again from Domain Wall to skyrmion the output Stage discussed in Section 3.2.2 has been used.

5.2 Complete structure simulation

Unfortunately it was not possible to create a single complete simulation because of the large mesh dimensions, consequently it was tested in pieces to make it easy.

The structure chosen from the list above is the Complete Structure with Ramp (Section 5.1.1).

The regions into which the structure is divided are listed below:

- **5.2.1 - Input T-Type**
- **5.2.2 - Conversion SingleLayer to Multilayer**
- **5.2.3 - Conversion MultiLayer to Single Layer**
- **5.2.4 - Output Stage**

5.2.1 Input T-Type

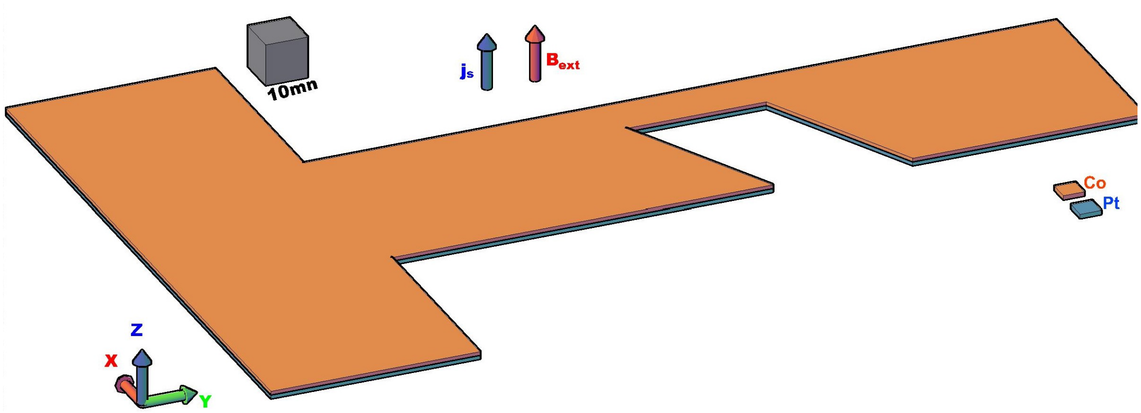

Figure 5.5: T-Type Input Stage SingleLayer

The input T-Type is shown in the Figure above [5.5]. This structure has been extensively described and analysed in Section 3.1.2 where there is an extract of a simulation that shows its principle functioning (Figure [3.8]).

5.2.2 Conversion SingleLayer to Multilayer

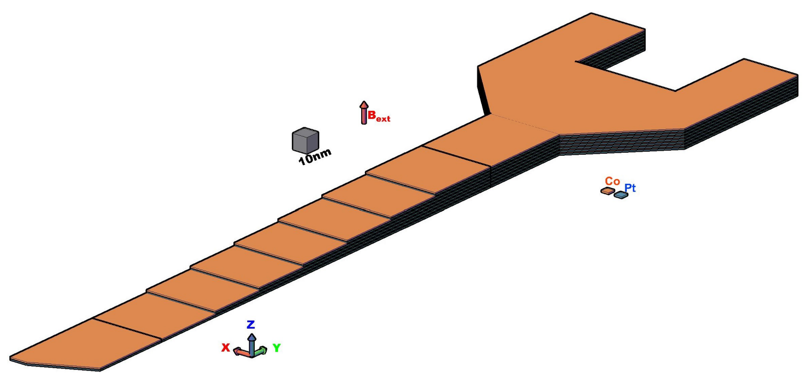

Figure 5.6: Conversion singleLayer to Multilayer plus horseshoe

In this case, a ramp has been used to switch from Singlelayer to Multilayer (Figure [5.6]). The difference with the ramp already discussed in Section 3.3.4 is that, the Domain Wall Pair must travel the ramp and nuclear the horseshoe of the inverter in half clock cycle, in order to be able to propagate in the processing unit pNML.

A simulation has been carried out and an extract is shown in Figure [5.7]

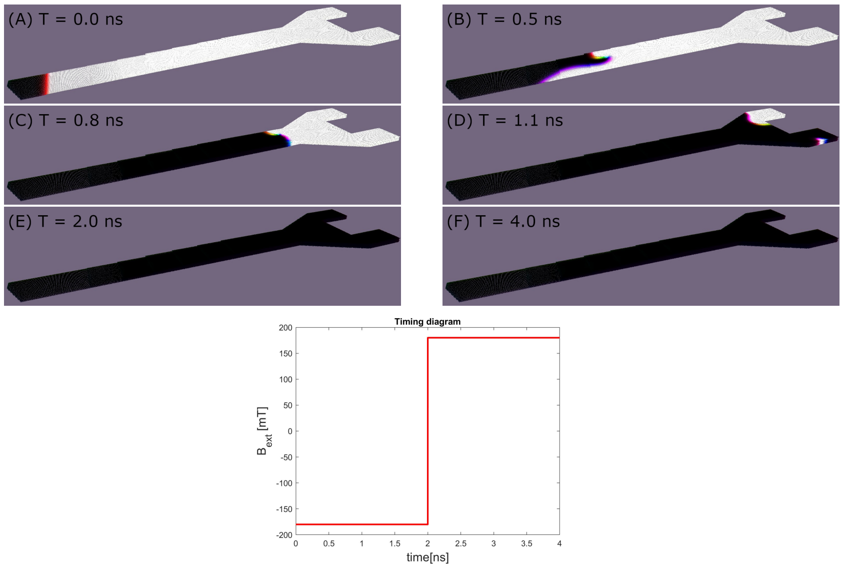

Figure 5.7: simulation of singleLayer to Multilayer plus horseshoe, A-D : $B_{ext} = -180mT$, E-F : $B_{ext} = 180mT$, timing diagram (bottom), result obtained with MuMax3

5.2.3 Conversion MultiLayer to Single Layer

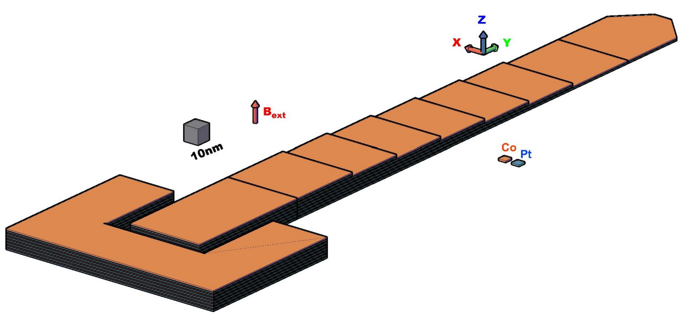

Figure 5.8: Conversion MultiLayer to Single Layer

After pNML processing, it is necessary to report the Domain Wall pair to a Single-layer, before converting it to skyrmion (See Figure [5.8]). Therefore in the simulation there is an inverter pNML that has as output a ramp, like that discussed in Section 3.4.3, also in this case the Domain Wall Pair must traveled in half clock cycle.

A simulation has been carried out and an extract is shown in Figures [5.9]

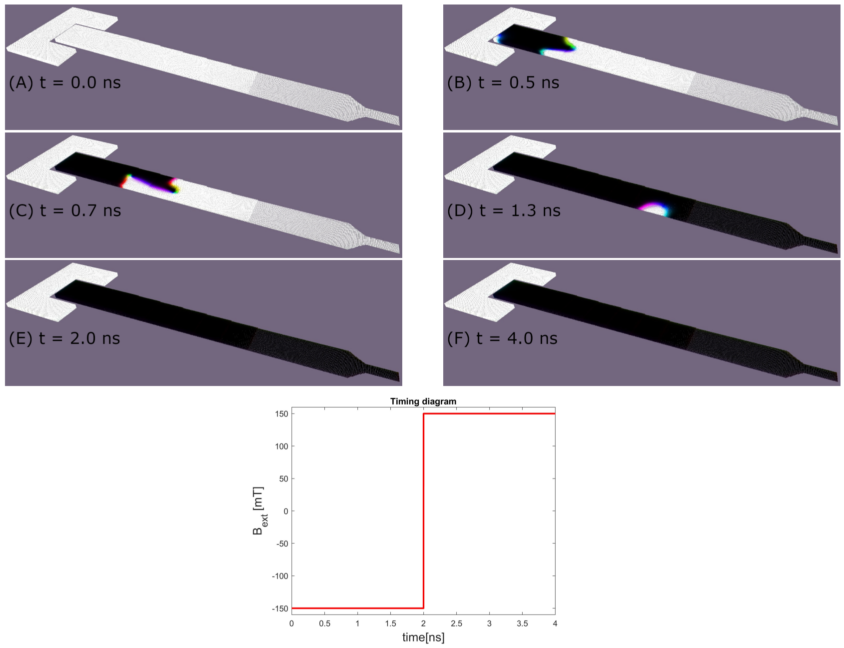

Figure 5.9: Simulation of inverter plus Multilayer to SingleLayer Converter,$B_{ext} = 150mT$, timing diagram (bottom), result obtained with MuMax3

5.2.4 Output Stage

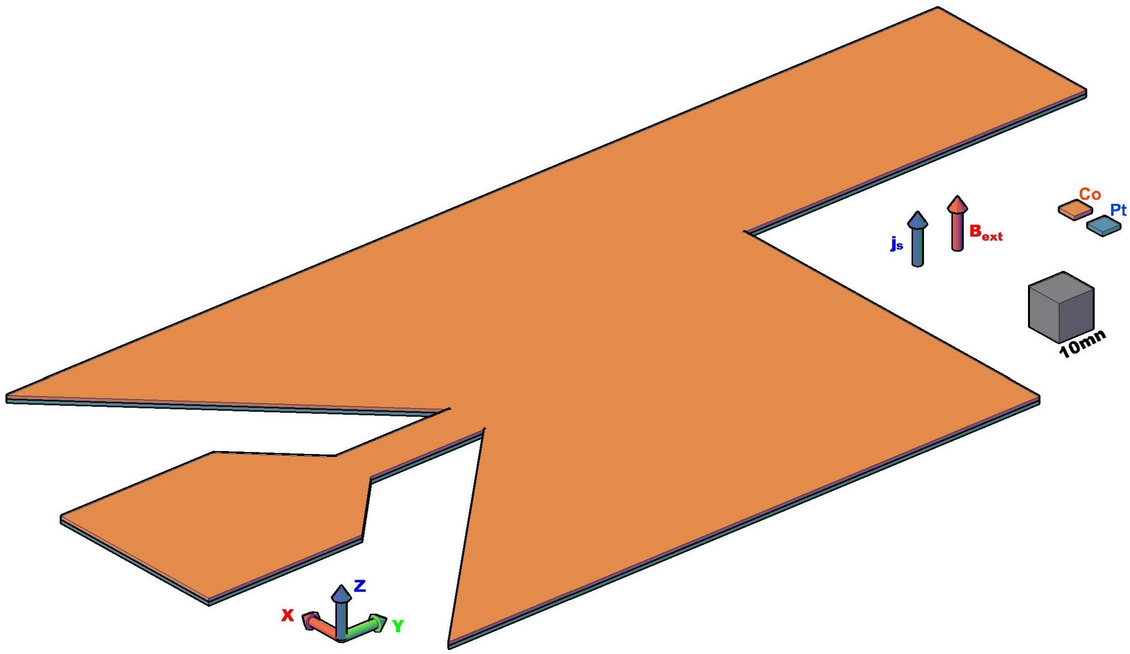

Figure 5.10: Output Stage V2 SingleLayer

When a Domain Wall Pair in Singlelayer is obtained, the block alredy discussed in Section 3.2.2 is used to convert it to skyrmion. Also in this case there is simulation that you can see in Figure [3.15].

Chapter 6

Lim architecture

A Logic in Memory structure is a natural application of these two technologies (pNML and Skyrmions), which lend themselves very well to this type of architecture.

There are innumerable articles in which the application of pNML technology is discussed.

6.1 Example of LiM system

A good starting point to use this hybrid technology is a max/min search system, in particular the one discussed in the Article [25], where it is proposed an architecture to find the minimum or the maximum.

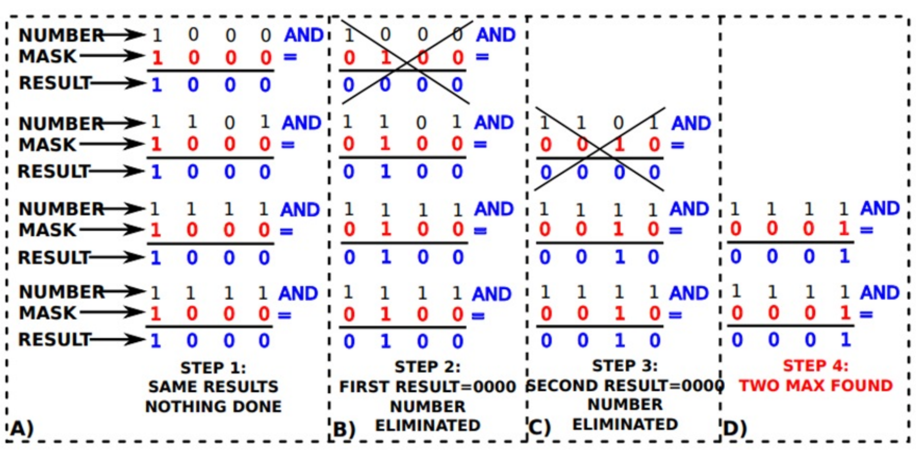

Figure 6.1: Lim algorithm extract from Article [25]

The algorithm is summarised in Figure [6.1], where to find the maximum N step (where N is the data bit number) are needed. At each step the data gets compared (AND function) to a mask, then is done the OR function of the result. If there is at least a "1" in the result, the data goes to the next step, otherwise it is excluded from the analysis because it is not a maximum (or minimum). So, only if the data arrives at the last step of the analysis a maximum (or minimum) has been found.

To make the algorithm a bit more complex, a system to count the number of maximum (or minimum) inside the memory has been added.

6.2 Hypothetical Skyrmions & pNML solution

To make the graphical representation of the system clearer, it was decided to represent the pNML gates as traditional logic gates and to add Special gates to the Skyrmions–Domain Wall conversion and vice versa (See Figure [6.2]).

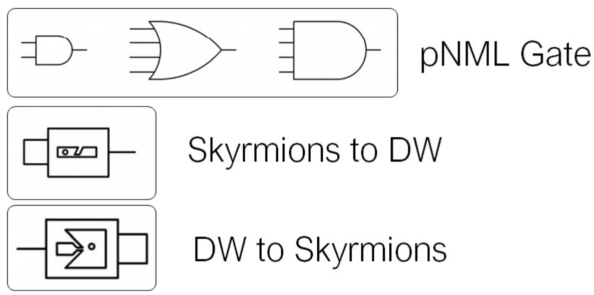

Figure 6.2: pNML gate and conversion gate

A first version is that shown in Figure [6.3].

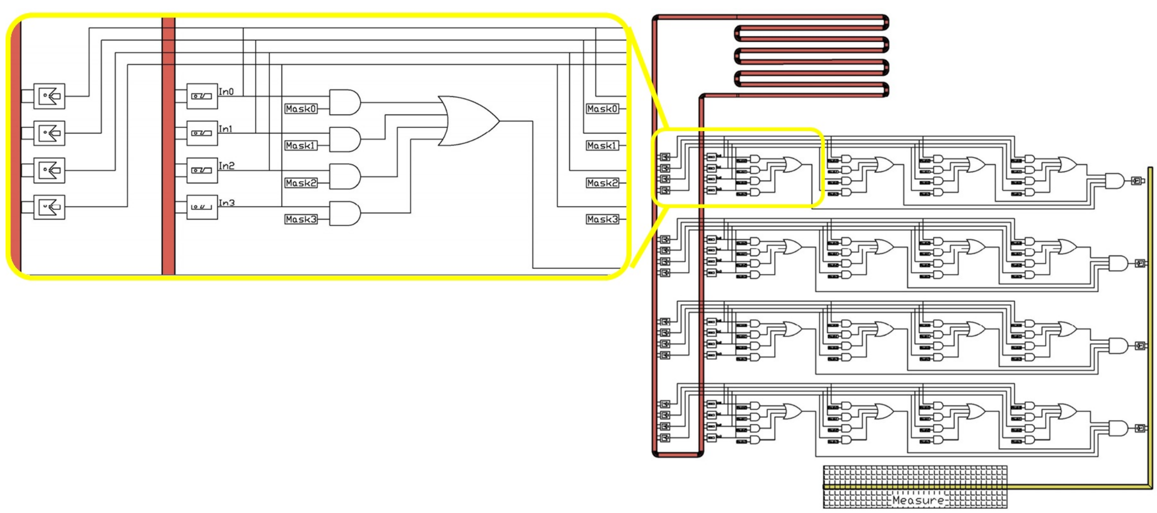

Figure 6.3: Lim algorithm circuit V1

When the data enters the pNML block it is duplicated (easy operation in the Domain wall) and rewritten in the skyrmions track so that it can be reinserted into memory.

The result does not return to the skyrmion's memory but every time a maximum (or minimum) is found, a skyrmion is generated in a new track where the number of Skyrmions is read with the magnetoresistance method.

In the new track the skyrmions are accumulated and they do not represent words. consequently it is possible to have a greater density so in the worst case this new line can be up to 5 * N times smaller than the main memory (N = bit Word).

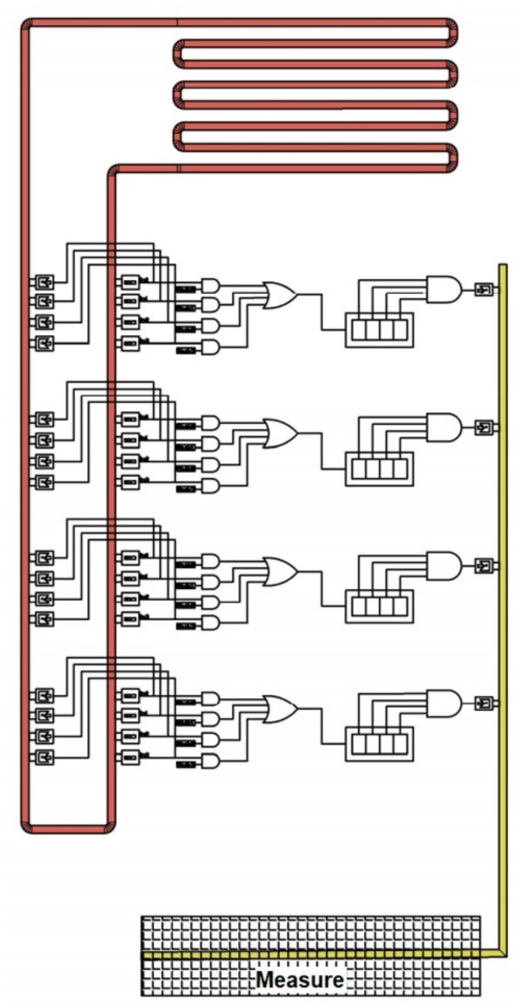

Figure 6.4: Lim algorithm circuit V2

In this structure, the overall dimensions are reduced by reducing the pNML processing unit by adding a ”Shift Register” in this way each horizontal branch can process an N bit data (N = 4 in the example) in N cycles.

Chapter 7

Conclusion

During the thesis work, countless studies were carried out to understand the skyrmions world and understand how to make the transition from Skyrmions to pNML and vice versa possible.

The results obtained were in fact very positive as can be seen in chapter 5 where there are some examples of possible hybrid skyrmions pNML structures. These structures could easily be used as basic building blocks for complex systems which fully exploit the potential of both technologies.

A system where it is possible to use this hybrid technology is proposed in chapter 6, where a LiM architecture is proposed to find the Max / min. This algorithm fits perfectly to our hybrid technology thanks to the density of the skyrmions memory and the computational capacity offered by the pNML.

As a further/future evolution, this technology could be used as a method of rapid encryption of information, for example through the AES algorithm.

Acronyms

$DW->Sk$ Domain Wall Pairs to Skyrmions conversion. 42, 117

$Sk->DW$ Skyrmions to Domain Wall Pairs conversion. 42, 43, 117

ANC Artificial Nucleation Center. 30, 58, 60, 71, 75, 82

CAM Content Addressable Memory. 32

CCK cross-coupled keeper. 34

CiM Computation-in-Memory. 33

CMOS Complementary MOSFET. 2, 29

CnM Computation-near-Memory. 33

Co Cobalt. 29

CPU central processing unit. 32

CwM Computation-with-Memory. 33

DCS dynamic current source. 34

DMI Dzyaloshinskii-Moriya. 18–20, 22, 25

DOS density of states. 25

DW Domain Wall. 21, 29, 43, 44, 48, 52, 53, 57

DWL Domain Wall Logic. 29

FD finite difference. 36

FIB Focused ion beam. 30

FM ferromagnetic. 19, 20, 26

HM heavy metal layer. 25

iNML in-plane Nano Magnetic Logic. 29

ITRS International Tecnology Roadmap for Semiconductors. 29

Ku Uniaxial Anisotropy Constant. 58, 60, 64, 66, 67, 72, 75, 77, 78, 82

LiM Logic in Memory. 32, 33

LLT Landau-Lifshitz torque. 36, 37

LUT lookup table. 32

MTJ Magnetic Tunnel Junction. 25, 34

MuMax3 GPU-accelerated micromagnetism software. 36, 37, 40, 45–47, 49, 51, 53, 54, 56, 61, 63, 65, 68, 69, 73, 74, 76, 79, 80, 84, 89, 92, 93, 95, 96, 98–100, 102, 103, 105–107, 109, 116, 122, 123

PMA perpendicular magnetic anisotropy. 29, 30, 33

pNML perpendicular Nanomagnetic Logic. 29, 30, 43

Pt Platinum. 29

SHE Spin Hall Effect. 23, 25

SLT Slonczewski spin-transfer torque. 37

SOC Spin-Orbit-Coupling. 19, 20

STT Spin Transfer Torque. 20, 22, 23

THE the Hall effect. 25

ZLT Zhang-Li spin-transfer torque. 37

List of Symbols

The next list describes several symbols that will be later used within the body of the document

α	Damping constant (material constant)
β	coefficent of non-adiabatic effect (material constant)
ϵ_0	Dielectric constant of vacuum
μ_0	Magnetic permeability of vacuum
ρ	Electric charge density
$\vec{\tau}_{LL}$	Landau-Lifshitz torque
$\vec{\tau}_{SL}$	Slonczewski spin-transfer torque
$\vec{\tau}_{ZL}$	Zhang-Li spin-transfer torque
$\vec{m}$	reduced magnetization
B	Magnetic flux field
C	Coupling field strength
c	Speed of light in a vacuum inertial frame
$C(r)$	Magnetic coupling field
C_{eff}	Effective coupling field strength
E	Electric field
E_{ani}	Anisotropy energy
E_{demag}	Demagnetization energy
$E_{exchange}$	Exchange energy

E_{total} Total energy

E_{Zeeman} Zeeman energy

G_L Free energy of the system

g_L Free energy of the system undder non zero input h

H Magnetic field

j Electric current density

j_c Depining current

M Magnetization

M_s Saturation magnetization [A/m]

M_z Perpendicular magnetization (Z-Axis)

Q_h helicity

Q_s Pontryagin number

Q_v Vorticity

T Temperature [K]

t Time [s]

Bibliography

[1] G. G. Shahidi. Evolution of cmos technology at 32 nm and beyond. In *2007 IEEE Custom Integrated Circuits Conference*, pages 413–416, Sep. 2007.

[2] Scott E. Thompson and Srivatsan Parthasarathy. Moore's law: the future of si microelectronics. *Materials Today*, 9(6):20 – 25, 2006.

[3] K. Rupp and S. Selberherr. The economic limit to moore's law. *IEEE Transactions on Semiconductor Manufacturing*, 24(1):1–4, Feb 2011.

[4] The international technology roadmap for semiconductors (itrs):processintegration, devices, and structures(pids). 2013.

[5] The international technology roadmap for semiconductors (itrs). 2013.

[6] D. E. Nikonov and I. A. Young. Overview of beyond-cmos devices and a uniform methodology for their benchmarking. *Proceedings of the IEEE*, 101(12):2498–2533, Dec 2013.

[7] Giorgio Bertotti. Chapter 2 - types of hysteresis. In Giorgio Bertotti, editor, *Hysteresis in Magnetism*, Electromagnetism, pages 31 – 70. Academic Press, San Diego, 1998.

[8] Weifeng Zhang, Wei Han, Xin Jiang, See-Hun Yang, and Stuart S. P. Parkin. Role of transparency of platinum–ferromagnet interfaces in determining the intrinsic magnitude of the spin hall effect. *Nature Physics*, 11, 2012.

[9] Cros V. Sampaio J. Fert A. Skyrmions on the track. *Nature Nanotech*, 8:152, 2013.

[10] Alexey A. Kovalev and Shane Sandhoefner. Skyrmions and antiskyrmions in quasi-two-dimensional magnets. *Frontiers in Physics*, 6:98, 2018.

[11] Edoardo Mandalari. *Logic in Memory implementation of an AES algorithm based on skyrmions*. thesis, 2020.

[12] Ezawa M. Zhou Y. A reversible conversion between a skyrmion and a domain-wall pair in a junction geometry. *Nature Communications*, 2014.

[13] Mochizuki M. Nagaosa N. Iwasaki J. Current-induced skyrmion dynamics in constricted geometries. *Nature Nanotechnology*, 2013.

[14] Fangohr H. et al. Zhang X., Zhao G. Skyrmion-skyrmion and skyrmion-edge

repulsions in skyrmion-based racetrack memory. *Scientific Reports*, 2015.

[15] Rohart S. et al Sampaio J., Cros V. Nucleation, stability and current-induced motion of isolated magnetic skyrmions in nanostructures. *Nature Nanotechnology*, 2013.

[16] Sara G. Miralles. *Molecular Spintronic Devices: from Molecular Spin Valves to Spin-OLEDs*. Phd thesis, 2017.

[17] Maverick Chauwin, Xuan Hu, Felipe Garcia-Sanchez, Neilesh Betrabet, Alexandru Paler, Christoforos Moutafis, and Joseph S. Friedman. Skyrmion logic system for large-scale reversible computation. *Phys. Rev. Applied*, 12:064053, Dec 2019.

[18] S. Breitkreutz, J. Kiermaier, I. Eichwald, C. Hildbrand, G. Csaba, D. Schmitt-Landsiedel, and M. Becherer. Experimental demonstration of a 1-bit full adder in perpendicular nanomagnetic logic. *IEEE Transactions on Magnetics*, 49(7):4464–4467, July 2013.

[19] S. Breitkreutz, J. Kiermaier, I. Eichwald, X. Ju, G. Csaba, D. Schmitt-Landsiedel, and M. Becherer. Majority gate for nanomagnetic logic with perpendicular magnetic anisotropy. *IEEE Transactions on Magnetics*, 48(11):4336–4339, Nov 2012.

[20] Giulia Santoro, Giovanna Turvani, and Mariagrazia Graziano. New logic-in-memory paradigms: An architectural and technological perspective. *Micromachines*, 10(6), 2019.

[21] F. Riente, G. Ziemys, G. Turvani, D. Schmitt-Landsiedel, S. B. Gamm, and M. Graziano. Towards logic-in-memory circuits using 3d-integrated nanomagnetic logic. In *2016 IEEE International Conference on Rebooting Computing (ICRC)*, pages 1–8, Oct 2016.

[22] S. Matsunaga, J. Hayakawa, S. Ikeda, K. Miura, T. Endoh, H. Ohno, and T. Hanyu. Mtj-based nonvolatile logic-in-memory circuit, future prospects and issues. In *2009 Design, Automation Test in Europe Conference Exhibition*, pages 433–435, April 2009.

[23] Arne Vansteenkiste, Jonathan Leliaert, Mykola Dvornik, Mathias Helsen, Felipe Garcia-Sanchez, and Bartel Van Waeyenberge. The design and verification of mumax3. *AIP Advances*, 4(10):107133, 2014.

[24] E. Motohiko Z. Xichao and Z. Yan. Magnetic skyrmion logic gates: conversion,

duplication and merging of skyrmions. *Scientific Reports*, Mar 2015.

[25] M. Vacca, Y. Tavva, A. Chattopadhyay, and A. Calimera. Logic-in-memory architecture for min/max search. In *2018 25th IEEE International Conference on Electronics, Circuits and Systems (ICECS)*, pages 853–856, Dec 2018.

[26] C. A. Mack. Fifty years of moore's law. *IEEE Transactions on Semiconductor Manufacturing*, 24(2):202–207, May 2011.

[27] Bernd Hoefflinger. *ITRS: The International Technology Roadmap for Semiconductors*, pages 161–174. Springer Berlin Heidelberg, Berlin, Heidelberg, 2012.

[28] M. G. Bardon, P. Raghavan, G. Eneman, P. Schuddinck, M. Dehan, A. Mercha, A. Thean, D. Verkest, and A. Steegen. Group iv channels for 7nm finfets: Performance for socs power and speed metrics. In *2014 Symposium on VLSI Technology (VLSI-Technology): Digest of Technical Papers*, pages 1–2, June 2014.

[29] Giorgio Bertotti. Chapter 1 - magnetic hysteresis. In Giorgio Bertotti, editor, *Hysteresis in Magnetism*, Electromagnetism, pages 3 – 30. Academic Press, San Diego, 1998.

[30] Giorgio Bertotti. Chapter 3 maxwell's equations in magnetic media. In Giorgio Bertotti, editor, *Hysteresis in Magnetism*, Electromagnetism, pages 73 – 102. Academic Press, San Diego, 1998.

[31] L. LANDAU and E. LIFSHITZ. 3 - on the theory of the dispersion of magnetic permeability in ferromagnetic bodiesreprinted from physikalische zeitschrift der sowjetunion 8, part 2, 153, 1935. In L.P. PITAEVSKI, editor, *Perspectives in Theoretical Physics*, pages 51–65. Pergamon, Amsterdam, 1992.

[32] Rudolf Hubert, Alexand Schäfer. *Domain Theory*, pages 99–335. Springer Berlin Heidelberg, Berlin, Heidelberg, 1998.

[33] T. L. Gilbert and J. M. Kelly, editors. *Anomalous rotational damping in ferromagnetic sheets*, June 1955.

[34] Soo-Man Seo, Kyoung-Whan Kim, Jisu Ryu, Hyun-Woo Lee, and Kyung-Jin Lee. Current-induced motion of a transverse magnetic domain wall in the presence of spin hall effect. *Applied Physics Letters*, 101(2):022405, 2012.

[35] W. Kang, Y. Huang, X. Zhang, Y. Zhou, and W. Zhao. Skyrmion-electronics: An overview and outlook. *Proceedings of the IEEE*, 104(10):2040–2061, Oct 2016.

[36] W. Kang, X. Chen, D. Zhu, S. Li, Y. Huang, Y. Zhang, and W. Zhao. Magnetic skyrmions for future potential memory and logic applications: Alternative information carriers. In *2018 Design, Automation Test in Europe Conference Exhibition (DATE)*, pages 119–124, March 2018.

[37] Kubetzka A. Dupé B. Romming N. von Bergmann K Wiesendanger R. Heinze S. Hanneken C., Otte F. Electrical detection of magnetic skyrmions by tunnelling non-collinear magnetoresistance. *Nature Nanotechnology*, 2015.

[38] D. A. Allwood, G. Xiong, C. C. Faulkner, D. Atkinson, D. Petit, and R. P. Cowburn. Magnetic domain-wall logic. *Science*, 309(5741):1688–1692, 2005.

[39] S. Breitkreutz, G. Ziemys, I. Eichwald, J. Kiermaier, G. Csaba, W. Porod, D. Schmitt-Landsiedel, and M. Becherer. Domain wall gate for magnetic logic and memory applications with perpendicular anisotropy. In *2013 IEEE International Electron Devices Meeting*, pages 22.4.1–22.4.4, Dec 2013.

[40] The international technology roadmap for semiconductors (itrs):emerging research devices (erd), 2013. [online].available:http://www.itrs.net/links/2013itrs/2013chapters/2013erd.pdf. 2013.

[41] M. Becherer, G. Csaba, R. Emling, W. Porod, P. Lugli, and D. Schmitt-Landsiedel. Field-coupled nanomagnets for interconnect-free nonvolatile computing. In *2009 IEEE International Solid-State Circuits Conference - Digest of Technical Papers*, pages 474–475, Feb 2009.

[42] S. Breitkreutz, J. Kiermaier, X. Ju, G. Csaba, D. Schmitt-Landsiedel, and M. Becherer. Nanomagnetic logic: Demonstration of directed signal flow for field-coupled computing devices. In *2011 Proceedings of the European Solid-State Device Research Conference (ESSDERC)*, pages 323–326, Sep. 2011.

[43] M. Becherer, J. Kiermaier, S. Breitkreutz, I. Eichwald, G. Csaba, and D. Schmitt-Landsiedel. Nanomagnetic logic clocked in the mhz regime. In *2013 Proceedings of the European Solid-State Device Research Conference (ESSDERC)*, pages 276–279, Sep. 2013.

[44] J. Kiermaier, S. Breitkreutz, I. Eichwald, M. Engelstädter, X. Ju, G. Csaba, D. Schmitt-Landsiedel, and M. Becherer. Information transport in field-coupled nanomagnetic logic devices. *Journal of Applied Physics*, 113(17):17B902, 2013.

[45] J. Kiermaier, S. Breitkreutz, I. Eichwald, X. Engelstädter, M. andJu, G. Csaba,

D. Schmitt-Landsiedel, and M. Becherer. Information transport in field-coupled nanomagnetic logic devices. *Journal of Applied Physics*, 113(17):17B902, 2013.

[46] A. M. Peskin. A logic-in-memory architecture for large-scale-integration technologies. In *Proceedings of the ACM Annual Conference - Volume 1*, ACM '72, page 12–25, New York, NY, USA, 1972. Association for Computing Machinery.

[47] D. H. Kim, K. Athikulwongse, M. B. Healy, M. M. Hossain, M. Jung, I. Khorosh, G. Kumar, Y. Lee, D. L. Lewis, T. Lin, C. Liu, S. Panth, M. Pathak, M. Ren, G. Shen, T. Song, D. H. Woo, X. Zhao, J. Kim, H. Choi, G. H. Loh, H. S. Lee, and S. K. Lim. Design and analysis of 3d-maps (3d massively parallel processor with stacked memory). *IEEE Transactions on Computers*, 64(1):112–125, Jan 2015.

[48] Shaahin Angizi, Zhezhi He, and Deliang Fan. Pima-logic: A novel processing-in-memory architecture for highly flexible and energy-efficient logic computation. In *Proceedings of the 55th Annual Design Automation Conference*, DAC '18, New York, NY, USA, 2018. Association for Computing Machinery.

[49] R. Kaplan, L. Yavits, R. Ginosar, and U. Weiser. A resistive cam processing-in-storage architecture for dna sequence alignment. *IEEE Micro*, 37(4):20–28, 2017.

[50] Shoun Matsunaga, Jun Hayakawa, Shoji Ikeda, Katsuya Miura, Haruhiro Hasegawa, Tetsuo Endoh, Hideo Ohno, and Takahiro Hanyu. Fabrication of a nonvolatile full adder based on logic-in-memory architecture using magnetic tunnel junctions. *Applied Physics Express*, 1:091301, aug 2008.

[51] G. Causapruno, F. Riente, G. Turvani, M. Vacca, M. Ruo Roch, M. Zamboni, and M. Graziano. Reconfigurable systolic array: From architecture to physical design for nml. *IEEE Transactions on Very Large Scale Integration (VLSI) Systems*, 24(11):3208–3217, Nov 2016.

[52] Stephan Werner Georg Breitkreutz von Gamm. *Perpendicular Nanomagnetic Logic: Digital Logic Circuits from Field-coupled Magnets*. thesis, 2015.